1985

Phase-Sensitive Detection and the Back-Action Evasion of Amplifier Force Noise (Measurement Theory, Transducers, Antenna, Gravitational Radiation, Accelerometer).

Gary W. Spetz
Louisiana State University and Agricultural & Mechanical College

INFORMATION TO USERS

This reproduction was made from a copy of a document sent to us for microfilming. While the most advanced technology has been used to photograph and reproduce this document, the quality of the reproduction is heavily dependent upon the quality of the material submitted.

The following explanation of techniques is provided to help clarify markings or notations which may appear on this reproduction.

1. The sign or "target" for pages apparently lacking from the document photographed is "Missing Page(s)". If it was possible to obtain the missing page(s) or section, they are spliced into the film along with adjacent pages. This may have necessitated cutting through an image and duplicating adjacent pages to assure complete continuity.

2. When an image on the film is obliterated with a round black mark, it is an indication of either blurred copy because of movement during exposure, duplicate copy, or copyrighted materials that should not have been filmed. For blurred pages, a good image of the page can be found in the adjacent frame. If copyrighted materials were deleted, a target note will appear listing the pages in the adjacent frame.

3. When a map, drawing or chart, etc., is part of the material being photographed, a definite method of "sectioning" the material has been followed. It is customary to begin filming at the upper left hand corner of a large sheet and to continue from left to right in equal sections with small overlaps. If necessary, sectioning is continued again—beginning below the first row and continuing on until complete.

4. For illustrations that cannot be satisfactorily reproduced by xerographic means, photographic prints can be purchased at additional cost and inserted into your xerographic copy. These prints are available upon request from the Dissertations Customer Services Department.

5. Some pages in any document may have indistinct print. In all cases the best available copy has been filmed.

University
Microfilms
International

300 N. Zeeb Road
Ann Arbor, MI 48106

Spetz, Gary W.

PHASE-SENSITIVE DETECTION AND THE BACK-ACTION EVASION OF AMPLIFIER FORCE NOISE

The Louisiana State University and Agricultural and Mechanical Col. PH.D. 1985

PLEASE NOTE:

In all cases this material has been filmed in the best possible way from the available copy. Problems encountered with this document have been identified here with a check mark __✓__.

1. Glossy photographs or pages _____
2. Colored illustrations, paper or print _____
3. Photographs with dark background ✓
4. Illustrations are poor copy _____
5. Pages with black marks, not original copy _____
6. Print shows through as there is text on both sides of page _____
7. Indistinct, broken or small print on several pages ✓
8. Print exceeds margin requirements _____
9. Tightly bound copy with print lost in spine _____
10. Computer printout pages with indistinct print _____
11. Page(s) _____ lacking when material received, and not available from school or author.
12. Page(s) _____ seem to be missing in numbering only as text follows.
13. Two pages numbered _____. Text follows.
14. Curling and wrinkled pages _____
15. Dissertation contains pages with print at a slant, filmed as received ✓
16. Other _____

_____

_____

PHASE-SENSITIVE DETECTION AND THE BACK-ACTION EVASION OF AMPLIFIER FORCE NOISE

A Dissertation

Submitted to the Graduate Faculty of the
Louisiana State University and
Agricultural and Mechanical College
in partial fulfillment of the
requirements for the degree of
Doctor of Philosophy

in

The Department of Physics and Astronomy

by
Gary W. Spetz
B.S., University of Illinois, Urbana, Illinois, 1974
M.S., University of Illinois, Urbana, Illinois, 1977
May 1985

ACKNOWLEDGEMENTS

It is impractical for me to acknowledge everyone who participated in my development, training, and research during the past few years. I first and foremost wish to express my gratitude to my major professor, William O. Hamilton. I have been enriched greatly through my personal and professional association with him and I am proud and fortunate to have him as an advisor and friend. I deeply appreciate the guidance and patience he showed me throughout this period.

I want to thank Dr. Tony Mann for his friendship, lab assistance and expertise, and unflagging encouragement and interest in my work. He also proofread the preliminary versions of this dissertation, for which I am extremely grateful.

I am indebted to Prof. William Oelfke for getting me started on the project and his encouragement throughout this work.

There have been a number of people associated with the gravitational radiation detection group here at LSU during my tenure. I am fortunate to have had the opportunity to work with, and benefit from, Allen Sibley, Bu-Xin Xu, Ricky Campisi, Dale Darling, Bruce Pipes, and

Gentom Wang. I thank Khachig Jerjian for his moral support. I also wish to thank Prof. Robert F. O'Connell for tutoring me in quantum optics.

I thank my mother, Ann, and brother, Keith, for their faith and support in me. I deeply regret that my father did not live to see me finish, for no one would be any prouder of me right now than he.

I also want to thank my father- and mother-in-law, John and Mildred Ruston, for taking me into their hearts as if I were their own son.

None of this would have any value, nor would have been possible, without the constant love and support I have received from my wife, Martha. I wish to express my love to her and tell her how much joy she brings me. I wish to dedicate this dissertation, as I have chosen to dedicate my life, to her and our new daughter, Lauren Allison, who is not quite seven weeks old as I write these words and so can not yet call me 'Doctor Dad'.

TABLE OF CONTENTS

Page

Page

LIST OF FIGURES

ABSTRACT

Limitations on the sensitivity for detecting a weak classical force acting on a harmonic oscillator are imposed by the quantum mechanical properties associated with a "standard" amplitude-and-phase measurement and, classically, by the back reaction noise associated with the finite noise temperature of the amplifier used to process the measurement. These are known as the "standard quantum limit" and the "standard amplifier limit", respectively.

We present the theoretical motivation behind the quest to circumvent these limits, and examine a single-transducer back-action evading measurement scheme designed to perform a phase-sensitive coupling to the oscillator, with the concomitant circumvention of the standard amplifier limit via the "squeezing" of amplifier back reaction noise. The applicability of squeezing in the detection of gravitational radiation is explored via the dependence of detection sensitivity on the physical temperature and quality factor of the resonant-bar gravitational radiation antenna, on the noise temperature of the amplifier, and on the squeezing factor of the back-action evading measurement; the success of back-action evasion in improving

upon the optimum amplitude-and-phase detection sensitivities depends critically upon these parameters.

Using the LSU superconducting dual-cavity accelerometer as a test platform, we present direct evidence for the establishment of a phase-sensitive coupling to an oscillator, along with a variety of indirect corroborating evidence. This data indicates that our phase-sensitive measurement scheme is indeed more sensitive to one component of the oscillator than to the other component.

We also present the first evidence for the existence of back-action evasion of amplifier back reaction noise. We show theoretical expectations and experimental results for the dependence of squeezing on: input signal phases, amplitudes, and frequencies; amplifier back reaction levels; background noise; mechanical oscillator frequency; and coherent carrier contribution at the cavity resonance frequency. Squeezing factors of up to fifteen were achieved by our back-action evading measurement scheme.

CHAPTER 1

INTRODUCTION

The nature of gravitational radiation detection has spawned a variety of spin-off research, not the least of which entertains the fascinating names of "quantum nondemolition" (QND) and "back-action evasion" (BAE). QND/BAE is a product of the intermingling of two scientific urgings: the pragmatic desire to improve on the potential sensitivity of working gravity wave antennas and the broader need to better understand the theory of measurement, particularly as it applies to the interaction of detection systems with very weak classical forces.

The LSU gravitational radiation detection group was the first group in this country to initiate an experimental investigation designed to test the basic ideas behind QND/BAE, this dissertation being the result of the investigation. In Chapter 2 we present the semi-classical arguments giving birth to the existence of a quantum mechanical limitation to the sensitivity for a "standard" measurement of the amplitude and phase of a harmonic oscillator (the "standard quantum limit", or SQL) and the subsequent principle of QND/BAE. We also discuss the noise contribution of a linear amplifier, which gives rise to the "standard amplifier limit" (SAL) and amplifier back action.

In Chapter 3 we analyze an equivalent-circuit model of the LSU test accelerometer and compare and contrast SQL-limiting and SQL-circumventing model parameters. The QND/BAE designs give rise to two interrelated but distinct phenomena: the "phase-sensitive" (PS) detection of only one oscillator coordinate (as opposed to the two coordinates that are monitored under amplitude and phase (AP) measurements), and the back action evasion (BAE) of amplifier back reaction force noise (i.e. the insertion of these noise effects into only one coordinate, also called "squeezing").

The applicability of BAE to gravity wave transducers and resonant bar antenna sensitivity is discussed in Chapter 4. Interestingly, the squeezing of amplifier back reaction not only reduces the effective amplifier noise temperature but it also raises the effective physical temperature of the antenna. Also examined is the relationship between detection sensitivity and the squeezing factor, resonant bar quality factor, antenna physical temperature, and amplifier noise temperature. These results are also compared between two operating modes of the transducer.

Chapter 5 describes the experimental apparatus used to conduct this investigation, including the LSU accelerometer; cavity design and preparation; cryogenic and vacuum support; and microwave input-signal

preparation and detection circuitry. The operation and characteristics of the accelerometer are also discussed.

The experimental results confirming both the establishment of phase-sensitive detection and the back-action evasion of amplifier force noise are shown in Chapters 6 and 7. Chapter 6 shows PSD and BAE evidence for cavity input signals generated by a doubly-balanced mixer, and some limited parameter dependences are verified. The last half of Chapter 6 is a reprint of a publication appearing in Physics Letters in September 1984. Chapter 7 also shows PSD and BAE evidence, but for input signals that are independently generated, allowing greater flexibility and enabling even more parameter dependences to be tested. These results are overwhelming in their support for the principles behind, and the establishment of, phase-sensitive detection and the back-action evasion of amplifier force noise.

CHAPTER 2

MEASUREMENT STRATEGIES: GENERAL CONSIDERATIONS

A. Introduction

In this chapter we explore the general theory of amplitude and phase (AP) and phase-sensitive (PS) measurements of a harmonic oscillator. We also discuss back-action evasion (BAE) in the same context, and compare the implications of AP and PS/BAE measurement strategies on force detection sensitivity. We follow, for the most part, the conventions established in the fine seminal review on this subject by Caves, et al. in Reviews of Modern Physics.[1] (We also refer the reader to other references at the end of this chapter.)

B. Amplitude and Phase Measurements

Consider a (quantum) harmonic oscillator with mass m, angular frequency ω, coordinate x, and (canonical) momentum p. The oscillator free Hamiltonian is

$$H_0 = \frac{p^2}{2m} + \frac{1}{2} m\omega^2 x^2 \qquad (2.1)$$

and the number of quanta is given by

$$N = \frac{H_0}{\hbar\omega} - \frac{1}{2} \tag{2.2}$$

Of course, the uncertainty principle for position and momentum is

$$\Delta x \cdot \Delta p \geq \frac{\hbar}{2} \tag{2.3}$$

The oscillator's phase plane can be labelled by Cartesian coordinates x and $p/m\omega$. Classically, the state of an oscillator is given by a point in this plane and rotates clockwise under free evolution. Quantum mechanically, the state is identified by an uncertainty region defined by the uncertainty principle. This uncertainty region is a minimum when it is a circle; then the uncertainties in the two coordinates are equal:

$$\Delta x = \frac{\Delta p}{m\omega} = \left(\frac{\hbar}{2m\omega}\right)^{1/2} \tag{2.4}$$

as illustrated in Figure 2.1. Quantum mechanical states obeying (2.4) are called minimum uncertainty, or coherent, states.[2] Carruthers and Nieto have shown[3] that an oscillator is put into a coherent state when acted upon by a classical force.

Usually, the oscillator is described in terms of its complex amplitude, X_1+iX_2, where

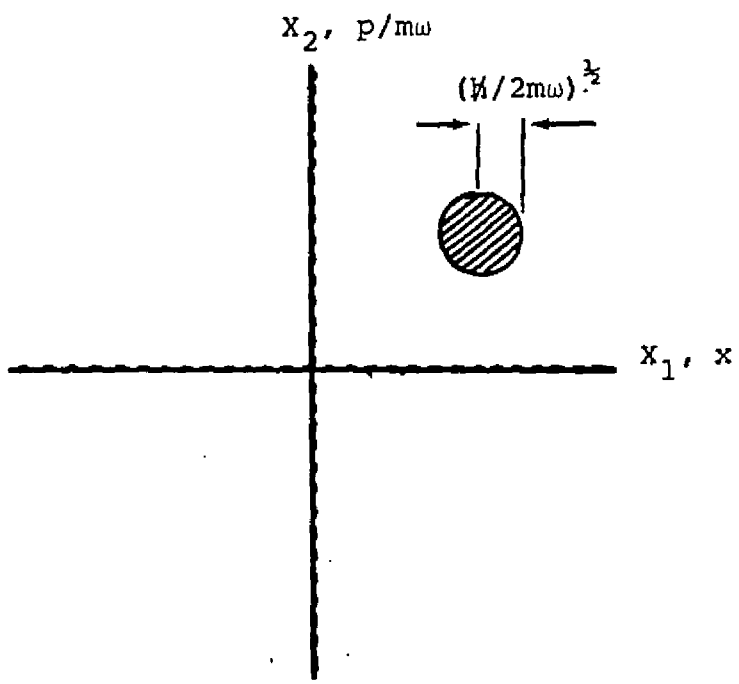

Figure 2.1 Error Circle for an Ideal Amplitude-and-Phase Measurement

$$X_1(t) = x(t)\cos\omega t - \frac{p(t)}{m\omega}\sin\omega t \qquad (2.5a)$$

$$X_2(t) = x(t)\sin\omega t + \frac{p(t)}{m\omega}\cos\omega t \qquad (2.5b)$$

and,

$$x + i\frac{p}{m\omega} = (X_1+iX_2)e^{-i\omega t} \qquad (2.6)$$

Classically, the amplitude of the oscillator motion is $A = \sqrt{(X_1^2+X_2^2)}$ and its phase given by $\tan\Phi = X_2/X_1$.

X_1 and X_2 obey an uncertainty principle derived from the fact that X_1 and X_2 obey the commutation relation $[X_1,X_2] = ih/m\omega$; thus

$$\Delta X_1 \cdot \Delta X_2 \geq \left(\frac{\hbar}{2m\omega}\right) \qquad (2.7)$$

The relationship between x and p and X_1 and X_2 can be seen in Figure 2.2.

At t=0, X_2 and p axes coincide and X_1 and x axes coincide. After a time t, the X_1-X_2 axes have rotated clockwise by an amount ωt; see (2.6). The significance of this is that the orientation of the X_1-X_2 plane is fixed with respect to the position of the state of the oscillator. That is, the complex amplitude is a constant of the motion for a free oscillator, or

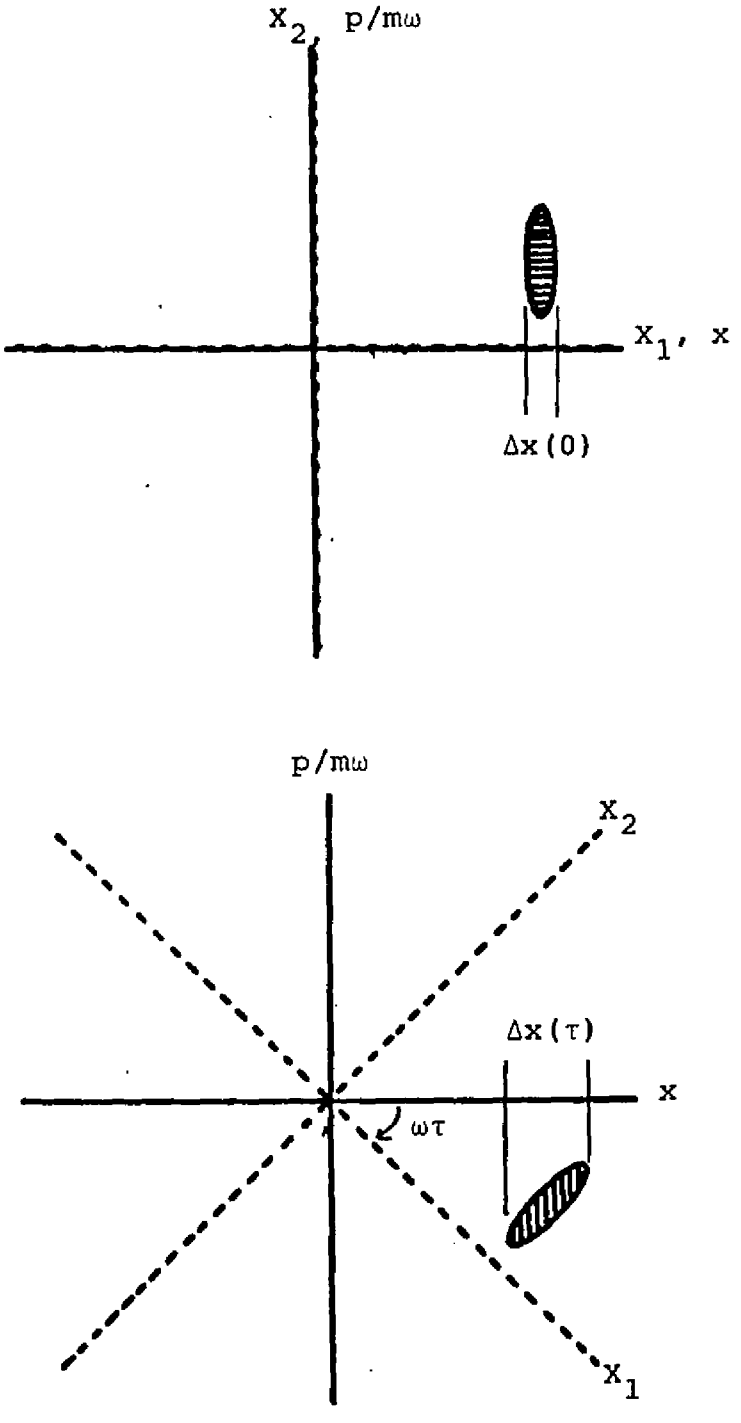

Figure 2.2 Relationship Between x, p and X_1, X_2, Highlighting Back-Action Effect of Δp on Δx During an AP Measurement

$$i\hbar \frac{d}{dt} (X_1+iX_2) = [X_1+iX_2,H_0] + i\hbar \frac{\partial}{\partial t} (X_1+iX_2) = 0 \qquad (2.8)$$

and

$$\frac{dX_1}{dt} = \frac{1}{i\hbar} [X_1,H_0] + \frac{\partial X_1}{\partial t} = 0 \qquad (2.9a)$$

$$\frac{dX_2}{dt} = \frac{1}{i\hbar} [X_2,H_0] + \frac{\partial X_2}{\partial t} = 0 \qquad (2.9b)$$

The minimum uncertainty in X_1 and X_2 for an AP measurement, from (2.7), is

$$\Delta X_1 = \Delta X_2 = (\frac{\hbar}{2m\omega})^{1/2} \qquad (2.10)$$

This is called the standard quantum limit (SQL) for AP measurements.[4]

Suppose now that a classical force, F(t), acts on the oscillator. The equations of motion (2.9) for X_1 and X_2 become

$$\frac{dX_1}{dt} = - \frac{F(t)}{m\omega} \sin \omega t \qquad (2.11a)$$

$$\frac{dX_2}{dt} = \frac{F(t)}{m\omega} \cos \omega t \qquad (2.11b)$$

The force, after a time τ, displaces the phase plane location of the center of the oscillator's uncertainty circle by the amount $\int_0^\tau \frac{F(t)}{m\omega} ie^{i\omega t}\, dt$, while leaving the circle unchanged. the SQL implies the best that an AP measurement can monitor the effects of a force on the complex amplitude of a harmonic oscillator is to within (approximately) the dimension of the uncertainty circle.

C. Phase Sensitive Measurements

We next consider the measurement of just one of the components of the complex amplitude, e.g. X_1. From (2.11a) we see that, in the absence of forces acting on the oscillator, X_1 is a constant of the motion. If a measurement of X_1 is made with a given accuracy, subsequent measurements of X_1 will continue to give this accuracy as the oscillator freely evolves. This is the property defining a quantum nondemolition (QND) measurement.[1,5,6] It can be understood quantum mechanically by considering a precise measurement of just x, which by (2.3) implies that p is given an unknown "kick". As the oscillator evolves, this unknown change in p is passed on to raise the uncertainty of the next measurement of x. This process of one variable's uncertainty affecting the uncertainty of its conjugate pair is

called "back-action; see Figure 2.2 for a phase plane picture highlighting this effect.

Measurements designed to avoid this back-action between conjugate pairs are called back-action evasion (BAE) measurements.[1,5,6] Consequently, a measurement of just X_1 (or X_2) is a BAE measurement. Measurements of X_1 are also called phase-sensitive (PS), as the phase of the oscillator is being "tracked" by the measurement process, so to speak. Throughout this paper we will use the term back-action evasion to refer to any measurement scheme whose net result is to improve on AP detection-imposed sensitivity limits, and phase-sensitive (PS) detection for any scheme measuring mainly X_1 or X_2.

Formally, BAE observables (e.g., X_1) $O(t)$ satisfy[6]

$$[O(t_i), O(t_j)] = 0 \tag{2.12}$$

We can apply this requirement to the position operator for a (free) harmonic oscillator; then

$$[x(t), x(t+\tau)] = \frac{i\hbar}{m\omega} \sin \omega\tau \tag{2.13}$$

This does not satisfy the formal requirement for BAE, as is expected (the momentum operator, however, does satisfy (2.12)). However, if the measurements are

made at times separated by half of the oscillator period, then $\sin \omega\tau = 0$ and (2.12) is satisfied. These types of measurements are called stroboscopic QND measurements.[7,8]

X_1 and X_2 do satisfy (2.12) for all times. A measurement sequence of X_1 can be made with arbitrary precision, with a concomitant loss of information about X_2. Integrating (2.11a) over a time interval τ gives

$$X_1(\tau) = X_1(0) - \int_0^\tau \frac{F(t)}{m\omega} \sin \omega t \, dt \tag{2.14}$$

If a measurement of X_1 at $t = 0$ leaves the oscillator in an eigenstate $|\sigma(0)>$ of X_1 with eigenvalue $\sigma(0)$, then a measurement of X_1 at time τ leaves the eigenstate unchanged, with an eigenvalue

$$\sigma(\tau,0) = \sigma(0) - \int_0^\tau \frac{F(t)}{m\omega} \sin \omega t \, dt \tag{2.15}$$

This points out the "nondemolition" aspect of QND, i.e. that the state vector, aside from its overall phase, remains unchanged even when a classical force is acting. (2.15) also provides the prescription for monitoring the force: record the time evolution of $\sigma(\tau,0)$ and from it derive $F(t)$ by

$$F(t) = - \frac{m\omega}{\sin \omega t} \left(\frac{d\sigma}{dt}\right) \tag{2.16}$$

Although $F(t)$ blows up when $\sin \omega t = 0$, this can be avoided by constructing a second oscillator and monitoring X_2, whereby $F(t) = (m\omega/\cos \omega t)(d\sigma/dt)$. In this way, complete knowledge can be had of the force with no uncertainty principle limitations on the sensitivity, although the uncertainty principle (2.7) is of course still valid.

D. Force Detection Sensitivity: Amplitude and Phase

We now consider force detection in more detail by including oscillator damping, characterized by an amplitude decay time τ_d or the quality factor $Q = \omega\tau_d/2$. We also assume $F(t)$ is of the form

$$F(t) = \begin{cases} F_0 \sin \Omega t & 0 < t < \tau \\ 0 & t > \tau \\ & t < 0 \end{cases} \qquad (2.17)$$

where F_0 is the force amplitude, Ω its angular frequency, and τ the duration time. We also assume that the force is a pulse, i.e. $\Omega\tau \simeq 1$, and that it is on resonance, i.e. $\Omega \simeq \omega$. We also have one more time interval to introduce, and that is the measurement time, τ_m.

We previously discussed the sensitivity limits to X_1 and X_2 when making an amplitude and phase measurement of any duration, i.e. $\delta X_1 = \sqrt{(h/2m\omega)}$. Because

of damping, however, the force detection sensitivity will depend on the measurement time, force duration, and on the amount the force is off-resonance.[9]

There are two conditions of interest: one in which $\tau < \tau_d$, and one in which $\tau > \tau_d$. For the former, a longer acting force means that more change will be produced in X_1. That is, the change in X_1 due to the force (2.17) acting for time $\tau < \tau_d$ is

$$\delta X_1 \cong - \left(\frac{F_0}{2m\omega}\right)\tau \qquad (2.18)$$

If we now require that $X_1 \geq \sqrt{(h/2m\omega)}$, then the minimum detectable force is

$$F_0(\min) \cong \left(\frac{2\hbar m\omega}{\tau^2}\right)^{1/2} \qquad \tau \leq \tau_m \leq \tau_d \qquad (2.19)$$

Increasing τ only improves sensitivity as long as $\tau < \tau_d$; when the force duration surpasses the decay time, the damping eliminates any improvement in sensitivity. Instead, we use a measurement time comparable to the force duration time, and divide the measurement time into a sequence of smaller "measurements" of length τ_d. Each of these "measurements" determines the force amplitude with an accuracy given by (2.19), with τ replaced by τ_d. There are τ/τ_d intervals in this sequence,

giving a minimum detectable force for the entire sequence of

$$F_0(\min) \cong \left(\frac{2\hbar m\omega}{\tau_d \tau}\right)^{1/2} \qquad \tau_m \cong \tau \gtrsim \tau_d \tag{2.20}$$

The resonant bar detector used by the LSU group is designed to detect burst forces with sensitivities satisfying (2.19), while the near-free mass laser interferometer detectors are best suited to detect continuous-wave forces with sensitivities limited by (2.20).

E. Force Detection Sensitivity: Back-Action Evasion

We have seen that a measurement of X_1 requires both a position and a momentum transducer. The difficulty is that a momentum transducer is not readily realizable in practice.[1] However, there is a way to improve on the SQL without using a momentum transducer, as fully explored by Caves in his Reviews of Modern Physics article.

Caves' idea is to couple to $x(t)\cos \omega t$; since

$$x(t)\cos \omega t = \frac{1}{2}\,(X_1 + X_1 \cos 2\omega t + X_2 \sin 2\omega t) \tag{2.21}$$

then low pass filtering a signal of this form would predominantly extract information on X_1. Likewise,

this signal could be upconverted to any appropriate frequency, and the X_1 information extracted via bandpass filtering. Because this scheme does not involve p(t) in any way, it is referred to as a single-transducer, back-action evading measurement scheme.

The sensitivity limit for a measurement of X_1 is[9,10,11]

$$\Delta X_1 \geq \left(\frac{\hbar}{2m\omega}\right)^{1/2} \left(\frac{\Delta\Omega_0}{\omega}\right)^{1/2} \tag{2.22}$$

where $\Delta\Omega_0$ is the bandwidth of the bandpass filter used to process the signal in obtaining X_1 (this will be derived in the next chapter). This limit imposes, for a force detection measurement, the extra constraint that $\Delta\Omega_0 < \omega$, necessitating a measurement bandwidth $(1/\tau)$ that is no larger than $\Delta\Omega_0$.

Since $\Delta\Omega_0/\omega$ can be much less than one, ΔX_1 can be small enough such that the effect of fluctuations introduced by contact with a zero-temperature heat reservoir (for simplicity, we will ignore finite temperature effects) must be considered. In a time t these fluctuations introduce an uncertainty in X_1 equal to[9] (see Appendix 2)

$$\delta X_1 \geq \left(\frac{\hbar}{2m\omega}\right)^{1/2} \left(1 - e^{-2t/\tau_d}\right)^{1/2} \tag{2.23}$$

Substituting $t = \tau_d(\Delta\Omega_0/\omega)$ in (2.23) we observe that $\delta X_1(\text{fluct.}) \approx \delta X_1(\text{BAE})$. Thus an upper limit on the measurement time is set by when these fluctuations become significant. So we first look at force durations of less than, and then greater than, this time interval, as we did in the previous section.

For $\tau < \tau_d(\Delta\Omega_0/\omega)$, the minimum detectable force is (with the proviso that the measurement time satisfy bandwidth requirements)

$$F_0(\text{min}) \approx \left(\frac{2\hbar m\omega}{\tau^2}\right)^{1/2} \left(\frac{\Delta\Omega_0}{\omega}\right)^{1/2} \qquad \tau < \tau_m \leq \tau_d \left(\frac{\Delta\Omega_0}{\omega}\right) \qquad (2.24)$$

Thus this back-action evasion measuring scheme improves on the standard amplitude and phase technique by a factor $\sqrt{(\Delta\Omega_0/\omega)}$.

For $\tau > \tau_d(\Delta\Omega_0/\omega)$, the measurement is again divided into intervals of duration $\tau_d(\Delta\Omega_0/\omega)$. The minimum detectable force for the entire sequence is then

$$F_0(\text{mm}) \approx \left(\frac{2\hbar m\omega}{\tau_d\tau}\right)^{1/2} \qquad \tau_m = \tau \geq \tau_d \left(\frac{\Delta\Omega_0}{\omega}\right) \qquad (2.25)$$

Of particular interest here is that, for $\tau > \tau_d$, the standard quantum limit for force detection is not improved on. This is because the zero point fluctuations keep the uncertainty of X_1 from going below the SQL.

We can also extend this analysis to determine how well BAE technique can do in principle. Although we would like to make $\Delta\Omega_0$ as small as possible, it can't be made so small that τ_m is larger than $\tau_d(\Delta\Omega_0/\omega)$, or that $1/\Omega_0 \simeq \tau_d(\Delta\Omega_0/\omega)$ or $\sqrt{(\Delta\Omega_0/\omega)} = Q^{-1/4}$. Thus, the best improvement offered by a single transducer, BAE measurement over the standard quantum limit is a factor of $Q^{1/4}$.

Up to now we have not looked at any specific experimental setup; however, we have already established some parameters that must be met. We later introduce the LSU accelerometer; its diaphragm/reentrant cavity arrangement already contains, built-in, the mechanical oscillator, bandpass filter, and upconverting capability. We shall also see that, with the appropriate input signal, it is possible to experimentally establish a single-transducer, back-action evading coupling to X_1 of the oscillator.

F. Fundamental Noise Limit of Linear Amplifiers

We have seen the role played by uncertainty relations in establishing the character of two different measurement strategies. The uncertainty principle also plays a key role in determining the minimum noise introduced by an amplifier. We now discuss the oft-cited article by Heffner[12] and Cave's subsequent amendments.[13,14]

The basis of Heffner's arguments rests on the uncertainty relation between number and phase

$$\Delta n \; \Delta\phi \geq \frac{1}{2} \tag{2.26}$$

where n is the number of quanta in the oscillator and ϕ the oscillator phase. The conclusion to be tested from this relationship is that it is impossible to construct a noiseless linear amplifier. We prove the statement by assuming a noiseless linear amplifier, and then showing that such a device would then violate (2.26).

First suppose that there exists a noiseless linear amplifier, linear meaning that, during any given time interval, the number of output photons n_2 is related to the number of input photons n_1 by G, the gain of the amplifier, visa vis

$$n_2 = G \cdot n_1 \tag{2.27}$$

and that the amplifier is phase preserving so that the output phase Φ_2 is equivalent to the input phase Φ_1 to within additive phase shift θ

$$\phi_2 = \phi_1 + \theta \tag{2.28}$$

Now assume that this ideal amplifier is connected to an ideal detector, i.e. one that can detect the number of output photons n_2 and the output ϕ_2 to within a minimum uncertainty

$$\Delta n_2 \cdot \Delta \phi_2 = \frac{1}{2} \tag{2.29}$$

Equations (2.27) and (2.28) imply that the uncertainty in the measurement of the input photons and phase is

$$\Delta n_1 \cdot \Delta \phi_1 = \frac{1}{2G} \tag{2.30}$$

However, (2.30) violates the uncertainty principle first cited. Hence a noiseless linear amplifier cannot exist, and thus must add noise.

Heffner then assumes that the input to the amplifier is noiseless, and that the amplifier has a bandwidth B. He requires that the amplifier and the detector be matched, necessitating measurement times of $\tau = 1/2B$. The additive noise is assumed to be white noise. The added noise number A characterizes the noise added to each quadrature (X_1 and X_2) and is determined by the uncertainty principle (2.26) to be[13]

$$A \geq \frac{1}{2} \left(1 - \frac{1}{G}\right) \tag{2.31}$$

A gives the added noise in units of number of quanta, referred to the amplifier input. For a high-gain amplifier, where G >> 1, the minimum added noise is 1/2 quantum.

This noise number can be expressed as a noise temperature

$$T_n \geq \left[\ln \frac{(2 - \frac{1}{G})}{(1 - \frac{1}{G})} \right]^{-1} \frac{\hbar\Omega}{k_B} \qquad (2.32)$$

For G >> 1, this gives the now famous minimum linear amplifier temperature[12] $T_n(\min) = \hbar\Omega/k_B \ln 2$.

Caves' work,[13,14] based on that of Haus and Mullen,[15] is a quantum mechanical one that includes unitary conditions (not included in Heffner) along with the uncertainty relation. Their work discusses why an amplifier adds noise. Essentially, a high gain linear amplifier must have one or more internal modes whose interaction with the input signal produces the amplified output. The internal modes must have at least the quantum mechanical zero-point fluctuations, and these fluctuations are amplified along with the input signal to produce noise at the output. Since the amplified internal mode fluctuations are uncorrelated, they add in quadrature to produce the total output noise.

We discuss in Chapter 4 just how the noise added by an amplifier can feed back, channeled by the transducer, to affect the mechanical oscillator. We refer to the AP sensitivity limits imposed by this amplifier noise back reaction as the "standard amplifier limit" (SAL).[6] The SAL and SQL are comparable for an ideal, minimum noise, linear amplifier.

References

1. C. M. Caves, K. S. Thorne, R. W. P. Drever, V. D. Sandberg, and M. Zimmerman, Reviews of Modern Physics 52, 341 (1980).

2. R. J. Glauber, Phys. Rev. 131, 2766 (1963), Phys. Rev. 130, 2529 (1963), Phys. Rev. Letts. 10, 84 (1963); D. Stoler, Phys. Rev. D1, 3217 (1970), Phys. Rev. D4, 1925 (1971), and Phys. Rev. D4, 2309 (1971).

3. P. Carruthers, and M. M. Nieto, Am. J. Phys. 33, 537 (1965).

4. K. S. Thorne, C. M. Caves, V. D. Sandberg, and M. Zimmerman, in Sources of Gravitational Radiation, L. Smarr, ed., (Cambridge University Press, New York, 1979).

5. W. G. Unruh, Phys. Rev. D19, 2888 (1979).

6. V. B. Braginsky, Y. I. Vorontsov, Science 209, 547 (1980).

7. V. B. Braginsky, Y. I. Vorontsov, and F. Y. Khalili, JETP Letters 27, 276 (1978).

8. K. S. Thorne, R. W. P. Drever, C. M. Caves, M. Zimmerman, and V. D. Sandberg, Phys. Rev. Letts. 40, 667 (1978).

9. C. M. Caves, Proc. Int. Symp. Foundations of Quantum Mechanics, Tokyo, p. 195 (1983).

10. W. W. Johnson, and M. Bocko, Phys. Rev. Letts. 47, 1184 (1981).

11. M. F. Bocko, and W. W. Johnson, Phys. Rev. Letts. 48, 1371 (1982).

12. H. Heffner, Proc. IRE, 50, 1604 (1962).

13. C. M. Caves, in Quantum Optics, Experimental Gravitation, and Measurement Theory.

14. C. M. Caves, Phys. Rev. D26, 1817 (1982).

15. H. A. Haus, and J. A. Mullen, Phys. Rev. 128, 2407 (1962).

CHAPTER 3

THEORETICAL CONSIDERATIONS OF, AND APPLICATIONS TO, THE LSU ACCELEROMETER

A. Introduction

We turn now to a classical analysis of the equivalent circuit model of the LSU accelerometer reentrant cavity/diaphragm system. We establish AP and PS cavity input signal requirements. We also provide the connection between PS measurements and back-action evasion (BAE) of amplifier force noise and introduce the squeezing factor Σ. We conclude with a semiclassical analysis of the time evolution of X_1 and X_2 during AP and BAE couplings to the oscillator for the back reaction forces specific to our system.

B. Equivalent Circuit Model

The LSU accelerometer used as the back-action evading test device can be represented as a parallel RLC circuit (Figure 3.1) with a harmonically varying capacitor, driven by a constant current source,[1] as can any capacitance-modulated resonator. The capacitor plate separation is given by $x(t) = x_0 \cos(\omega t+\Phi)$, with a capacitance of $C(t) = C_0(1+\alpha \cos(\omega t+\Phi))$, where

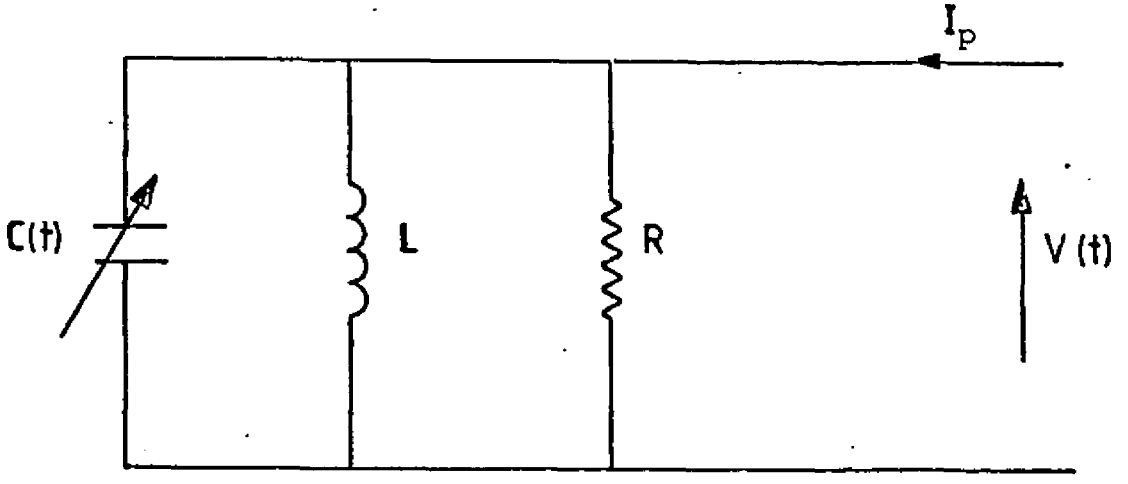

Figure 3.1 Equivalent Circuit Model for LSU Accelerometer

$\alpha = -x_0/d_0 << 1$ (actually, less than $\approx 10^{-10}$) with d_0 being the equilibrium plate spacing and representing the reentrant cavity gap. The time varying capacitor modulates the voltage across it. We choose a general form of the input current

$$I_p = i_{0c} \cos \Omega_0 t + i_{0s} \sin \Omega_0 t + i_{+c} \cos \Omega_+ t + i_{+s} \sin \Omega_+ t$$
$$+ i_{-c} \cos \Omega_- t + i_{-s} \sin \Omega_- t + i_{2+c} \cos \Omega_{2+} t$$
$$+ i_{2+s} \sin \Omega_{2+} t + i_{2-c} \cos \Omega_{2-} t + i_{2-s} \sin \Omega_{2-} t \qquad (3.1)$$

where Ω_0 is the circuit (cavity) resonant frequency at $x = 0$ and $\Omega_{n\pm} \equiv \Omega \pm n\omega$. Typically, ω is several orders of magnitude less than Ω_0.

Since the modulation factor α is so small and the $i_{2\pm}$ currents much smaller than the others, the third harmonic and higher sidebands are negligible. Thus the output voltage is assigned the form

$$V(t) = V_p \{c_0 \cos \Omega_0 t + s_0 \sin \Omega_0 t + s_+ \sin \Omega_+ t$$

$$+ s_- \sin \Omega_- t + c_+ \cos \Omega_+ t + c_- \cos \Omega_- t$$

$$+ s_{2+} \sin \Omega_{2+} t + s_{2-} \sin \Omega_{2-} t$$

$$+ c_{2+} \cos \Omega_{2+} t + c_{2-} \cos \Omega_{2-} t\} \qquad (3.2)$$

We next define

$$T \equiv 2Q_e \omega/\Omega_0 = 2\omega/(\Delta\Omega_0) \qquad (3.3)$$

where Q_e is the quality factor of the circuit (i.e. the cavity) and $\Delta\Omega_0$ the bandwidth of the resonance. This factor plays an important role in the succeeding discussions concerning phase-sensitive detection and back-action evasion.

Solving the current conservation equation, $I_p = i_c + i_l + i_r$, we obtain the output voltage coefficients as shown in Appendix 1.

We now have the tools to determine the output signal for any input currents describable by the form of (3.1). With this information, we can now explore the necessary requirements for phase-sensitive detection and the back-action evasion of amplifier noise.

C. Detected Cavity Output

The cavity output is typically at a low power level ($\leq$ -50 dBm, where 0 dBm = 1mW), so it is amplified before being demodulated by a doubly balanced mixer (DBM) (see Chapter 5). The phase of the local oscillator (LO) signal to the mixer is adjustable by a line stretcher. For the output of (3.2) and a given LO phase (which we will call the BAE phase), the detected (test cavity) output contains components at DC, ω, and 2ω:

DC component (BAE) phase of detected output:

$$V_{DC} = \frac{RQ_e}{4(1+T^2)d_0}\{\frac{2d_0(1+T^2)i_{0s}}{Q_e} + (-Ti_{+s} + i_{+c} + Ti_{-s} + i_{-c})X_1$$

$$+ (i_{+s} + Ti_{+c} - i_{-s} + Ti_{-c}))X_2\} \qquad (3.4a)$$

ω-component (BAE phase):

$$V_\omega = \frac{RQ_e}{2(1+T^2)d_0}\{[\frac{d_0}{Q_e}(Ti_{-s} + i_{-c} + Ti_{+s} - i_{+c})$$

$$- i_{0c}TX_1 - i_{0c}X_2]\sin\omega t$$

$$+ [\frac{d_0}{Q_e}(i_{+s} + Ti_{+c} + i_{-s} - Ti_{-c}) - i_{0c}X_1 + i_{0c}TX_2]\cos\omega t\}$$

(3.5a)

2ω-component (BAE phase):

$$V_{2\omega} = \frac{RQ_e}{4(1+T^2)(1+4T^2)d_0}\{[\frac{2(1+T^2)d_0}{Q_e}(2Ti_{2-s} + i_{2-c} + 2Ti_{2+s} - i_{2+c})$$

$$+ (3Ti_{-3} + (1-2T^2)i_{-c} - 3Ti_{+s} + (1-2T^2)i_{+c})X_2$$

$$+ (-(1-2T^2)i_{-s} + 3Ti_{-c} + (1-2T^2)i_{+s}$$

$$+ (3Ti_{-s} + (1-2T^2)i_{-c} - 3Ti_{+s} + (1-2T^2)i_{+c})X_2$$

$$+ (-(1-2T^2)i_{-s} + 3Ti_{-c} + (1-2T^2)i_{+s} + 3Ti_{+c})X_1]\sin 2\omega t$$

$$+ [\frac{2(1+T^2)d_0}{Q_e}(i_{2+s} + 2Ti_{2+c} + i_{2-s} - 2Ti_{2-c})$$

$$+ (-3Ti_{+s} + (1-2T^2)i_{+c} + 3Ti_{-s} + (1-2T^2)i_{-c})X_1$$

$$+ (-(1-2T^2)i_{+s} - 3Ti_{+c} + (1-2T^2)i_{-s} - 3Ti_{-c})X_2]\cos 2\omega t\} \qquad (3.6a)$$

Changing the LO phase so that it is in quadrature to the BAE phase gives the following detected (test cavity) output:

DC component (quad phase) of detected output:

$$V_{DC} \cong \frac{RQ_e}{4(1+T^2)d_0} \{ \frac{2(1+T^2)d_0\, i_{0c}}{Q_e} + (-i_{+s} - Ti_{+c} - i_{-s} + Ti_{-c})X_1 + (-Ti_{+s} + i_{+c} - Ti_{-s} - i_{-c})X_2 \} \quad (3.4b)$$

ω-component (quad phase):

$$V_\omega \cong \frac{RQ_e}{2(1+T^2)d_0} \{ [\frac{d_0}{Q_e} (i_{+s} + Ti_{+c} - i_{-s} + Ti_{-c}) - Ti_{0s} X_1 - i_{0s} X_2] \sin \omega t + [\frac{d_0}{Q_e} (Ti_{-s} + i_{-c} - Ti_{+s} + i_{+c}) - i_{0s} X_1 + i_{0s} TX_2] \cos \omega t \} \quad (3.5b)$$

2ω-component (quad phase):

$$V_{2\omega} \cong \frac{RQ_e}{4(1+T^2)(1+4T^2)d_0} \{[\frac{2(1+T^2)d_0}{Q_e}(i_{2+s} + 2Ti_{2+c} - i_{2-s} + 2Ti_{2-c})$$

$$+ (-3Ti_{+s} + (1-2T^2)i_{+c} - 3Ti_{-s} - (1-2T^2)i_{-c})X_1$$

$$+ (-(1-2T^2)i_{+s} - 3Ti_{+c} - (1-2T^2)i_{-s} + 3Ti_{-c})X_2] \sin 2\omega t$$

$$+ [\frac{2(1+T^2)d_0}{Q_e}(-2Ti_{2+s} + i_{2+c} + 2Ti_{2-s} + i_{2-c}) + (-(1-2T^2)i_{+s}$$

$$-3Ti_{+c} - (1-2T^2)i_{-s} + 3Ti_{-c})X_1 + (3Ti_{+s} - (1-2T^2)i_{+c}$$

$$+ 3Ti_{-s} - (1-2T^2)i_{-c})X_2] \cos 2\omega t\} \qquad (3.6b)$$

D. Amplitude and Phase Measurements of Diaphragm

The standard use of the LSU accelerometer, and all other transducers, for that matter, is to make AP measurements. In the LSU case, this is done with an input current with a single component at Ω_0.[2] The cavity modulation creates output voltage sidebands at $\Omega_\pm$, whose amplitudes are proportional to α (and consequently are very small compared to the pump signal) and contain information on x, or, equivalently, X_1 and X_2. This can be seen by examining (3.5a) for an input current of the form $I_p = i_{0c} \cos \Omega_0 t$:

$$V_\omega \alpha (TX_1 + X_2) \sin \omega t + (X_1 - TX_2) \cos \omega t \qquad (3.7)$$

An AP measurement would then necessarily consist of monitoring either (or both) of the modulation sidebands. As mentioned in Chapter 2, even the best detection system will introduce noise to the oscillator via amplifier back reaction. This noise can be represented by $i_{\pm s,c}$ (see (3.5a)), depending on what sideband is being monitored, and adds noise to each of the terms in (3.7).

E. Phase Sensitive Measurements of Diaphragm

Consider now an input current of the form $I_p = i_{+c} \cos \Omega_+ t + i_{-c} \cos \Omega_- t = 2I \cos \omega t \cos \Omega_0 t$ if $i_{+c} = i_{-c} \equiv I$. We can use (3.4a) to determine that the DC component of the detected test cavity output (BAE phase) is

$$V_{DC} \propto \frac{X_1}{T} + X_2 \tag{3.8}$$

This input current establishes a classical coupling scheme which is sensitive to predominantly one of the two oscillator coordinates, in this case X_2. It is more sensitive to X_2 by a factor T; only in the limit that the filter bandwidth approaches zero does the coupling scheme give exact coupling to one coordinate. We have assumed no noise sources, and that the "two-stick" or dual-sideband input (so called because of its appearance in the frequence domain) be symmetric about Ω_0. In a later section on amplifier noise back-action evasion we will look at the effect of pump signal imperfections.

To represent the phases of the individual sticks we can rewrite the $\Omega_\pm$ components of the general input current

$$I_p = (i_+ \cos \phi_+) \cos \Omega_+ t - (i_+ \sin \phi_+) \sin \Omega_+ t$$

$$+ (i_- \cos \phi_-) \cos \Omega_- t - (i_- \sin \phi_-) \sin \Omega_- t \qquad (3.9)$$

where ϕ_+ and ϕ_- refer to the phases, and i_+ and i_- the amplitudes, of the upper and lower sidebands, respectively. The ϕ's and i's can be varied through the front panel controls of the two synthesizers used to generate the independent sidebands.

We use the same cavity detection scheme as before except that the source of the LO input is different (see Chapter 5). The detected DC output (BAE phase) of the IF (intermediate frequency) port of the DBM is then

$$V_{DC} \cong \frac{RQ_e}{4(1+T^2)d_0} \{(Ti_+ \sin \phi_+ + i_+ \cos \phi_+ - Ti_- \sin \phi_-$$

$$+ i_- \cos \phi_-) (x_0 \cos \Phi)$$

$$+ (-i_+ \sin \phi_+ + Ti_+ \cos \phi_+ + i_- \sin \phi_-$$

$$+ Ti_- \cos \phi_-) (-x_0 \sin \Phi)\} \qquad (3.10)$$

where $X_1 = x_0 \cos \phi$ and $X_2 = -x_0 \sin \phi$.

It is important to be able to establish the phase relationship between the synthesizers. There are three phase "degrees of freedom" in this experiment: the LO phase adjustment and the $\phi_{+,-}$ settings. To help establish these phases, and to later verify a PS coupling scheme, we look at the predicted ω-component of the test cavity detected output for, first, the LO BAE phase setting:

$$V_\omega \approx \frac{RQ_e}{2(1+T^2)d_0} \{[\frac{d_0}{Q_e} \ (-Ti_+ \sin \phi_+ - i_+ \cos \phi_+$$

$$- Ti_- \sin \phi_- + i_- \cos \phi_-) + i_{0c} TX_1 + i_{0c} X_2] \sin \omega t$$

$$+ [\frac{2d_0}{Q_e} (-i_+ \sin \phi_+ + Ti_+ \cos \phi_+ - i_- \sin \phi_- - Ti_- \cos \phi_-)$$

$$+ i_{0c} X_1 - i_{0c} TX_2] \cos \omega t\}$$

(3.11a)

and, second, for the quad LO phase:

$$V_\omega \cong \frac{RQ_e}{2(1+T^2)d_0} \{[\frac{d_0}{Q_e}(-i_+ \sin\phi_+ + Ti_+ \cos\phi_+$$

$$+ i_- \sin\phi_- + Ti_- \cos\phi_-) - i_{0s} TX_1 - i_{0s}X_2] \sin\omega t$$

$$+ [\frac{d_0}{Q_e}(-Ti_- \sin\phi_- + i_- \cos\phi_- + Ti_+ \sin\phi_+ + i_+ \cos\phi_+)$$

$$- i_{0s} X_1 + i_{0s} TX_2] \cos\omega t\} \qquad (3.11b)$$

We will apply this analysis in Chapter 7 when examining experimental results for independent sideband input currents.

F. Back Reaction Forces: AP Versus BAE

We have just determined the output voltage for the accelerometer equivalent circuit for a general input current. This voltage gives rise to a rf time-averaged force on the oscillator given by[1]

$$\overline{F(t)}^{rf} = \frac{d}{dx}\left(\overline{\left(\tfrac{1}{2} CV^2\right)}^{rf}\right)\Big|_{x_0 = 0} \qquad (3.12)$$

The force components effecting the diaphragm are those at frequency ω; thus pairs of currents separated in frequency by ω will contribute to the back-action forces. We earlier saw the input currents required for AP and PS measurement schemes, and now examine the back-action forces associated with these currents.

We have established that an AP coupling (with noise at Ω_+) to the oscillator can be achieved by the following input current:

$$I_p = i_{0c} \cos \Omega_0 t + i_{+c} \cos \Omega_+ t + i_{+s} \sin \Omega_+ t \qquad (3.13)$$

If we let $\sqrt{(i_{+c})^2} = \sqrt{(i_{+s})^2} \equiv i_a$, then the back-action force associated with this current is

$$F_{ba}(AP) = \frac{C_0 R^2 i_{0c} i_a}{2(1+T^2)^{1/2} d_0} [\cos \omega t + \sin \omega t] \qquad (3.14)$$

In contrast, the following PS coupling (with noise at Ω_0)

$$I_p = I(\cos \Omega_+ t + \cos \Omega_- t) + i_a(\cos \Omega_0 t + \sin \Omega_0 t) \quad (3.15)$$

gives a back-action force of

$$F_{ba}(\text{BAE}) = \frac{C_0 R^2 I i_a}{2d_0(1+T^2)} [\cos \omega t + T \sin \omega t] \quad (3.16)$$

Equation (3.14) shows that the back-action diaphragm force has equal components in the two phases (sin ωt and cos ωt), while (3.16) reveals that one of the phase components is a factor T larger than the other. We know that the PS current (3.15) couples predominantly to X_2. Thus (3.16) indicates that, for $T > 1$:

a. the amplifier noise back reaction is preferentially injected into one oscillator coordinate (X_1), (since F_{ba} is in quadrature to $x(t) = X_1 \cos \omega t + X_2 \sin \omega t$), and

b. the noise is predominantly injected into the coordinate to which the measurement is least sensitive (X_1).

This shunting of back-action force noise into the least coupled coordinate is called "back-action evasion" (BAE); it is also called classical "squeezing".[3]

We saw in Chapter 2 that an AP measurement gives rise to a minimum uncertainty circle with $\Delta X_1(AP) = \Delta X_2(AP) = \sqrt{(h/2m\omega)}$. A BAE measurement gives rise to an uncertainty ellipse having approximately the same area as the AP circle (the AP circle is "squeezed" by the BAE measurement). Equation (3.16) indicates that (for a BAE measurement)

$$\frac{\Delta X_1(BAE)}{\Delta X_2(BAE)} = T \tag{3.17}$$

Since $\Delta X_1(BAE)\cdot\Delta X_2(BAE) = [\Delta X_1(BAE)/\Delta X_2(BAE)]\cdot(\Delta X_2(BAE))^2 \approx \Delta X_1(AP)\cdot\Delta X_2(AP)$, then $T(\Delta X_2(BAE))^2 \approx (\Delta X_2(AP))^2$ and

$$\Delta X_2(BAE) = \frac{\Delta X_2(AP)}{T^{1/2}} \geq \left(\frac{\hbar}{2m\omega}\right)^{1/2} \left(\frac{\Delta\Omega_0}{2\omega}\right)^{1/2} \tag{3.18a}$$

$$\Delta X_1(BAE) = \Delta X_2(AP)\cdot T^{1/2} \geq \left(\frac{\hbar}{2m\omega}\right)^{1/2} \left(\frac{2\omega}{\Delta\Omega_0}\right)^{1/2} \tag{3.18b}$$

We introduce a squeezing factor Σ, defined by

$$\Sigma \equiv \frac{\Delta X_1}{\Delta X_2} \tag{3.19}$$

The term "squeezing" was first used by Hollenhorst[1] to refer to circumvention of the SQL. We will use the term to also denote circumvention of the SAL.

We find that, for the current of (3.15), $\Sigma = T = 2\omega/\Delta\Omega_0$. This result is in basic agreement with the different treatments of Braginsky,[4] Caves,[5] and Bocko and Johnson.[6]

G. Time Evolution of X_1 and X_2 Under Classical AP, BAE Back-Action Forces

Although we have just examined the classical analogue of squeezing and back-action evasion, it is illuminating to consider the semi-classical treatment of the same problem (classical force, quantum mechanical description).[7] We will deal specifically with the equations of motion of X_1 and X_2 (it should be noted that in this section X_1 and X_2 are operators).

Consider the AP back-action force on the diaphragm given by (3.15). Since the Heisenberg equation of motion for the complex amplitude is

$$\frac{d}{dt}(X_1 + iX_2) = \frac{F(t)}{m\omega}(-\sin\omega t + i\cos\omega t) \tag{3.20}$$

then the equations of motion for X_1 and X_2, due to this back-action force, are

$$\left.\frac{dX_1}{dt}\right|_{ba} = -\frac{C_0 R^2 i_{0c} i_a}{4d_0 m\omega(1+T^2)^{1/2}} [1 - \cos 2\omega t + \sin 2\omega t] \quad (3.21a)$$

$$\left.\frac{dX_2}{dt}\right|_{ba} = \frac{C_0 R^2 i_{0c} i_a}{4d_0 m\omega(1+T^2)^{1/2}} [1 + \cos 2\omega t + \sin 2\omega t] \quad (3.21b)$$

If the $2\omega t$-terms are averaged to zero, the magnitudes of the rate of change of X_1 and X_2 are equal, indicating that they are each equally disturbed by the back-action forces.

Continuing the semiclassical analysis[7] of the system equations reveals that one can detect changes with uncertainty given by

$$(\Delta\bar{X}_1)^2 = (\Delta\bar{X}_2)^2 \simeq \frac{k_B T_n}{m\omega^2}\left(\frac{\omega\tau}{Q}\right) + A\left(\frac{\hbar}{2m\omega}\right)\left(\frac{1}{\beta\omega\tau} + \beta\omega\tau\right) \quad (3.22)$$

where $k_B T_n >> h\omega$ and $\omega\tau/Q << 1$, and where β is the electromechanical energy transfer coefficient (see Chapter 4), given by

$$\beta = \frac{\pi^2 \Omega_0 C_0}{16 m\omega^3} \left(\frac{V_p}{d_0}\right)^2 \qquad (3.23)$$

The first term in (3.22) is due to thermal fluctuations in the mechanical oscillator, and the second term is the contribution of the amplifier noise, which itself consists of two terms. The first amplifier noise term is due to the additive (forward) amplifier noise and the second is due to the amplifier back reaction. The thermal and back reaction contributions are proportional to τ as each is due to a random force acting on the oscillator; the additive noise is proportional to $1/\tau$ because of the bandwidth of the measurement associated with the measurement time τ (bandwidth $\approx 1/\tau$). A is called the added noise number, related to T_n by

$$A = (e^{\hbar\Omega/k_B T_n} - 1)^{-1} \qquad (3.24)$$

where Ω is the operating frequency of the amplifier.

If the thermal noise term is negligible then $(k_B T_n/h\omega Q) << \beta A$, and if the measurement time is chosen to be equal to $1/\beta\omega$, then we obtain

$$\Delta X_1(\text{min}) = \Delta X_2(\text{min}) = \left(\frac{A\hbar}{m\omega}\right)^{1/2} \geq \left(\frac{\hbar}{2m\omega}\right)^{1/2} \qquad (3.25)$$

where the last inequality follows from the quantum mechanical limit on the performance on any high-gain amplifier, i.e. $A \geq 1/2$.[8,9]

We next consider the results for a BAE coupling to the mechanical oscillator, with the back-action force on the oscillator given by (3.16). The equations of motion become

$$\left.\frac{dX_1}{dt}\right|_{ba} = -\frac{C_0 R^2 I i_a}{4d_0 m\omega(1+T^2)} [T - T \cos 2\omega t + \sin 2\omega t] \quad (3.26a)$$

$$\left.\frac{dX_2}{dt}\right|_{ba} = \frac{C_0 R^2 I i_a}{4d_0 m\omega(1+T^2)} [1 + \cos 2\omega t + T \sin 2\omega t] \quad (3.26b)$$

The $2\omega t$-terms average away, leaving X_1 disturbed more strongly (by a factor of T) than X_2. Semiclassical analysis further reveals[7,10] that, if thermal fluctuations are neglected, the limit to the uncertainty in X_2 is

$$\Delta X_2 \cong \left(\frac{A\hbar}{m\omega}\right)^{1/2} \left(\frac{1}{\beta\omega\tau}\right)^{1/2} \geq \left(\frac{\hbar}{2m\omega}\right)^{1/2} \left(\frac{1}{\beta\omega\tau}\right)^{1/2} \quad (3.27)$$

However, because the oscillator is not exactly coupled to X_2, X_1 information "leaks" through to disturb

X_2 and thereby prevent the uncertainty in X_2 from being reduced arbitrarily by increasing τ. When $\tau \geq \tau_d/\beta$, the uncertainty in X_2 reaches a lower bound of

$$\Delta X_2 \equiv \left(\frac{\hbar}{2m\omega}\right)^{1/2} \left(\frac{1}{\omega\tau_d}\right)^{1/2} \tag{3.28}$$

References

1. R. Giffard, and H. J. Paik, Stanford University Report, unpublished, (June, 1977); D. Darling, Experimental Relativity Group Technical Memorandum, (1978).

2. W. C. Oelfke, and W. O. Hamilton, Acta. Astron. 5, 87 (1978).

3. J. N. Hollenhorst, Phys. Rev. D19, 1669 (1979).

4. V. B. Braginsky, in Gravitational Radiation, N. Deruelle and T. Piran, eds., (North Holland, New York, 1983).

5. C. M. Caves, Proc. Int. Symp. Foundations of Quantum Mechanics, Tokyo, p. 195 (1983).

6. M. F. Bocko, and W. W. Johnson, Phys. Rev. Letts. 48, 1371 (1982).

7. C. M. Caves, in Quantum Optics, Experimental Gravitation, and Measurement Theory, P. Meystre, and M. O. Scully, eds., (Plenum Press, New York, 1983).

8. H. Heffner, Proc. IRE 50, (1962).

9. C. M. Caves, Phys. Rev. D26, 1817 (1982).

10. C. M. Caves, et al., Reviews of Modern Physics 52, 341 (1980).

CHAPTER 4

BACK-ACTION EVASION AND RESONANT-BAR GRAVITATIONAL WAVE DETECTORS

A. Introduction

Gravitational radiation detection research was responsible for the development of PS measurements and BAE. In this chapter we apply the concept of squeezing to the business of detecting gravity waves, that is, to transducers monitoring gravity wave resonant bar antennae and to the LSU transducer in particular. We compare the energy detection sensitivity offered by AP transducer couplings to BAE couplings; these comparisons are made as functions of the amplifier noise temperature, antenna physical temperature, antenna quality factor, squeezing factor, and operating mode of the transducer.

B. Electromechanical Model of Transducer-Antenna System

The LSU accelerometer was designed to be used as a displacement sensor for the LSU gravitational radiation resonant bar antenna.[1] The antenna is an aluminum cylinder 2500 kg in mass and 3 m in length. At 4.2° K, its fundamental longitudinal mode is at ≈ 900 Hz with a quality

factor Q_a of 10-50 million. See Table 4.1 for antenna and transducer parameters. Attached to the cylinder face, the accelerometer acts as a transducer converting antenna mechanical motion to a processable electrical signal. The properties of the transducer and its coupling of amplifier and antenna can be described by the following electromechanical two-port model[2]:

$$F(t) = Z_{11}*u(t) + Z_{12}*I(t)$$

$$V(t) = Z_{21}*u(t) + Z_{22}*I(t) \qquad (4.1)$$

where F(t) and u(t) are the (mechanical) input force and velocity and V(t) and I(t) are the (electrical) output voltage and current.

The elements Z_{11} and Z_{22} represent the mechanical input and electrical output impedances, respectively. Z_{21}, the forward transconductance, represents the displacement sensitivity of the system (given by $Z_{21}*\omega_a$, with ω_a the antenna fundamental mode frequency). A forward energy coupling coefficient β_{21}, can be defined[3]

$$\beta_{21} \equiv \frac{|Z_{21}|^2}{M\ \omega_a |Z_{22}|} \qquad (4.2)$$

where M is the antenna mass. Z_{12}, the reverse transconductance, is responsible for characterizing the

Table 4.1

Nominal Operating Parameters

Antenna:		
mass	M	2500 kg
quality factor	Q_a	50 million
angular frequency	ω_a	900 Hz
temperature	T_a	4.2 °K
beat period	τ_b	0.22 s
Transducer:		
1) cavity		
capacitance gap	d_0	10
angular frequency	Ω_0	600 MHz
quality factor	Q_e	600,000
capacitance	C_0	28 pF
gap electric field	E_0	100,000 V/m
2) diaphragm		
mass	m	0.02 g
frequency	ω	4-13 kHz
quality factor	Q_m	50,000
squeezing factor	T	1-20

effect that amplifier noise back reaction has on the antenna. This noise coupling can be expressed through the reverse energy coupling coefficient

$$\beta_{12} \equiv \frac{|Z_{12}|^2}{M\,\omega_a |Z_{22}|} \tag{4.3}$$

and the usual (i.e. Gibbons-Hawking[4]) electromechanical coupling coefficient is defined by

$$\beta \equiv (\beta_{12}\beta_{21})^{1/2} = \frac{|Z_{12}||Z_{21}|}{M\,\omega_a |Z_{22}|} \tag{4.4}$$

β, as defined in Gibbons-Hawking,[4] represents the ratio of the energy of the electrical output signal of the transducer to the elastic energy of the antenna. There is an alternative interpretation due to Caves,[5] where β is defined approximately by

$$\beta = \frac{\{\#\text{ of quanta transferred to the amplifier in one period of mech. osc.}\}}{\{\#\text{ of quanta in the mech. osc.}\}} \tag{4.5}$$

β determines how rapidly the transducer transfers information to the amplifier.

The transducer-antenna system comprises a set of coupled harmonic oscillators. Energy of the antenna is transferred to the transducer in a time equal to one-half the beat period, τ_B, of the two oscillators,[6] or

$$\frac{\tau_B}{2} = \frac{\pi}{\omega_a [\Delta^2 + \frac{m}{M}]^{\frac{1}{2}}} \tag{4.6}$$

where Δ is the relative frequency difference between the transducer and antenna mechanical frequencies ($\Delta \cong |\omega_a - \omega|/\omega_a$), and m is the diaphragm mass. When $\Delta = 0$, the transducer is said to be resonant; then $\tau_B = (\sqrt{M/m})(2\pi/\omega_a)$ and the impedances $|Z_{12}|$ and $|Z_{21}|$ are increased by $\sqrt{M/m}$ and β by M/m (for measurement times greater than $\tau_B/2$). Thus the relationship between nonresonant (NR) or resonant (R) transducer operation can be expressed[6] as

$$\beta_R = \beta_{NR} \cdot \frac{M}{m} \cdot \sin^2 \left(\frac{\pi\tau}{\tau_B}\right) \tag{4.7}$$

where τ is the measurement time. The $\sin^2$ term is replaced by unity if $t > \tau_B$.

C. Energy Detection Sensitivity

The resonant bar antenna must respond optimally to gravity wave bursts, i.e. energy that is deposited in times shorter than τ_a, the decay time of the antenna. If we consider a linear (AP) operation of the accelerometer followed by a voltage amplifier, then the detectability criterion for detecting an amount of energy E_a deposited in the antenna is[7]

$$E_a \geq \frac{k_B T_a \tau}{\tau_a} + k_B T_N \left[\frac{|z_{12}|^2 \tau}{2MR_0} + \frac{2MR_0 \left(1 + \frac{|z_{22}|^2}{R_0^2}\right)}{|z_{21}|^2 \tau} \right] \tag{4.8}$$

where τ is the measurement time, T_a is the antenna physical temperature, τ_a the antenna decay time, R_0 ($\equiv\sqrt{(S_e/S_i)}$) the optimum source impedance of the amplifier, T_n ($\equiv (S_e S_i)^{1/2}\ \Omega_0/2k_B$) the amplifier noise temperature, and k_B is Boltzmann's constant (S_e and S_i refer to the amplifier voltage and current noise spectral densities, respectively).

The first term on the right hand side of (4.8) is the antenna Brownian noise contribution to the total noise; the second term contains the amplifier back reaction (narrowband) and forward (wideband) contributions,

respectively, to the total noise (referenced to the input of the amplifier). The transducer itself is assumed to be ideal and noiseless.

The total noise is minimized by matching the transducer output impedance to the amplifier input impedance ($R_0 \approx |Z_{22}|$) and by optimizing the measurement time τ. This optimization gives

$$\tau_0 = \frac{2\sqrt{2}\ \underline{\Sigma}}{\omega_a\ \beta\left[\frac{2}{T_N}\ \left(\frac{T_a}{Q_a}\right)\ \left|\frac{Z_{21}}{Z_{12}}\right|\ \frac{\underline{\Sigma}^2}{\beta} + 1\right]^{1/2}} \tag{4.9}$$

where the $\underline{\Sigma}$ appears only for BAE coupling of the transducer, and is replaced by unity for AP couplings. This τ_0 leads to the minimum detectable antenna signal energy

$$E_{min} \approx 4k_B\ \left|\frac{Z_{12}}{Z_{21}}\right|^{1/2}\ \left(\frac{T_N}{\underline{\Sigma}}\right)^{1/2}\ \left[\left(\frac{T_a\underline{\Sigma}}{Q_a}\right)\ \frac{1}{\beta}\right.$$

$$\left. + \frac{1}{2}\left(\frac{T_N}{\underline{\Sigma}}\right)\left|\frac{Z_{12}}{Z_{21}}\right|\right]^{1/2} \tag{4.10}$$

with the same proviso for $\underline{\Sigma}$. All parameters in (4.9) and (4.10) are to reflect AP values.

The right hand side of (4.10) contains two terms, with the first term being the antenna thermal noise contribution to the total noise of the system, and is inversely proportional to the coupling and directly proportional to the squeezing. Although the effective amplifier noise temperature is reduced by the squeezing factor, the increase in the effective physical temperature of the antenna by this same factor has hitherto been unreported. Equation (4.10) indicates that if the thermal noise dominates then E_{min} will be independent of squeezing, and if the amplifier noise dominates than E_{min} will be inversely proportional to the squeezing factor.

The above expressions for BAE measurements take into account the change in the impedance matrix elements under back action evading coupling to the transducer. It can be shown in a high-Q limit, or equivalently a high T ($T >> 1$) limit, that

$$|Z_{12}|(AP) \cong \frac{E_0}{4\omega} \tag{4.11a}$$

$$|Z_{21}|(AP) \cong (\frac{E_0}{4\omega}) \ (\frac{\Omega_0}{\omega}) \tag{4.11b}$$

and that, for BAE operation,

$$|Z_{12}|(\text{BAE}) \cong \left(\frac{E_0'}{4\omega}\right) \frac{1}{\Sigma} \quad (4.12a)$$

$$|Z_{21}|(\text{BAE}) \cong \left(\frac{E_0'}{4\omega}\right) \left(\frac{\Omega_0}{\omega}\right) \quad (4.12b)$$

where E_0 and E_0' are the electric fields in the capacitance gap under each respective operation mode. If we assume that $E_0 \approx E_0'$, then 4.11 and 4.12 show that the forward transductance, Z_{21}, does not change when a BAE scheme is implemented, indicating that additive voltage noise is not increased by the technique; they also show that the reverse transductance, Z_{12}, is diminished by the factor Σ during BAE, which is not unexpected considering the definition of this matrix element in the two-port model. Z_{11} and Z_{22} are also unchanged by back action evasion. Another conclusion from 4.4, 4.11 and 4.12 is that β(BAE) is reduced by a factor of Σ from (AP).

D. AP Versus BAE: Specific Application to LSU Transducer-Antenna System

The litmus test of the application of BAE principles to working gravity wave detection antennas is in how squeezing competes with non-squeezing measurement energy

sensitivities for optimal measurement times. The transducer parameters assumed in the following are equivalent to the BAE/AP test platform transducer with two exceptions: 1) the diaphragm mass, which was 2.0×10^{-5} kg in the test system, is now assumed to be 0.05 kg in order to achieve high enough diaphragm mechanical Q's such that the transducer thermal noise does not dominate over the antenna thermal noise and, 2) the Q_e of the cavity be at least three million (instead of the 600,000 of the test transducer) in order that squeezing factors on the order of ten be reached at 1 kHz. Both of these parameters are realistic and experimentally achievable with some care.

In the following, we examine the minimum detectable energy as a function of nonresonant and resonant operation, of temperature (at 4.2 °K and 0.050 °K), of antenna Q_a (10^7 and 10^8), and especially of amplifier noise temperature, assuming the transducer contributes negligible noise. The amplifier noise temperature plays a very important role; as we will soon see, the efficacy of BAE in improving energy sensitivity critically depends upon T_n. Note that the minimum noise temperature is given by $T_n(\text{min}) = \hbar\Omega_0/k_B \ln 2$, which is equal to 0.043 °K at 600 MHz. It is at this temperature that we will consider the SAL to reach the SQL.

a) $T_a = 4.2$ °K, $Q_a = 10^7$ ($T_a/Q_a = 4.2 \times 10^{-7}$)

1) Nonresonant Operation

Figure 4.1 shows E_{min} as a function of T_n for AP operation (Σ=1) and for BAE squeezing factors of 5, 10, and 15. It shows that for T_n's less than ten degrees, AP coupling provides much better energy sensitivity than BAE coupling. This is largely due to the very weak couplings involved, necessitating longer measurement times and hence allowing increased antenna thermal noise contributions. The AP coupling is 8×10^{-2}.

2) Resonant Operation

Figure 4.2 shows E_{min} vs T_n under resonant operation. It indicates that squeezing will improve sensitivity for amplifiers with noise temperatures over ≈1 °K, with significant improvement for $T_n > 7$ °K. Since the best reported 4 °K FET amplifier had a $T_n = 8$ °K,[8] it would seem that resonant operation offers real practical hope for energy sensitivity improvement for the pragmatic parameters assumed for the antenna/transducer system here, with an order of magnitude improvement in sensitivity at $T_n = 50$ °K. Resonant operation also offers almost two orders of magnitude improvement in sensitivity over nonresonant operation. Figure 4.2 also reveals the interesting feature that when T_n is less than 10 °K

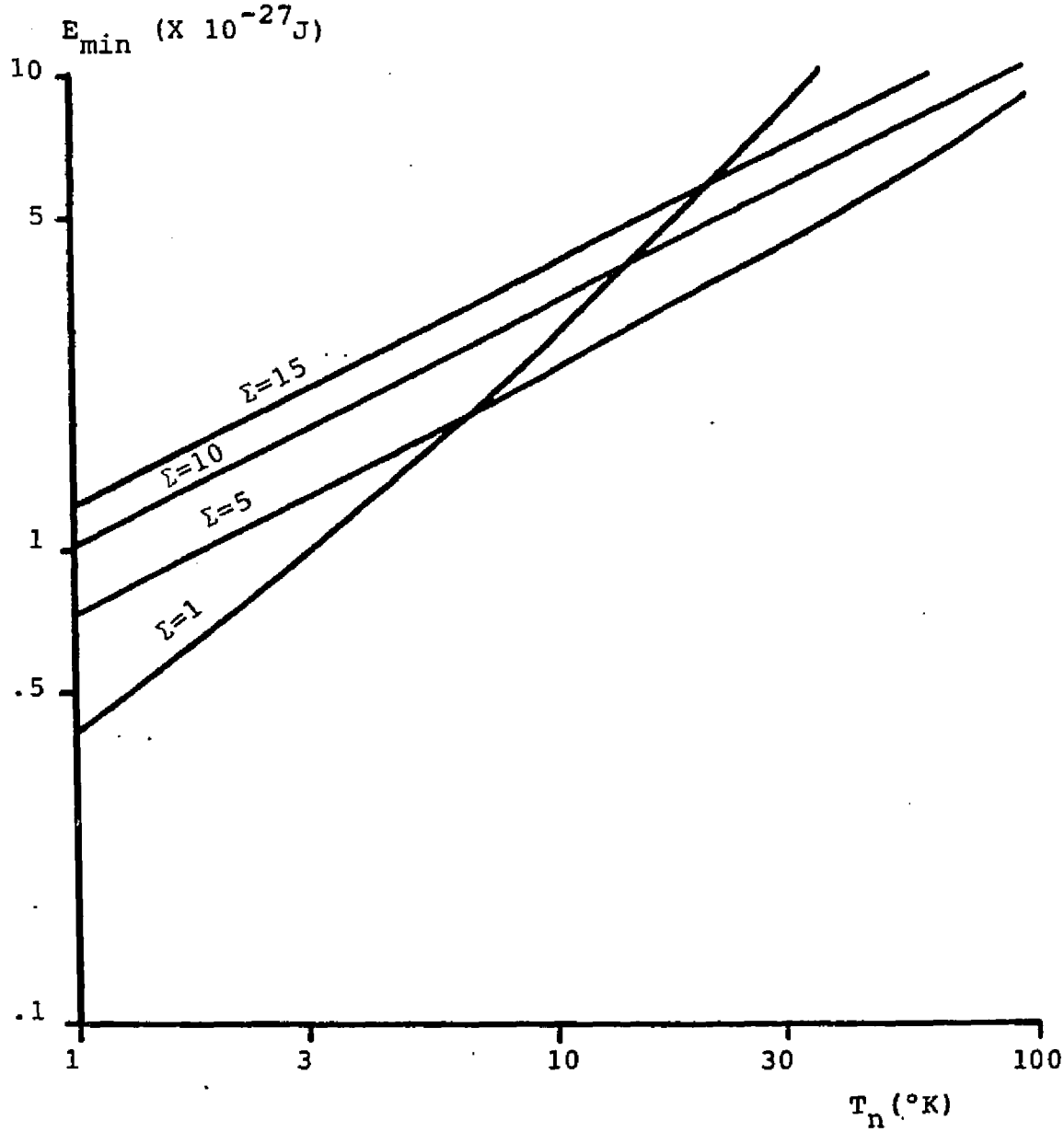

Figure 4.1 Minimum Energy Sensitivity versus T_n
(Nonresonant Operation)

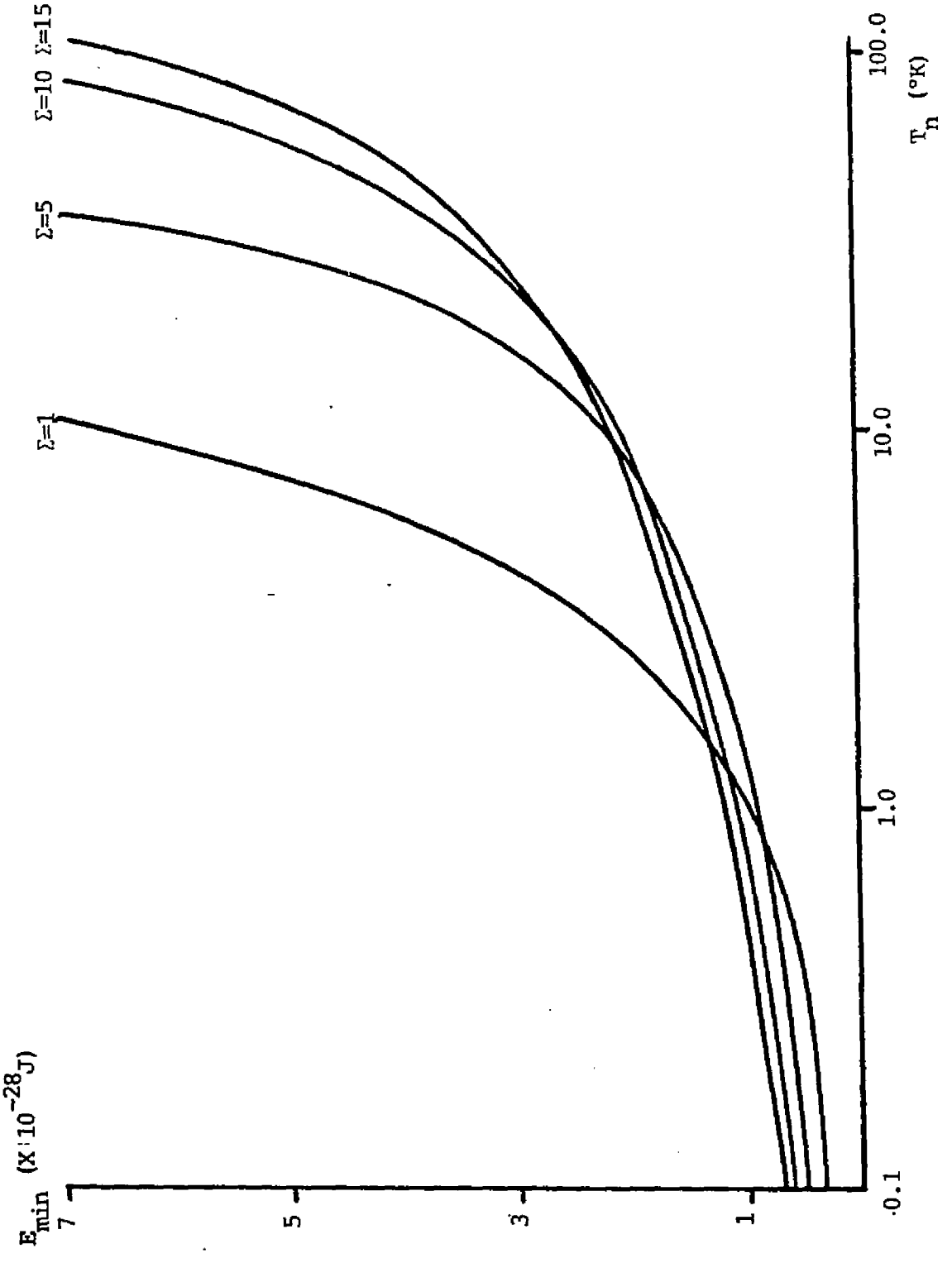

Figure 4.2 Minimum Energy Sensitivity versus T_n

(Resonant Operation)

there is not much squeezing dependence to the sensitivity. It should be remembered that the coupling is decreased by the squeezing factor, necessitating longer measurement times. At these low amplifier noise temperatures, longer measurement times allow enough thermal noise contamination such that BAE is of little help. Thus, depending on the thermal noise contribution and the amplifier noise temperature, there is a point of diminishing returns that is reached when determining the benefit of squeezing on sensitivity.

b) $T_a = 4.2\ ^\circ K$, $Q_a = 10^8$ $(T_a/Q_a = 4.2 \times 10^{-8})$

1) Nonresonant Operation

Figure 4.3 shows the sensitivity as a function of noise temperature with the antenna Q_a increased by a factor of ten. This increase could be achieved experimentally (the gravity wave group at the University of Western Australia has already reported un-loaded Q's of 250 million for their niobium bar[9]) by using an aluminum alloy 5056 antenna. This reduces the thermal noise contribution, and allows an improvement in sensitivity over the lower Q_a case. The Q_a increase also allows BAE to compete with AP around $T_n = 0.1\ ^\circ K$ for $\Sigma=5$, and at $T_n = 0.3\ ^\circ K$ for $\Sigma=15$.

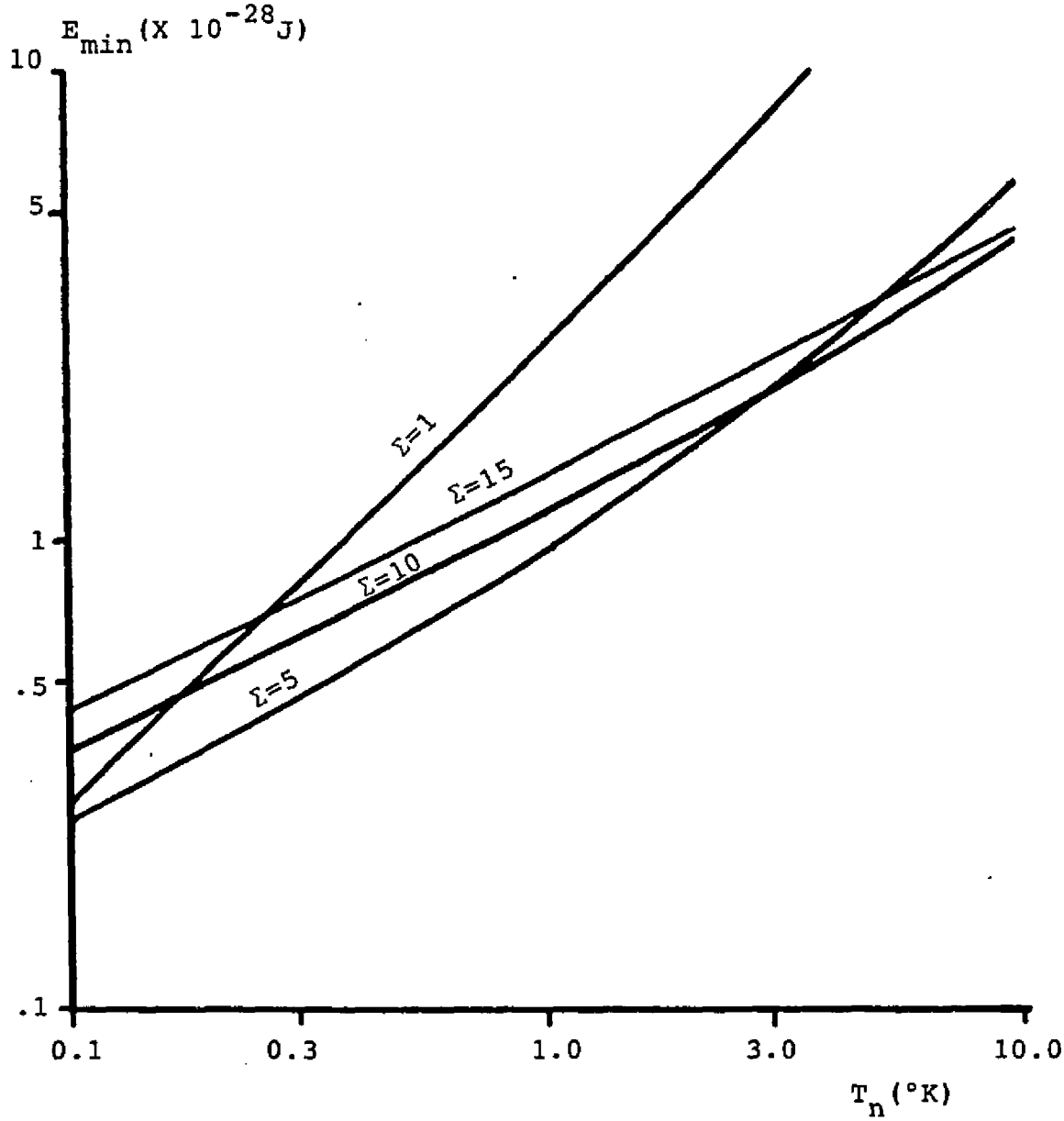

Figure 4.3 Minimum Energy Sensitivity versus T_n

(Nonresonant Operation)

2) Resonant Operation

Figure 4.4 displays sensitivity as a function of amplifier noise temperature for various Σ values. Compared with Figure 4.2, it indicates that the effect of increasing the antenna Q_a is to push the squeezing benefit toward lower amplifier noise temperatures; in this case squeezing improves on AP measurement sensitivity for $T_n > 0.2$ °K. Interestingly, larger values of squeezing do not result in improved sensitivity until after 1 °K or so. BAE is shown to have tremendous potential for improving upon the SAL of 8 °K FET amplifiers.

c) $T_a = 0.050$ °K, $Q_a = 10^7$ ($T_a/Q_a = 5.0 \times 10^{-9}$)

1) Nonresonant Operation

We present the results of sensitivity analysis similar to that in parts a) and b) in Figure 4.5, except now we are at dilution refrigerator temperatures. This capability was built into the LSU cryogenic support apparatus, and its implementation is being studied by Prof. Bruce Pipes at Dartmouth. The lower antenna temperature results in improved sensitivities, as expected, and allows squeezing to be beneficial for T_n's greater than 0.3 °K for Σ=5 and 2 °K for Σ=15.

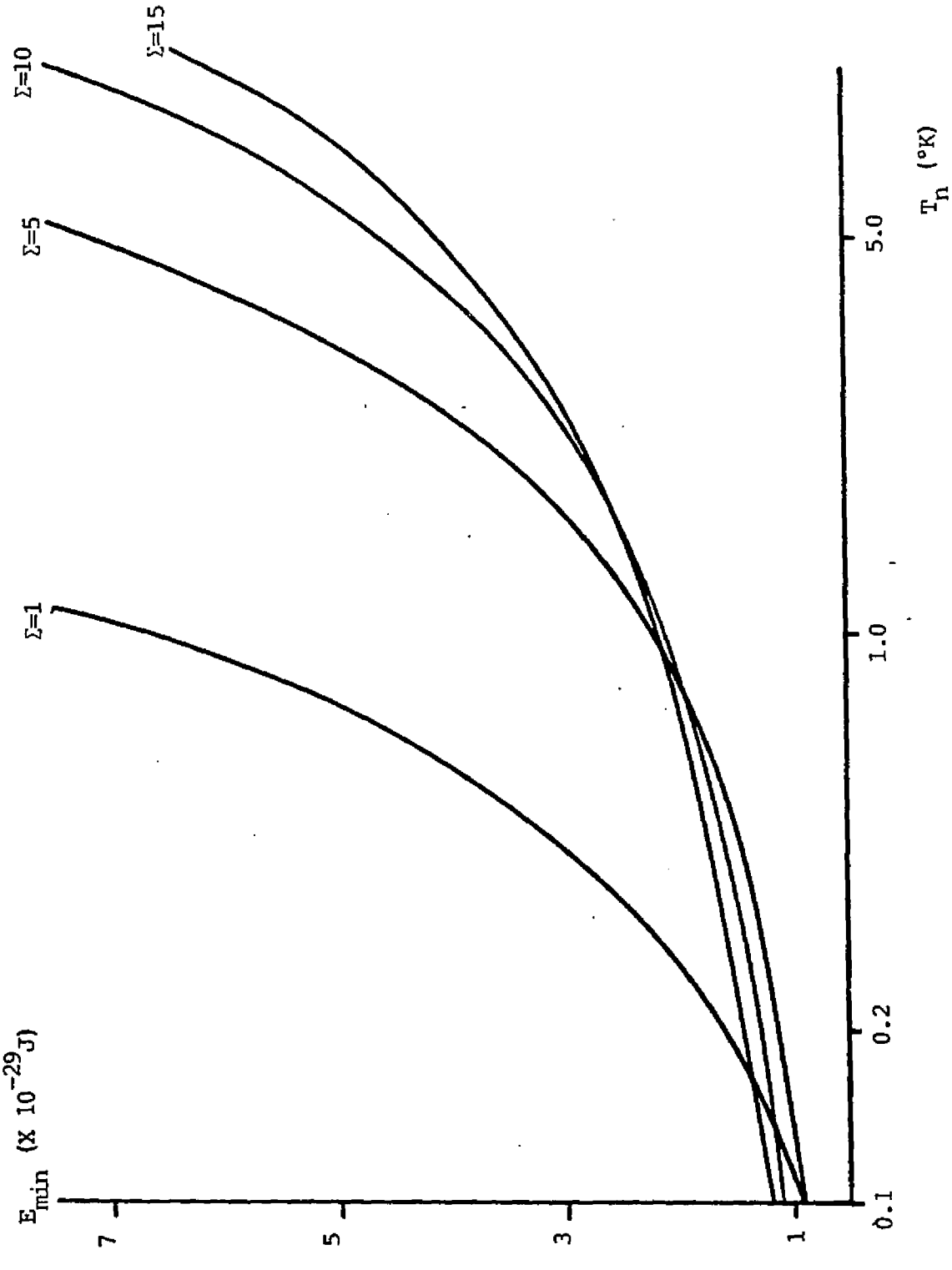

Figure 4.4 Minimum Energy Sensitivity versus T_n

(Resonant Operation)

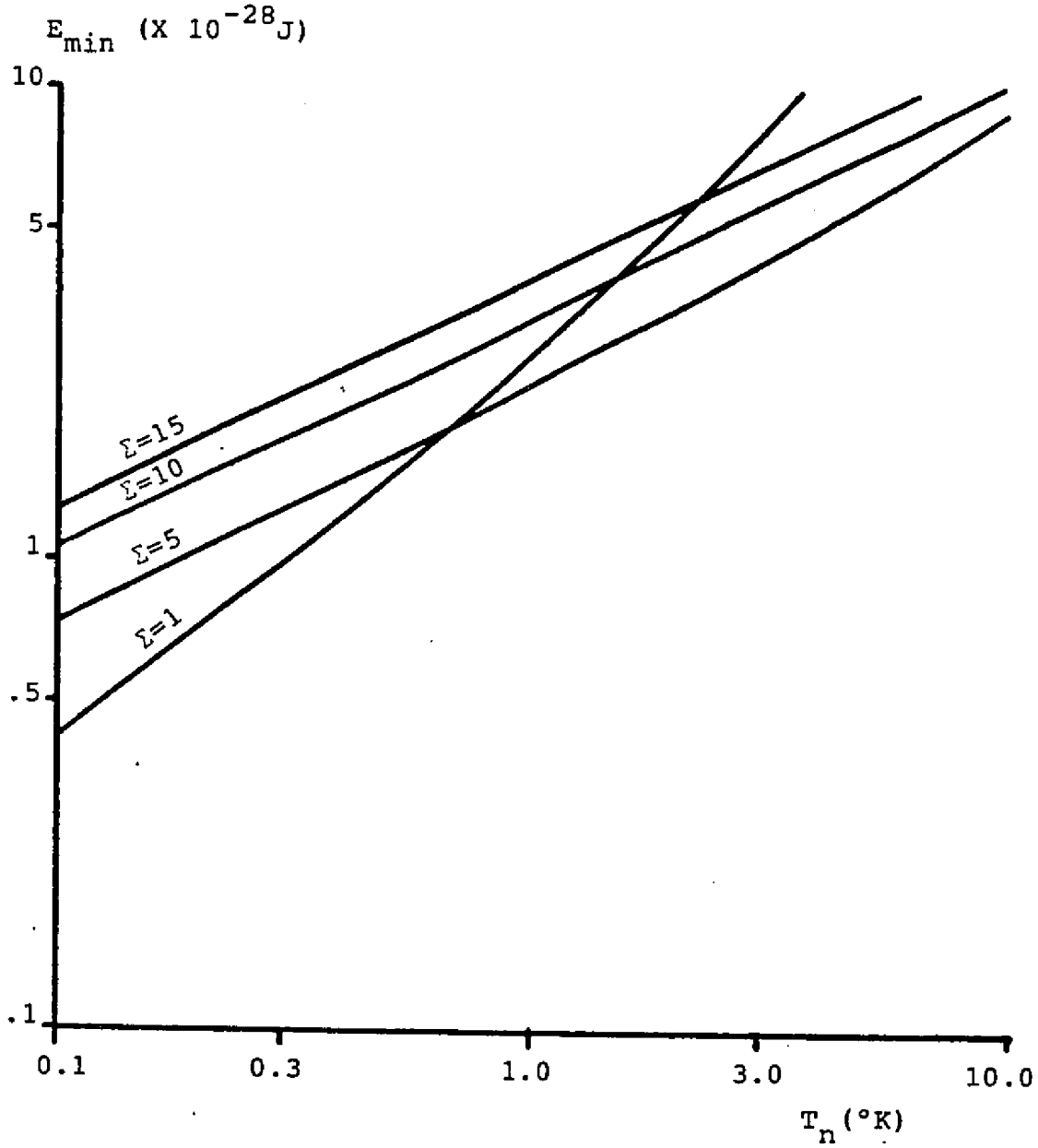

Figure 4.5 Minimum Energy Sensitivity versus T_n
(Nonresonant Operation)

2) Resonant Operation

Sensitivity curves under resonant operation are shown in Figure 4.6. Squeezing starts to improve on AP sensitivity after approximately 0.03 °K, with significant squeezing starting to occur at 0.1 °K. Sensitivity also starts to become Σ dependent after 0.1 °K. Since the SQL occurs at about 0.04 °K, the sensitivity curves show that there is improvement on the SQL under BAE; the relatively small amount of squeezing shown is "squeezing" in the original sense of the word, i.e., allowing the SQL to be circumvented.

d) $T_a = 0.050$ °K, $Q_a = 10^8$ $(T_a/Q_a = 5.0 \times 10^{-10})$

1) Nonresonant Operation

Figure 4.7 shows sensitivity curves for nonresonant operation with a higher antenna Q_a. The sensitivities here are equivalent to the resonant sensitivities for the $T_a = 4.2$ °K and $Q_a = 10^8$ system (Figure 4.2). The important difference is that this is a nonresonant mode with concomitant smaller coupling factors, and that BAE offers improvement over AP for $T_n = 0.01$ °K for Σ=5 and 0.2 °K for Σ=15. Nonresonant BAE operation offers significant improvement at the noise temperatures expected for the best FET amplifiers.

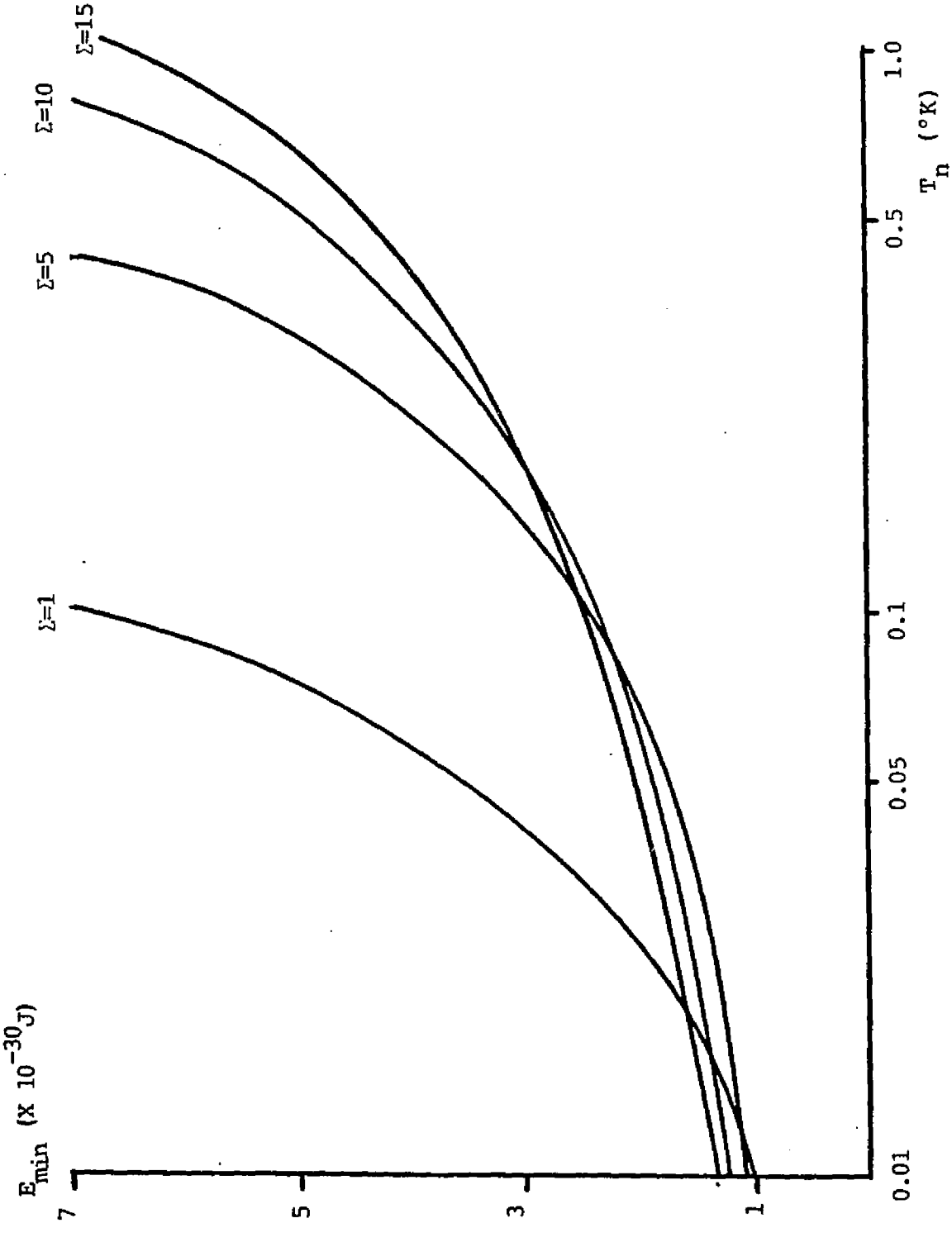

Figure 4.6 Minimum Energy Sensitivity versus T_n

(Resonant Operation)

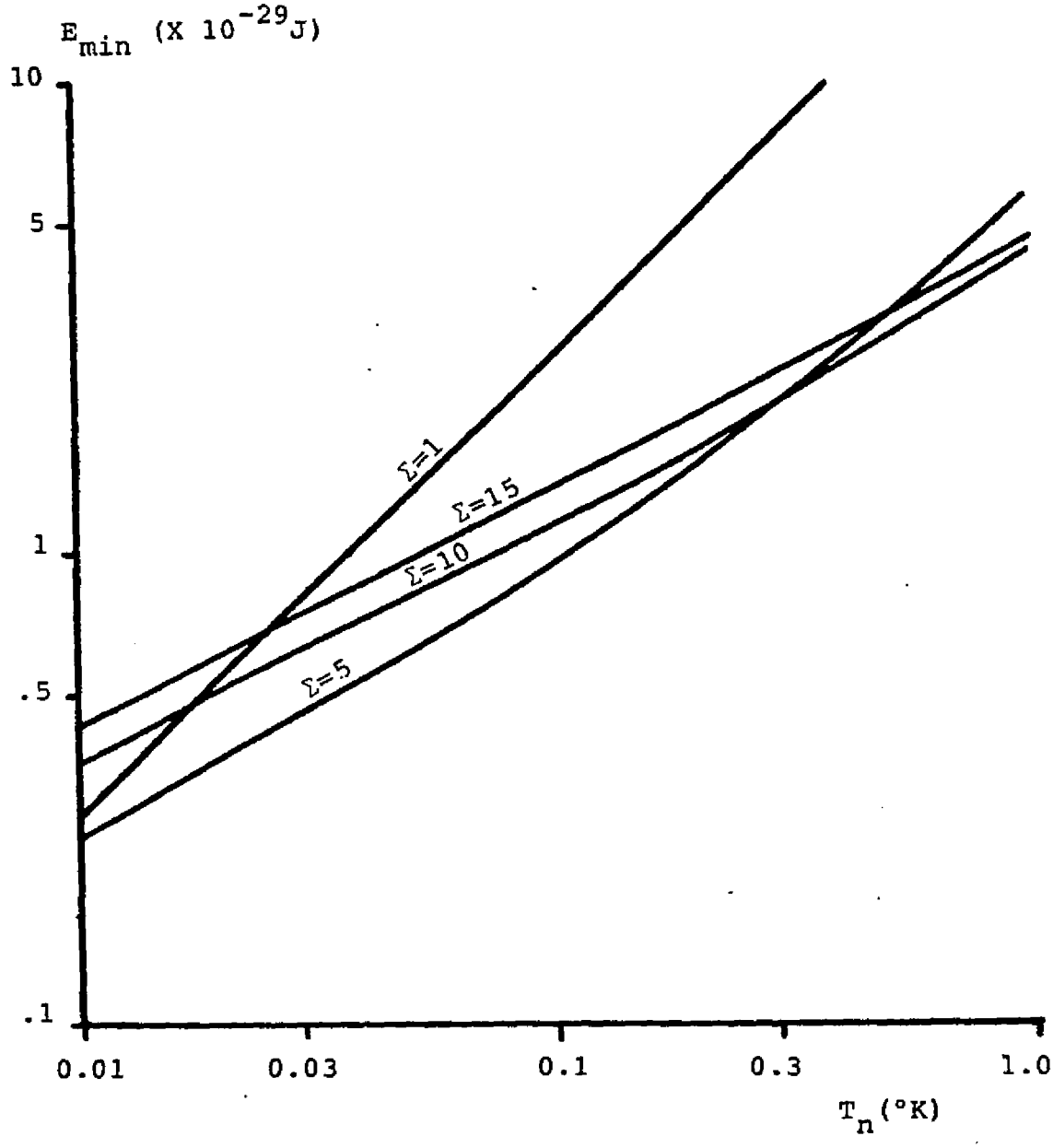

Figure 4.7 Minimum Energy Sensitivity versus T_n

(Nonresonant Operation)

2) Resonant Operation

See Figure 4.8. The BAE performance is very good, with significant squeezing effect occuring after 0.005 °K. Sensitivity starts becoming Σ dependent at 0.01 °K, and there is an approximate improvement in the SQL sensitivity of an order of magnitude for squeezing factors of 5-15. Sensitivities are almost four orders of magnitude smaller than those of T_a = 4.2 °K, $Q_a = 10^7$, under nonresonant operation. The β's under these final set of parameters are nearly unity, as expected since the antenna thermal noise has been so reduced.

The results of these considerations of energy detection sensitivities as a function of a variety of pertinent system parameters, and as a function of the amplifier noise temperature, lead to the following conclusions:

a. The establishment of classical squeezing of the amplifier back reaction noise by the transducer does not necessarily translate to improved antenna energy detection sensitivity, it depends critically on the level of amplifier back reaction present, on the antenna physical temperature, the quality factor of the antenna, and on the operational mode of the transducer.

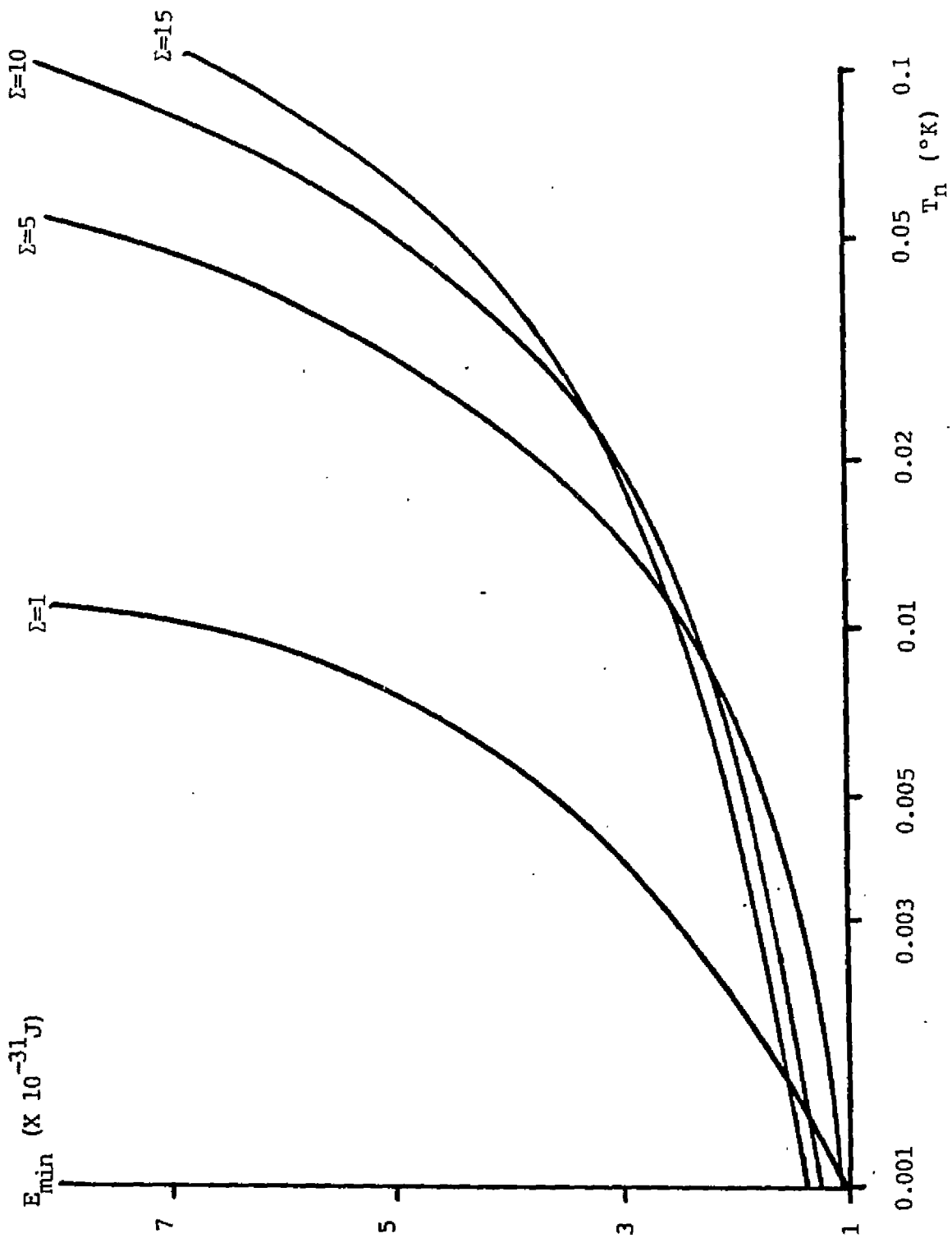

Figure 4.8 Minimum Energy Sensitivity versus T_n

(Resonant Operation)

b. For the experimentally feasible parameters considered, the detection sensitivity is not extremely dependent on the size of the squeezing factor for the lower amplifier noise temperatures. Generally, a small amount of squeezing (e.g. a factor of five) is much better than no squeezing, but not much worse than a significantly larger value (e.g., a factor of fifteen).

c. For the parameters considered, supercooling down to dilution refrigerator temperatures (0.05 °K) is a must if the SQL is to be circumvented.

d. Resonant operation of the transducer offers one to two orders of magnitude improvement

E. Effects of Oscillator Phase Noise

An important caveat to all of the preceeding analysis is that two very important assumptions have been made:

1. It has been assumed that the transducer contributes negligible noise, and
2. The assumptions are made that there is an ideal two stick input current and that there is negligible phase noise contributed by the pump oscillator.

We refer the reader to the discussion by Blair and Mann[10] and Mann[11] on possible sources of noise in an antenna readout system; we will not go into the noise contributions of the transducer per se except to say that the mechanical Q_m of the diaphragm should be as high as possible, particularly to minimize thermal noise.

The problem posed by pump phase noise is particularly relevant, as the LSU dual cavity accelerometer was designed in part to suppress the effects of pump phase noise.[1] Pump phase noise adds to the wideband amplifier noise; the amplitude noise is usually orders of magnitude smaller than the phase noise contribution,[12] and will be neglected.

We denote the phase noise spectral density by S_ϕ, with a noise energy contribution at the amplifier input given by[10]

$$E_\phi \cong \frac{[2M(2\omega_a^2)(\frac{\omega_a}{\Omega_0})^2 d_0^2]}{\tau} S_\phi = (1.1 \times 10^{-10}) \frac{S_\phi}{\tau} \qquad (4.13)$$

A good fixed oscillator can have a S_ϕ as low as 10^{-15} Hz^{-1}. To get an idea of the effect of this noise on the antenna sensitivity, we present in Table 4.2 the value of τ_0 for each of the previously examined operational modes (Figures 4.1, 4.4, 4.5, 4.6, 4.7, and 4.8) for T_n = 10 °K and the resulting energy contribution.

Table 4.2

AP

T_a/Q_a	τ(NR;sec)	E_ϕ(NR;J)	τ(R;sec)	E_ϕ(R;J)
4.2×10^{-7}	5.2×10^{-3}	2.1×10^{-23}	8.1×10^{-4}	1.4×10^{-22}
4.2×10^{-8}	5.6×10^{-3}	2.0×10^{-23}	8.2×10^{-4}	1.3×10^{-22}
5.0×10^{-9}	5.6×10^{-3}	2.0×10^{-23}	8.2×10^{-4}	1.3×10^{-22}
5.0×10^{-10}	5.6×10^{-3}	2.0×10^{-23}	8.2×10^{-4}	1.3×10^{-22}

BAE (Σ=10)

4.2×10^{-7}	4.5×10^{-2}	2.4×10^{-24}	2.6×10^{-3}	4.2×10^{-23}
4.2×10^{-8}	0.14	7.9×10^{-25}	3.6×10^{-3}	3.1×10^{-23}
5.0×10^{-9}	0.33	3.3×10^{-25}	3.8×10^{-3}	2.9×10^{-23}
5.0×10^{-10}	0.52	2.2×10^{-25}	3.8×10^{-3}	2.9×10^{-23}

It is clear from a comparison of the above results and of the energy sensitivity figures that the phase noise contribution is several orders of magnitude larger than the optimum sensitivities. This necessitates that one either take advantage of the phase noise cancelling properties offered by the LSU transducer or Rochester bridge design, or apply phase noise suppression techniques to the oscillator output ala Mann,[13] to obtain the indicated ≈60 dB suppression.

References

1. W. C. Oelfke, and W. O. Hamilton, Acta. Astron. 5, 87 (1978); D. Darling, W. O. Hamilton, and W. C. Oelfke, in Proc. of the Second Marcel Grossman Conf., R. Ruffini, ed., (North Holland, New York, 1982); W. O. Oelfke, and W. O. Hamilton, Rev. Sci. Instr. 54, 410 (1983).

2. F. V. Hunt, Electroacoustics, (Harvard Univ. Press, Cambridge, 1954).

3. R. P. Giffard, Stanford Univ. preprint, (December, 1975).

4. G. W. Gibbons, and S. W. Hawking, Phys. Rev. D4, 2191 (1971).

5. C. M. Caves, in Quantum Optics, Experimental Gravitational, and Measurement Theory, (Plenum Press, New York, 1983).

6. H. J. Paik, in Proc. of the Second Marcel Grossman Conf. (North Holland, New York, 1982).

7. R. P. Giffard, Phys. Rev. D14, 2478 (1976).

8. S. Weinreb, IEEE MIT-S Digest, p. 10 (1982).

9. P. J. Veitch, D. G. Blair, M. J. Buckingham, C. Edwards, J. Ferreirinho, F. van Kann, and T. Suzuki, abstract, Applied Superconductivity Conference-1984, San Diego, CA.

10. D. G. Blair, and A. G. Mann, Il Nuovo Cimento 61, 73 (1981).

11. A. G. Mann, Ph.D. Dissertation, Univ. of Western Australia (1982).

12. U. Rhode, Digital PLL Frequency Synthesizers: Theory and Design, (Prentice Hall, Englewood Cliffs, New Jersey, 1983).

13. A. G. Mann, IEEE Trans. MIT-33, 51 (1985).

CHAPTER 5

EXPERIMENTAL APPARATUS

A. Introduction

We describe the experimental apparatus in this chapter. The experiment can be divided into four interrelated sections: the accelerometer; the dewar and dewar insert; the microwave signal generating/processing apparatus; and the cryogenic and vacuum support. We go into some detail on the superconducting reentrant cavity design and surface preparation and on the operation and properties of the LSU accelerometer cavity/diaphragm system.

B. Accelerometer Design and Construction

The dual cavity LSU accelerometer is shown in Figure 5.1. It consists of two identical reentrant niobium cavities separated by a thin niobium diaphragm. The connecting flanges are attached via six 2-56 brass screws. The 1 mil diaphragm is put under radial tension via six pairs of tensioning screws prior to tightening the flange screws. The tuning diaphragms, about 20 mils thick, are tapped for a samarium cobalt magnet.[1]

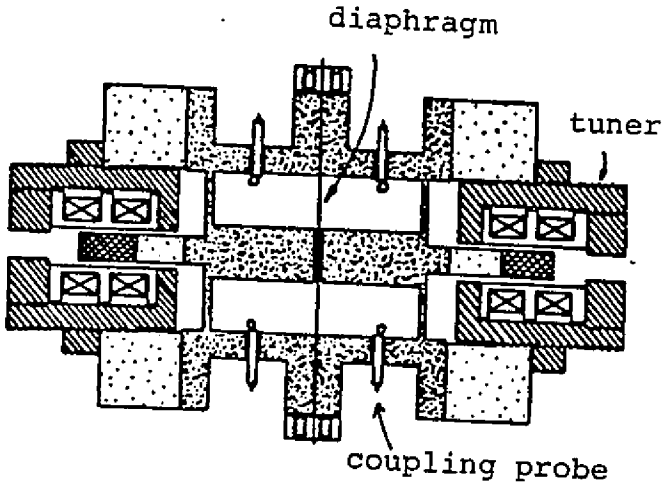

Figure 5.1 LSU Accelerometer

Attached to the flanges on the tuning diaphragm side of the cavity is a threaded housing designed to allow the tuning coil to be centered around the permanent magnet. The accelerometer is then attached by six more brass screws to an aluminum mounting pedestal which in turn is mounted on a 10 kg copper base. Mounted on the copper base are the superconducting tuning transformers and heat switches and an Allen-Bradley resistor for thermometry. Also mounted are anchoring attachments (to the mounting block) for the coaxial lines connected to the coupling probes. Holes are also tapped to allow the mounting of large PZT drivers.

C. Dewar and Dewar Insert

Figure 5.2 shows a cutaway view of the dewar insert, and dewar housing. The dewar insert has to provide for: the transfer of liquid nitrogen and helium; thermometry; vacuum at the micron level in the experimental can; signal input and retrieval for two rf cavities; the sustenance of liquid helium temperatures in the experimental can for hours at a time; the tuning of two cavity tuning assemblies; the driving of PZT's; vibration isolation of the accelerometer; and the recovery of evaporated helium gas. The dewar is 8" in diameter and made by SCT, Inc. The dewar insert satisfies

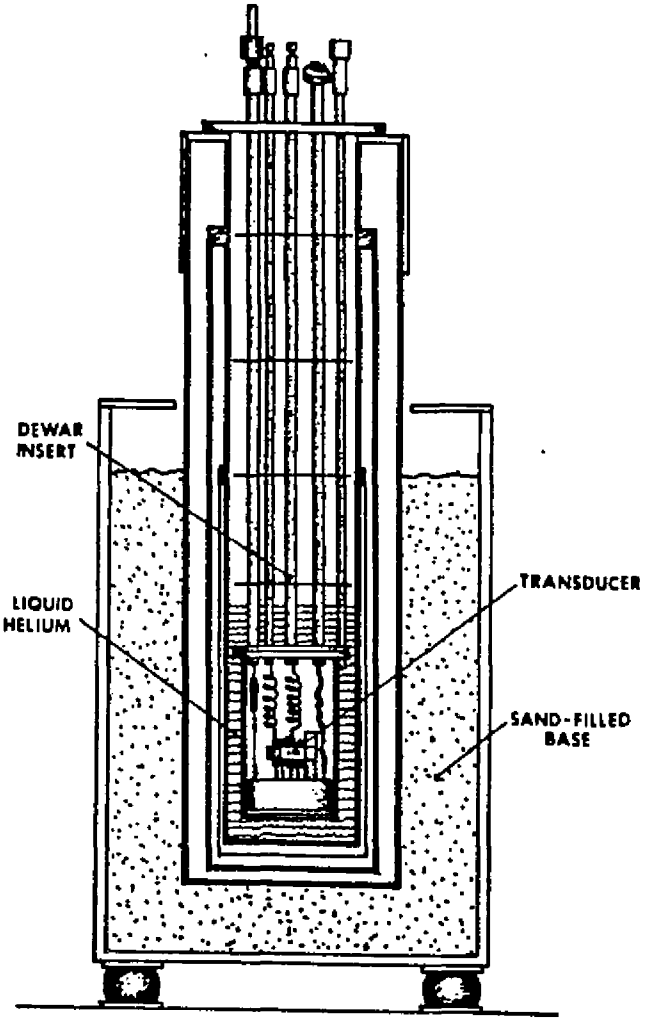

Figure 5.2 Dewar, Dewar Insert, and Dewar Housing

the above requirements through use of copper in the top plate and experimental can, with 1/2" stainless steel tubing used to provide access to the can. Copper reflectors help prevent radiation loss in the dewar. The can is sealed by an indium O-ring. Octal glass-to-metal feedthroughs are used for thermometry, tuning, and PZT driving; stainless steel 0.085" diameter coaxial cable (Uniform Tubes, type UT-85) is run through stainless tubes to conduct microwave power to and from the can. Allen-Bradley resistors are attached at various levels along the insert and in the experimental can. The dewar resides in a sand-filled plywood box resting on layered rubber and steel stacks in order to minimize ambient vibration from reaching the can. Three springs are used to isolate the copper mounting block from the dewar. Coiled UT-35 copper coax connects the cavities to the insert microwave lines. These coils are attached to the mounting block and are intended to minimize microphonic propagation to the cavities.

D. Vacuum and Cryogenic Support

The experiment is performed at 4.2 °K, although a pumping system acting on the liquid He bath lets 2 °K temperatures be reached. The vented He gas boiloff is collected and reprocessed by the helium liquifier.

With the dewar insert in place, it takes approximately 35 liters of helium, starting at 77 °K, to fill the dewar to the uppermost copper radiation shield. Liquid remains in the dewar to the top of the vacuum can for about 24 to 36 hours.

A helium exchange gas pressure of about 1000 μ is used during both liquid nitrogen precooling and helium transfers. The vacuum can is then evacuated to about 10 μ after cooling. It is possible for the accelerometer to remain at 4 °K for about 48-72 hours. A serious problem is thermal oscillations; their presence can warm the system to liquid nitrogen temperatures in less than 12 hours. They are eliminated by keeping the vacuum can pressure less than 150 μ. (A large thermal gradient, piping and can geometry, and line pressures all contribute to thermal oscillations. Typical remedies of this not-well-understood phenomenon include obstructing and breaking up gas flow, changing the liquid storage reservoir size and shape, and reducing line pressures.)

E. Microwave Signal Preparation

In order to test phase sensitive detection and back-action evasion, the input signal for the test cavity must meet at least two requirements: a "two-stick" spectrum centered on the cavity resonance frequency

and a means of inserting noise at Ω_0. Also, detection of back-action evasion requires that the monitor cavity have an input signal appropriate for an AP measurement. Although several different schemes were used during the course of the project, they fell into two basic categories: one in which a doubly balanced mixer was used to generate the two sticks and another in which two synthesizers were used to generate the sticks.

Figure 5.3 shows a design using a mixer to generate the two sticks. The accelerometer has two cavities: one is designated the test cavity and is used to test PS detection, and the other, the monitor cavity, and is used to (AP) monitor the back-action effects on the diaphragm. Synthesizer B is the source of the test cavity signal; the mixer is modulated by an audio frequency synthesizer set to the diaphragm mode of interest, giving rise to a dual sideband signal whose two sticks are separated about Ω_0 by ω. Synthesizer A provides the signal to both power the monitor cavity and to detect the monitor cavity output. The thermal noise chain is also shown; the thermal noise of a room temperature 50 Ω resistor is amplified by a 145 dB amplifier chain, with a high Q ($\approx$10,000) dielectric resonator to prevent amplifier saturation in the latter stages of the chain (I thank Dr. Tony Mann for use of his resonator[2]).

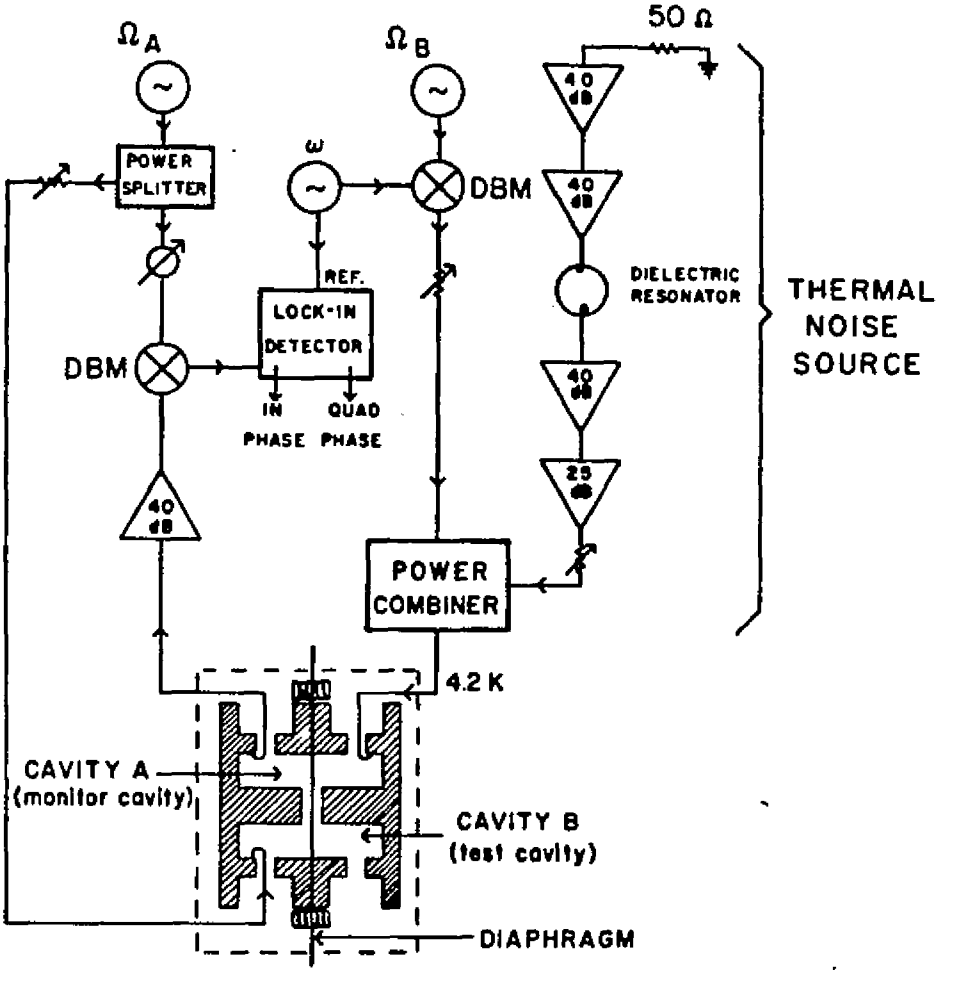

Figure 5.3 Schematic for Mixer-Generated BAE Input Signal Circuitry

Figure 5.4 displays the schematic wherein each sideband of the two-stick input is generated independently, which is a sterner experimental task but allowing much more flexibility in setting stick parameters. The requirements for this setup were that, besides independent two-stick input, the monitor cavity signal be phase-locked to the two-stick input. This is to insure that the phase relationships among the microwave signals be fixed, as they are in the mixer generated case. Four synthesizers were available: one audio frequency (Rockland model 5100), two low rf (< 25 MHz, HP 3325), and one high rf (< 1 GHz, HP 8660). The 600 MHz oscillator provided the monitor cavity AP input, as before. However, to insure a constant phase relationship between the monitor cavity input and the two stick input, a 10 MHz reference oscillator signal was multiplied up to 600 MHz and used in the two stick generation (I am indebted to Dr. Tony Mann for use of his X60 multiplier). The 60 MHz signal is then split and converted to the appropriate Ω_+ and Ω_- frequencies. The individual amplitudes and phases are adjusted at the front panels of the HP 3325's. The amplifier back reaction noise is added as before. Since there are three phase degrees of freedom (the LO phase and the phases of the two-sticks), a trial-and-error process is used to simultaneously adjust the three phases, with 3.11a and 3.11b

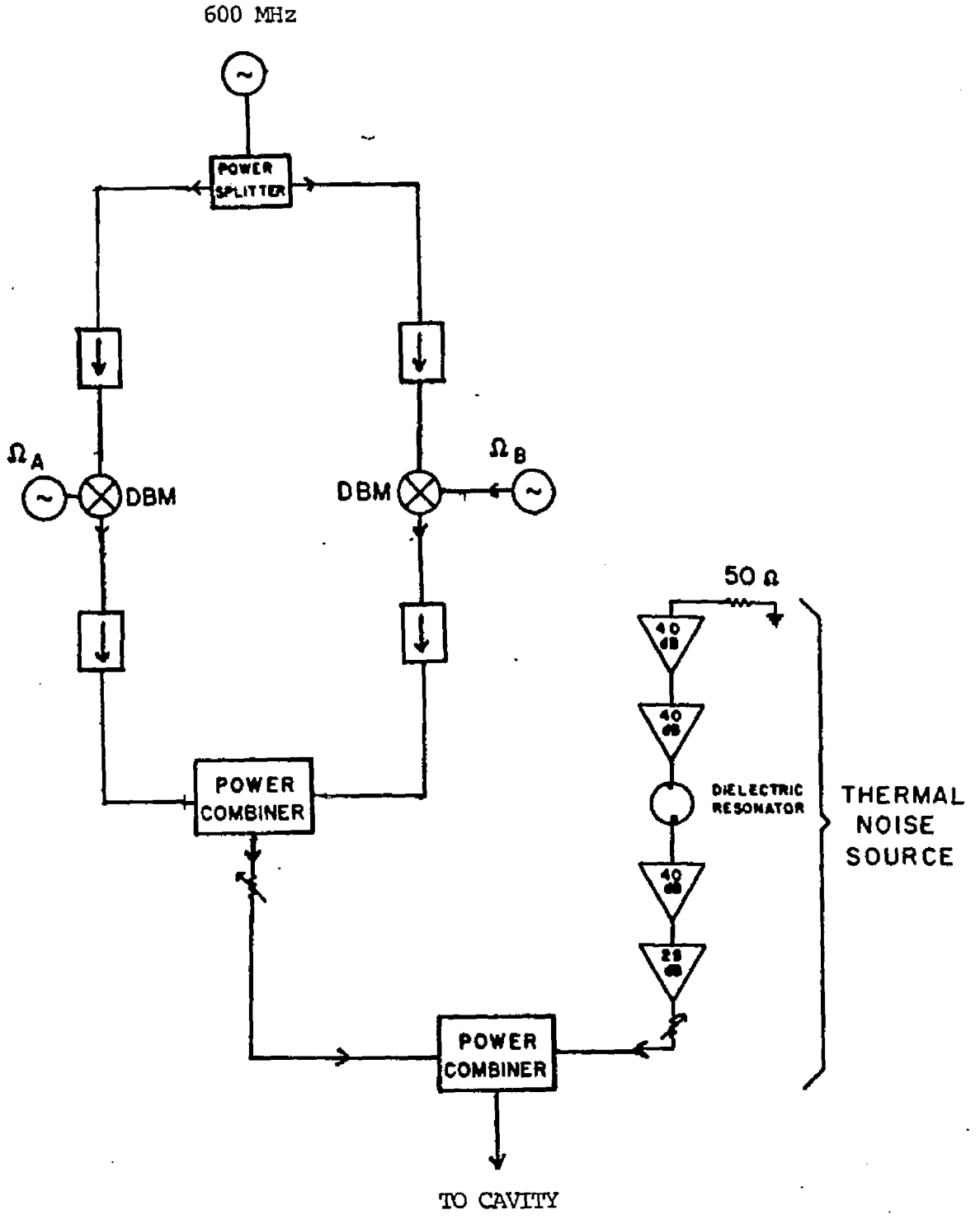

Figure 5.4 Schematic for Independent-Sideband BAE Input Signal Circuitry

used to ascertain the absolute phase values.

The amplified (40 dB) output signal of either cavity was detected via a doubly balanced mixer, demodulated at the cavity resonant frequency. See Figure 5.5. It is then processed by a PAR 129 two phase lock-in, with the Rockland providing the reference signal (at the diaphragm frequency). The in- and quad-phase output is used to determine the ω-component of the test cavity output. Squeezing data is obtained by comparing the lockin output signals after processing by a spectrum analyzer.

F. Reentrant Cavity Design and Preparation

The basic reentrant cavity design we consider is shown in Figure 5.6. Determination of the resonance frequency for this design is a non-trivial matter; however, if $l >> d$ then it can be treated as a lumped inductance (that of a short transmission line) shunted by the capacitance of the gap. The inductance is given by

$$L = \frac{\mu \ell}{2\pi} \ell n \left(\frac{b}{a}\right) \tag{5.1}$$

and the capacitance (including fringing capacitance) is

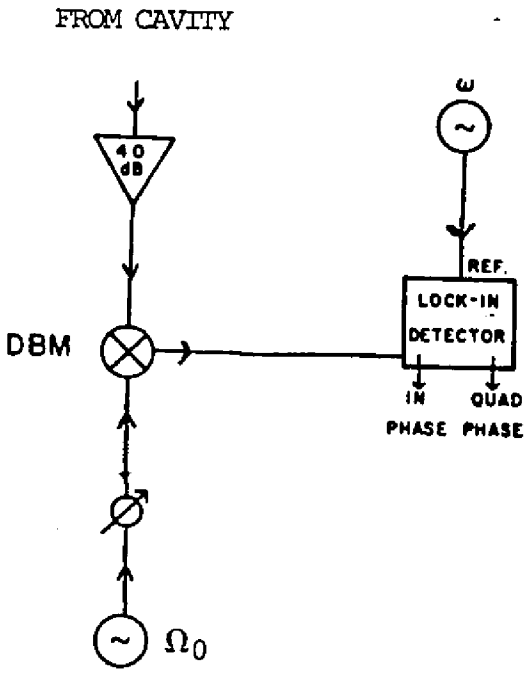

Figure 5.5 Schematic for Cavity Output Detection Circuitry

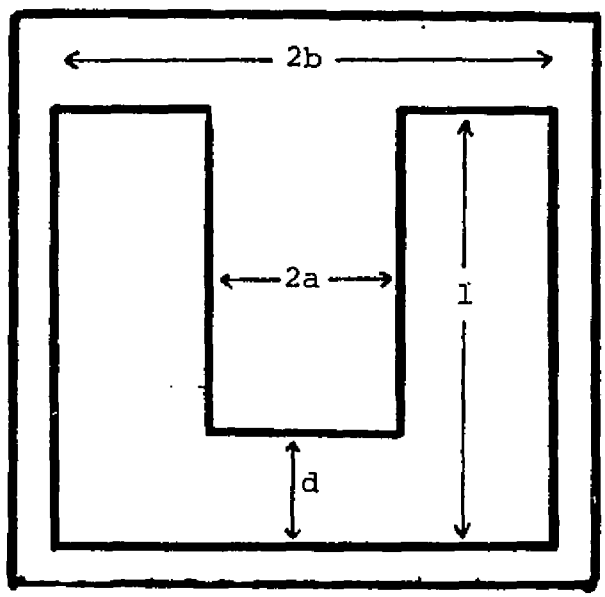

Figure 5.6 Reentrant Cavity Design

$$C = \varepsilon\left[\frac{\pi a^2}{d} - 4a\,\ell n\,\frac{0.765}{[\ell^2+(b-a)^2]^{1/2}}\right] \qquad (5.2)$$

The resonant frequency is then given by[3]

$$\Omega_0 = \frac{c}{\varepsilon^{1/2}}\left[a\ell\left(\frac{a}{2d} - \frac{2}{\ell}\,\ell n\,\frac{0.765}{[\ell^2+(b-a)^2]^{1/2}}\right)\ell n\left(\frac{b}{a}\right)\right]^{-1/2} \qquad (5.3)$$

The parameters for our cavities, intended to achieve nominal frequencies of around 600 MHz, are d = 10 μ, b - 0.75", a = 0.125", and l = 0.75". For these values, the logarithmic terms in (5.2) and (5.3) provide a negligible correction to lumped L-C circuit results. The relatively small size of these cavities is one of their most redeeming features. A resonant cylindrical cavity, to support a 600 MHz oscillation, would have a length of ≈ 50 cm or nearly 20 inches, whereas our reentrant cavity's largest dimension is 1.5 inches.

The benefit gained in size is offset by the loss in the cavity quality factor (Q_e), which will be discussed shortly. The quality factor is defined by

$$Q_e = \Omega_0\,\frac{\text{stored energy/cycle}}{\text{power loss/cycle}} \qquad (5.4)$$

The frequency separation between the half-power points, $\Delta\Omega_0$, also determines the Q_e:

$$Q_e \equiv \frac{\Omega_0}{\Delta\Omega_0} \tag{5.5}$$

The Q_e of a cavity resonator can be expressed approximately as

$$Q_e^{-1} = \left[\frac{\Omega_0 \mu (\text{enclosed volume})}{R_s\ (\text{surface area})}\right]^{-1} + \left[\frac{d_0}{2t\ \tan\phi}\right]^{-1} \tag{5.6}$$

where μ is the magnetic permeability, R_s is the surface resistance, t the thickness of the dielectric layer in the gap region, and $\tan\phi$ its loss tangent. Since, ignoring dielectric losses, the Q is roughly proportional to the volume of the cavity divided by the surface area, reentrant cavities tend to have smaller Q's than non-reentrant ones.

The magnetic losses described by R_s arise from the dissipative motion of the electrons within the penetration depth. Since in a superconductor the number of normal electrons approaches zero as T approaches zero, then it would seem that arbitrarily high Q's should be attainable by operating at arbitrarily low temperatures. This is not the case in practice; in fact, the Q is found to become independent of temperature below a certain temperature. This effect is described by an empirical residual surface resistance; although not

fully understood, possible contributors surface purity, surface crystal size, and surface smoothness.[5] The surface preparation techniques we have adopted are designed to maximize surface smoothness and purity.

A potentially significant contributor to residual surface resistance is that due to trapped magnetic flux.[4,6] Although there is a tendency for applied magnetic flux to be excluded by the Meissner effect, the relatively thin walls of typical cavities prevent appreciable macroscopic exclusion. There is no evidence, however, that leakage fields from the tuner magnet assemblies have a noticeable effect on our cavity quality factors.

The cavities were constructed from reactor grade niobium rod stock. Particular care is taken in preparing the surfaces which have significant electric fields across them, or which are part of a joint.[1] These surfaces include the face of the reentrant post and the flange joints. First, these surfaces are carefully ground to remove tool marks. They are then lapped to the desired dimensions using 400 and 600 grit paper. The final lapping was done on 5 μ and 2 μ grit silicon carbide coated polyester films. An optically flat lapping stone provided the working surface.

The niobium pieces are then cleaned in an ultrasonic cleaner with a detergent solution. Then the very

important process of removing the oxide layers is initiated. The pieces are dipped into a sulfate flux consisting of equal parts ammonium sulfate and concentrated sulfuric acid at a temperature of 250 °C. They are then rinsed in boiling water to remove the sulfate, and cycled through distilled water and ethanol baths. They are then stored in alcohol to prevent exposure to air. There are a variety of different oxides present on niobium surfaces and, like aluminum, niobium oxidizes quickly and strongly. Care is also taken to prevent skin oils from getting in contact with the niobium pieces.

What were the results of these careful preparations? During the course of our experiment, unloaded Q's were usually between 400,000 to 700,000, with a maximum value of 1.1 million. The indications are that, at least for the conditions of my experiment, the cavity performance is not very dependent on surface oxides. Either that, or the oxides bind so quickly that a steady state is reached prior to the first cooldown, making the surfaces during subsequent runs no different than the first.

Because of the existence of weak superconducting joints, e.g. between the cavity walls and diaphragm, the unloaded Q's can be degraded by sufficiently high power levels.[1] Prof. G. Wang has done some interesting work on optimizing the coupling in this situation.[7] For the work described here, couplings were set to one or

two orders of magnitude below critical to assure a maximum, non-degraded, Q.

G. LSU Accelerometer Operation

The LSU accelerometer is a dual reentrant cavity device designed to operate at liquid helium temperatures. The design and preparation of the cavities are discussed in the next section. The cavities are separated by a thin (1 mil) niobium diaphragm, with the spacing between the reentrant cavity posts and the diaphragm nominally being 10 μ. The tuning end of each cavity is approximately 0.025" thick and fitted with a small samarium cobalt magnet. The cavities can be individually tuned by driving the magnet right or left by superconducting coils in the tuning assembly. See Figure 5.7 for a photo of the accelerometer.

Assume that the accelerometer is AP coupled. Using the doubly balanced mixer detection scheme described earlier, the voltage response of the IF output as a function of frequency about the cavity resonance is shown in the oscilloscope photo in Figure 5.8a with labelling conventions in Figure 5.8b. This is the characteristic curve associated with the phase detection of a doubly balanced mixer. The properties of this curve determine the ultimate sensitivity of the

Figure 5.7 Photograph of LSU Accelerometer

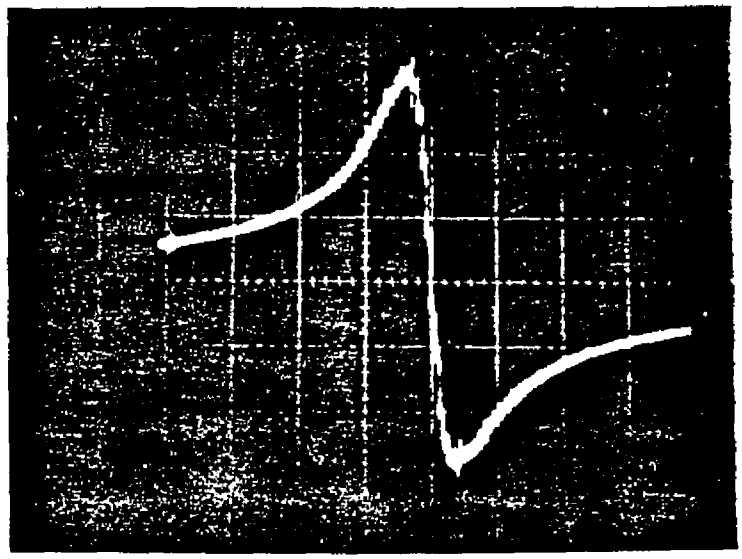

Figure 5.8 a) Oscilloscope Display of DBM-Detected Output About Cavity Resonance

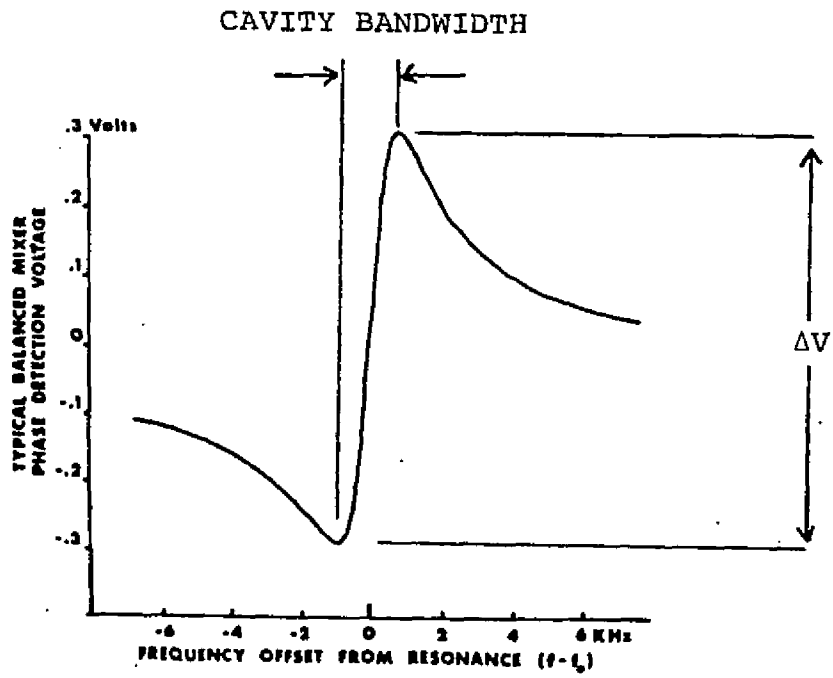

Figure 5.8 b) Labelling Conventions

accelerometer to displacements of the diaphragm. If the displacement in the diaphragm is dx, then

$$dx = \frac{2d_0}{f_0} \left(\frac{\partial f}{\partial V}\right) dV \tag{5.7}$$

where d_0 is the equilibrium gap spacing, f_0 the cavity resonance frequency, and dV the voltage response corresponding to the displacement. $(\partial f/\partial V)$ is the inverse slope of the curve at a given frequency. The accelerometer is consequently most sensitive when operated at the center of its passband. If the Q_e is large enough, then the approximation can be made

$$dx \cong \frac{2d_0}{Q_e} \left(\frac{dV}{\Delta V}\right) \tag{5.8}$$

For the parameters of the LSU accelerometer, with Q_e's near one million and maximum pump power of around -35 dBm, this approximation is correct to within 30%.

The sensitivity of the accelerometer, dV/dx, is then shown to be dependent on Q_e, the strength of the pump signal powering the cavity (ΔV), the pump frequency, and the gap spacing.

In the operation of high-Q superconducting cavities a number of unique instabilities may arise that can seriously affect the cavity response.[1] One set arises due to the interaction between the electromagnetic field

in the cavity and the diaphragm. We saw in Chapter 3 that there are back action forces on the diaphragm due to the presence of an electric field in the capacitance gap; we can express the force on the diaphragm as

$$F = \frac{1}{2} d_0 CE^2 = m\ddot{x} + b\dot{x} + kx \tag{5.9}$$

The lowest order component of this force tends to close the capacitance gap, pulling the resonance frequency to lower frequencies. Such an effect is observed when the cavity resonance frequency is measured as a function of rf drive level (see Figure 5.9[1]). If this force remains constant then it poses no problem.

The two higher order components of this force can cause serious instability problems even when the oscillator frequency is not being swept. The largest of these contribute to and modify both the spring constant k and damping coefficient b of the mechanical part of the transducer. These terms k_{em} and b_{em} display a dependence on cavity tuning ($\Delta \equiv \Omega - \Omega_0$) which, for the transducer signal matched to the cavity passband ($\Omega_0 \approx BW/2$), is given by[1]

$$k_{em} = \frac{E^2 C \Omega_0 \Delta}{2(\Delta^2 + (\frac{BW}{2})^2)} \tag{5.10a}$$

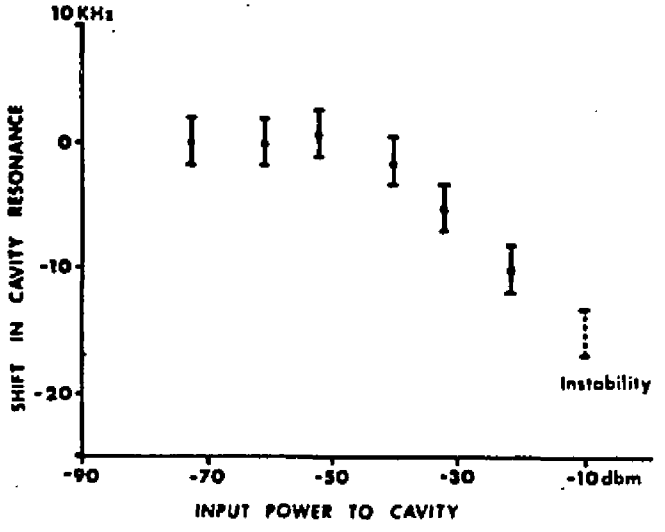

Figure 5.9 Cavity Resonance Frequency as a Function of Input Signal Power

$$b_{em} = -E^2 C\Omega_0 \cdot (BW) \cdot \Delta / (4(\frac{BW}{2})^4 + \Delta^4) \qquad (5.10b)$$

If the mechanical oscillator is a thin, well-damped diaphragm, its effective spring constant k will be modified by the additional electromagnetic term k_{em} given above. The size of k_{em} clearly depends on the rf power and on the driving frequency. If the cavity is operated near the high frequency side of its passband, $\Delta > 0$ and the effective spring constant is increased and the diaphragm is more rigid. If the cavity is operated near the low frequency side, $\Delta < 0$ and the effective spring constant is reduced, making the diaphragm less rigid. If Δ is negative enough such that $k+k_{em} < 0$, then bistability (oilcanning) may be displayed. If, however, the cavity is driven at resonance then k_{em} will be zero and these effects won't occur.

In the accelerometer applications at LSU, the diaphragm is not highly damped since the cavity is normally operated in a vacuum and the only mechanical damping is provided by acoustical losses in the niobium diaphragm. Thus b can be quite small, and the addition of b_{em} can make the total damping negative if $\Delta > 0$ or when the cavity is operated on the high frequency side of its passband. Under these conditions more rf energy is put into the mechanical resonance than is

removed and the diaphragm is driven into parametric oscillation. This kind of instability can be prevented if the cavity is operated at the center of its passband, or on the low frequency side, or if drive levels are kept sufficiently low.

During the course of the experimental research, different oscillatory modes of the diaphragm were used. Typically, three modes were strong enough to be used. Using normal mode analysis of a clamped diaphragm,[8] we present in Table 5.1 a comparison of the observed modes with their expected higher order values for one particular run.

Table 5.1

	f_{01}	f_{02}	f_{03}
Observed	5020	11560	18100 Hz
Expected	(5020)	11560	18150 Hz

The spectra of the diaphragm modes can be quite full; in Table 5.2 we show a complete set of ascertainable modes (associated with one run), with the predicted normal mode assignment and frequency value. As Paik[9] points out, the discrepancy between observed and expected values is due to the diaphragm not being exactly describable as a membrane or a plate, but displaying properties of each.

Table 5.2

	f_{01}	f_{21}	f_{02}	f_{03}	f_{23}
Observed	4140	8464	9279	13919	21514 Hz
Expected	(4140)	8860	9522	14904	19996 Hz

Figure 5.10 shows the behavior of some of these modes.[9]

Since there are two cavities, one technique to ascertain whether or not a given mode is a diaphragm mode is to search for it with each cavity. This will usually identify oscillations in the cavity endplates (i.e., in the tuning diaphragms). The easiest method of determining if a mode originates in the diaphragm is to determine if the mode can be driven into parametric oscillation. The lower-mass components of the mechanical system will be the most affected (for comparable quality factors), and the diaphragm is the lowest mass component in the system. This again is a good technique for isolating spurious modes of the tuning diaphragm from those of the diaphragm.

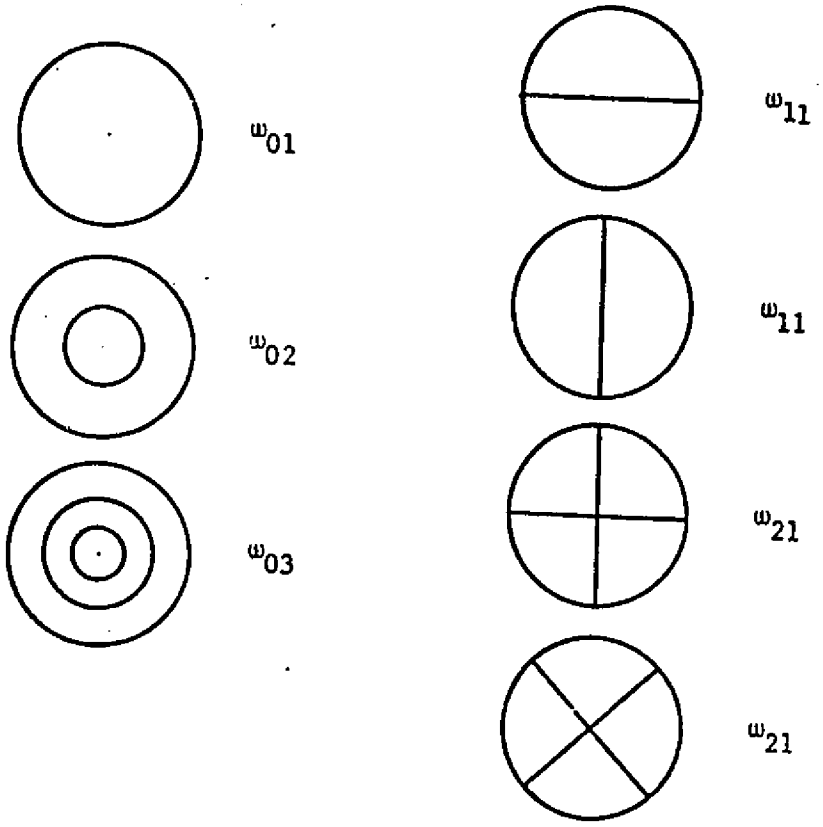

Figure 5.10 Diaphragm Behavior for Some of the Lower Modes

References

1. W. C. Oelfke and W. O. Hamilton, Rev. Sci. Instr. 54, 410 (1983).

2. A. G. Mann, IEEE Trans. MIT-33, 51 (1985).

3. This discussion can be found in most microwave engineering texts. Two good texts are E. L. Ginzton, Microwave Engineering, (McGraw-Hill, New York, 1957) and S. Y. Liao, Microwave Devices and Circuits, (Prentice Hall, Englewood Cliffs, New Jersey, 1980).

4. A. G. Mann, Ph.D. Dissertation, Univ. of Western Australia, (1982).

5. J. M. Pierce, Methods of Experimental Physics.

6. J. M. Pierce, Ph.D. Dissertation, Stanford University, (1967).

7. G. Wang, (1985) to be published.

8. H. Wyld, Methods of Mathematical Physics, lecture notes, (1976).

9. H. J. Paik, Ph.D. Dissertation, Stanford University, (1974).

CHAPTER 6

EXPERIMENTAL RESULTS FOR MIXER-GENERATED PS/BAE CAVITY INPUT

A. Introduction

In this chapter we present the experimental evidence for phase sensitive detection and back action evasion for mixer-generated two-stick input signals. The use of a doubly balanced mixer is crucial if a phase noise reduction technique such as the one devised by Mann[1] is to be employable (as this technique can only work on one oscillator). Within the limitations posed by the mixer, we determine the dependence of phase sensitivity and BAE to various parameters, such as frequency detuning and sideband amplitude differences. The first part of this chapter will deal with the evidence for PS detection; the final part will be a reprint of a Physics Letters A article[2] presenting evidence for BAE.

B. Experimental Evidence for Phase Sensitive Detection

The experimental evidence for PS detection is obtained through examination of the output of the mixer used to detect the cavity signal. The DC- and ω-components of this output have special forms and

dependences peculiar to the type of coupling to the diaphragm. We will explore some examples of PS behavior in this section and in the next chapter.

The cavity input signal is critical in establishing a PS coupling. As mentioned in Chapter 5, two methods for generating the input currents were used. The method applied in this chapter utilizes a doubly balanced mixer to generate the dual sidebands (see Section E, Chapter 5). The mixer allows the appropriate signal to be created with both minimal equipment and the desired fixed phase relationship between the sidebands. There are a couple of drawbacks to its use, however. First, the two-stick amplitudes are not exactly equal; the two different mixers used in dual sideband generation exhibited amplitude imbalances of between 2% and 6%. Second, the mixers also show fairly significant contributions at Ω_0 and equivalent contributions at $\Omega_{2\pm}$. Thus the mixer-generated sidebands only closely approximate the ideal single transducer coupling.

To compensate for the fixed nature of mixer-generated sideband amplitudes, a single-sideband (SSB) modulator was built to allow some degree of amplitude adjustment.[3] The set-up for the SSB modulator is shown in Figure 6.1. This device allows the upper (Ω_+) or lower Ω_-) sideband to be suppressed, letting simple amplitude dependences to be tested. The other way to test sideband

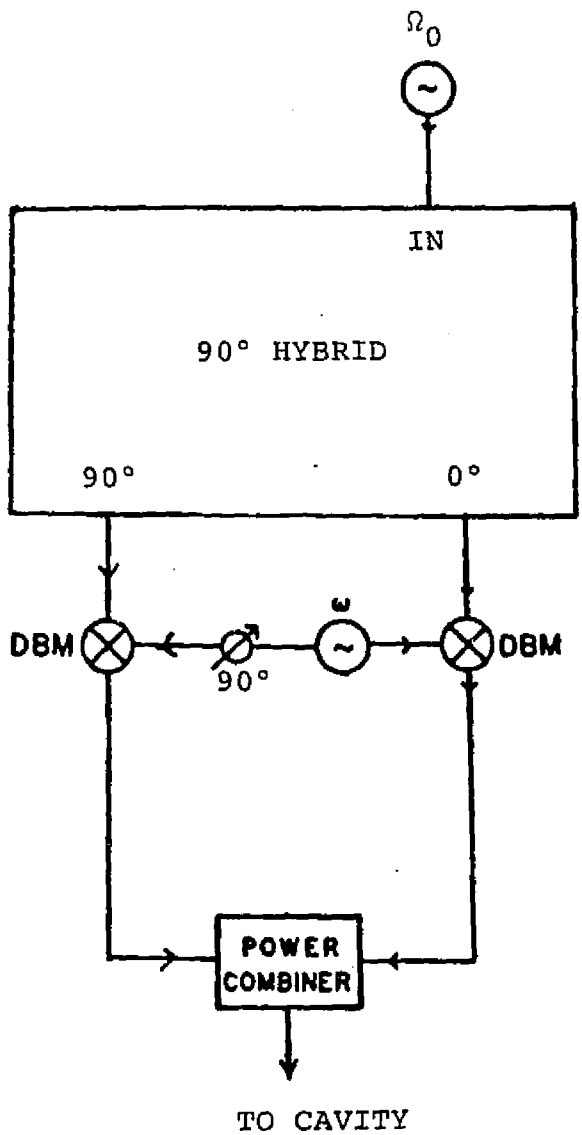

Figure 6.1 Schematic of the Single-Sideband Modulator Circuitry

dependences is to take advantage of the cavity passband; shifting the center of the two sidebands causes the passband filtering to alter the sideband amplitudes due to the cavity Lorentzian factor. However, relying on cavity filtering to adjust amplitudes also introduces unwanted relative phase shifts between the sidebands.

The non-ideal nature of the mixer generated signal does not preclude phase-sensitive detection or squeezing (which will be discussed later in the chapter). If we rewrite (3.10) to reflect the mixer input and take into account that $X_1 = x_0 \cos \Phi$ and $X_2 = -x_0 \sin \Phi$ and assume $i_{+c} = i_{-c} \equiv I$ (where $i_{\pm s} = 0$), then (for BAE phase)

$$V_{DC} = \frac{R\, Q_e\, I\, X_0}{4(1+T^2)d_0} \{\cos \Phi - T \sin \Phi\} \qquad (6.1)$$

where Φ is the PZT drive phase relative to the two sticks.

That the input couples to predominantly one of the diaphragm coordinates, i.e. phase-sensitively, can be shown by plotting the detected DC (mixer) output as a function of the phase of a PZT transducer driving the diaphragm. This is done in Figure 6.2, where the DC output data is plotted against $\cos \Phi - 6 \sin \Phi$ (the theoretical plot would be shifted some 40° to the right for $T = 1$). Other conclusive displays of PS detection

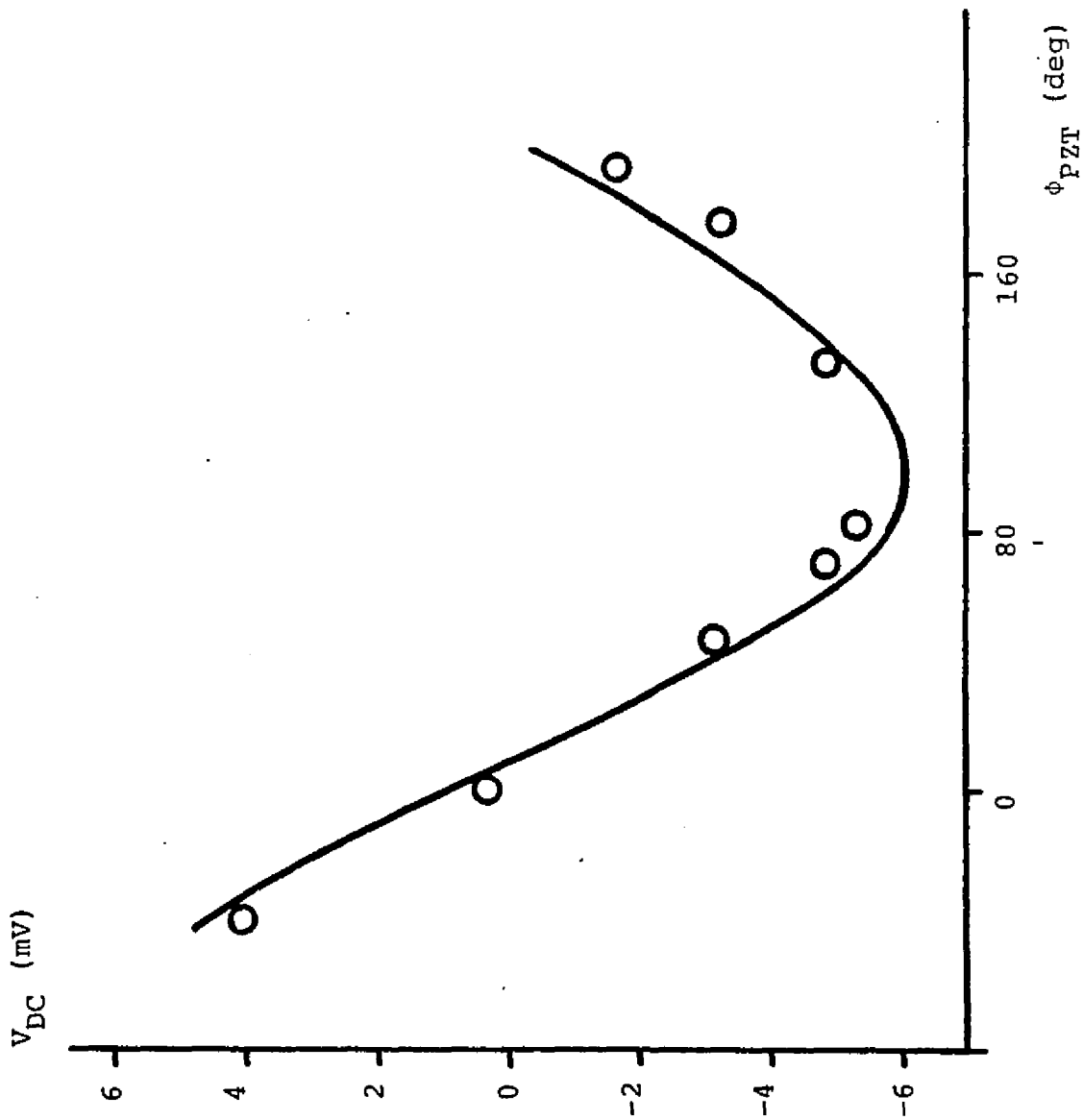

Figure 6.2 DBM DC-Component versus PZT Drive Phase

will be seen in the next chapter.

Figure 6.2 is direct evidence of PS detection, i.e., it will be this component of the DBM that will be monitored in an actual application of this technique. Thee are other ways to reinforce the claim for phase sensitive detection, and one of these is to examine the behavior of the ω-component of the detected output. Equation (3.11a) gives the general result, and for mixer-generated input signals becomes

$$V_\omega \cong \frac{RQ_e}{2(1+T^2)d_0} \{[i_{0c}\, TX_1 + i_{0c}\, X_2] \sin \omega t$$

$$+ [i_{0c}\, X_1 - i_{0c}\, TX_2] \cos \omega t\} \qquad (6.2)$$

Since $i_{+c} = i_{-c}$, the only contributions to this component are those X_1, X_2 terms containing the in-phase leakage at Ω_0. It is this result that allows the proper LO phase to be chosen: turn off the PZT drive and adjust the LO phase shifter to minimize the ω-component, and the proper detection phase will have been established. Evidence of the establishment of PS detection using the ω-component (6.2) of the detected output is shown in Figure 6.3. For a given PZT drive amplitude, the ratio of the in-phase lockin signal and the quad-phase lockin signal is presented as a function of the PZT

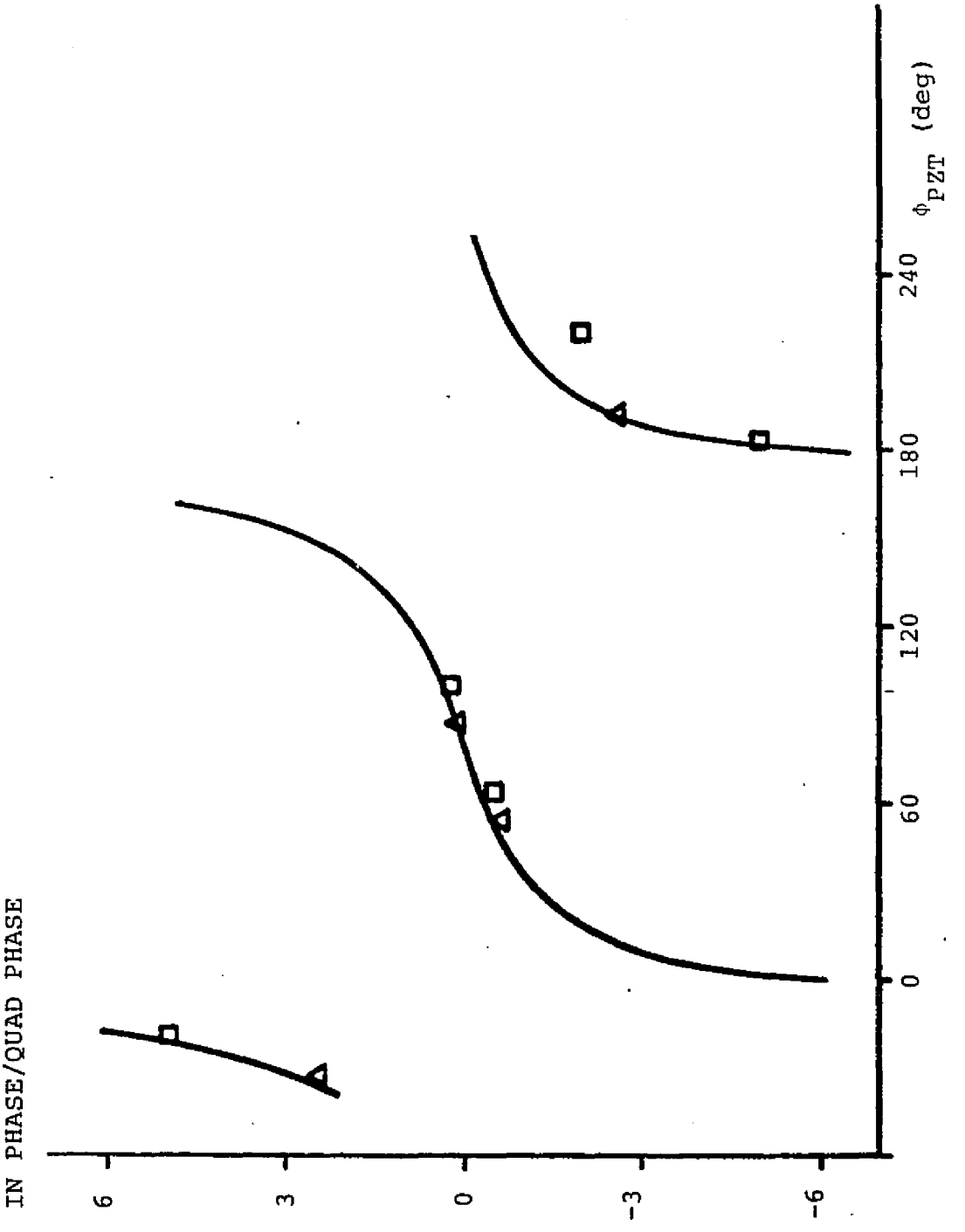

Figure 6.3 DBM ω-Component versus PZT Drive Phase

phase (for two chronologically separated runs), and compared to the theoretical expectation for T = 6. The close agreement between the data and the theoretical curve further substantiates the phase sensitive coupling of the two stick input.

A further validation of the initiation of a PS coupling scheme is given by the system response to imbalances in the two sidebands. Using the SSB modulator, for a given set of RF and LO power levels (mixer function is dependent upon these parameters) the spectrum looks as in Table 6.1, where the relative values of the amplitudes are given.

Table 6.1

Ω_-	Ω_0	Ω_+	
0.120	0.315	1.000	(upper sideband)
1.000	0.315	1.150	(lower sideband)
0.580	0.225	0.575	(dual sideband)

(The dual sideband output is obtained by disconnecting one of the SSB mixers, making this a single mixer generated output.)

Now, for $\alpha = 0$, the ratio of the quad LO phase ω-component divided by the BAE LO phase ω-component should be the same as the ratio $(i_{+c}-1_{-c})/(i_{+c}+i_{-c})$ for a PS

coupling to the diaphragm. This is verified in Table 6.2, where the experimentally determined ω-component ratios versus the ratios of the sideband imbalances are given.

Table 6.2

	ω-comp. ratio (BAE/quad LO phase)	$(i_{+c}-i_{-c})/(i_{+c}+i_{-c})$
(Upper sideband)	0.763 ± 3%	0.787 ±1%
(Lower sideband)	0.741 ± 3%	0.741 ±1%
(Dual sideband)	0.011 ±10%	0.003 ±1%

Amplitude dependence of PS coupling will be examined in more detail in the next chapter; in the meantime, this prototypical data was very encouraging, and typical of the success achieved in attaining PS detection even under non-ideal conditions.

Another property of PS coupling is its response to currents at Ω_0, as seen in the terms containing X_1 and X_2 in the ω-component expressions (see, e.g. (6.2)). The effect of i_{0c} can be tested using carrier suppression with balanced sidebands; the ratio of the ω-components (in the BAE LO phase) with and without carrier suppression should be the same as the ratio of the respective i_{0c}'s. This is verified experimentally, where a 15 dB (±.5 dB)

suppression of i_{0c} gives rise to a 15.6 dB (±.3 dB) decrease in the ω-component amplitude ratio. The quad LO phase can also be used to test the PS-coupled response (see (3.11b)) to i_{0c}, since the DC component is directly proportional to i_{0c}. This can be seen in oscilloscope photos in Figure 6.4, where Figure 6.4a shows the non-suppressed DC- and ω-components, and Figure 6.4b shows the system response to a carrier suppression of about 30 dB. The ω-component does not depend on i_{0c}, and this is also supported by the photos.

Standing alone, the data just presented provides conclusive evidence for the establishment of a phase-sensitive detection scheme with its preferred coupling to one of the oscillator coordinates (X_2 in this experiment). The next chapter expands upon these tests with the introduction of independent sidebands and their attendant flexibility.

C. Experimental Evidence for Back Action Evasion of Amplifier Force Noise: A Physics Letters A Publication [2]

This section presents in toto our Physics Letters publication of 9/20/84. The text is exactly as it was published, so portions of the article conform to certain definitions that are slightly different than those used elsewhere in this dissertation. The references at the end of the

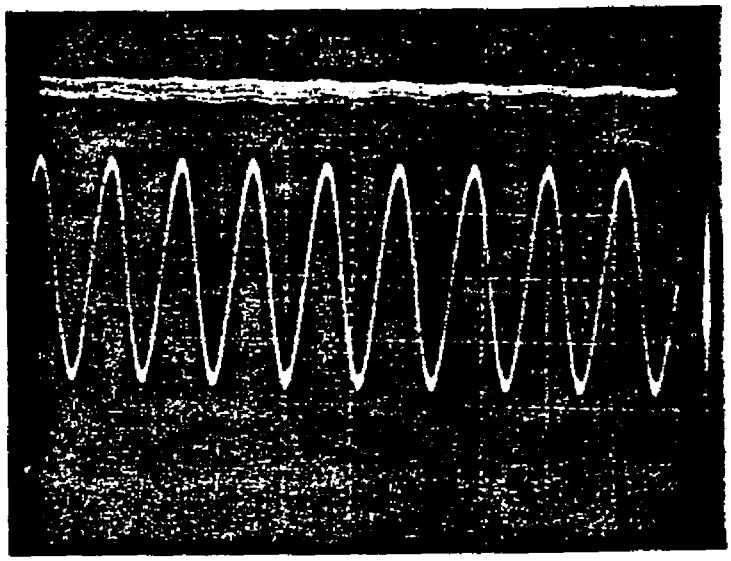

Figure 6.4 a) Oscilloscope Display Showing DBM DC- and ω-Components Without Carrier Suppression

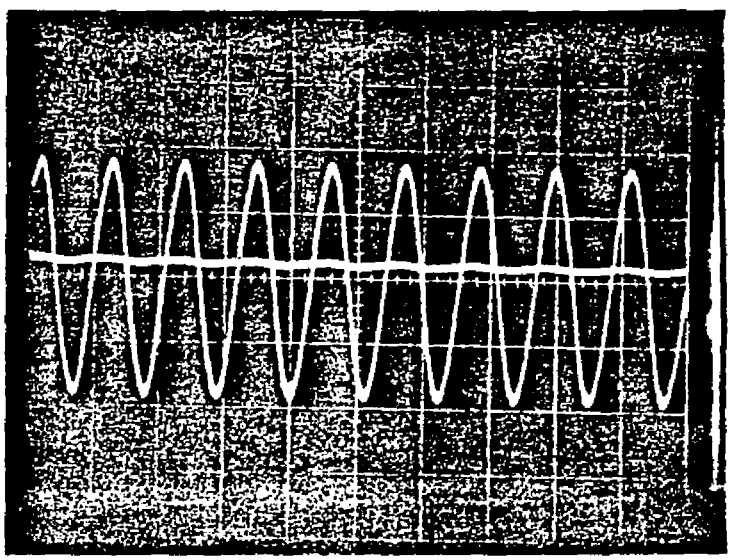

Figure 6.4 b) Oscilloscope Display Showing DBM DC- and ω-Components With Carrier Suppression

article will refer only to that article; the reference page at the end of this chapter will cover all other parts of the chapter.

We introduce the first reported evidence for back-action evasion in this article. The (AP-coupled) monitor cavity allows X_1 and X_2 to be monitored, and the effects of amplifier back reaction noise to be ascertained. Comparison of the effects of this noise on the two quadrature components of the diaphragm motion gives the squeezing factor. Squeezing evidence will be examined more thoroughly in the next chapter.

EXPERIMENTAL VERIFICATION OF A SINGLE TRANSDUCER BACK-ACTION EVADING MEASUREMENT SCHEME FOR A GRAVITATIONAL WAVE DETECTOR

The linear amplifier limit to the precision with which one can measure the symmetrical coordinates, X_1 and X_2, of a mechanical oscillator such as a resonant gravitational wave antenna, is given by the minimum uncertainty relation[1]

$$\Delta X_1 \Delta X_2 = kT_A(\Omega)/m\omega\Omega \equiv A^2 , \qquad (1)$$

where Ω is the frequency at which the amplifier operates, $T_A(\Omega)$ is the amplifier noise temperature, m is the oscillator effective mass and ω its frequency. In the case where Ω and ω are not identical, the displacement is sensed by a frequency-translating (parametric up-converter) transducer, such as a capacitance-modulated radio frequency LCR circuit, which produces frequency modulation sidebands at a high carrier frequency ($\Omega \gg \omega$) in response to the mechanical modulation at ω. X_1 and X_2 are related to the oscillator's position variable by

$$x = X_1 \sin \omega t + X_2 \cos \omega t . \qquad (2)$$

Conventional transducers measure X_1 and X_2 with equal precision, which constitutes an amplitude and phase (A&P) measurement. Hence the quantity A is referred to as the linear (or standard) amplifier limit (SAL) in the classical regime ($kT_A >> \hbar\Omega$), and the linear amplifier (or standard) quantum limit (SQL) when $kT_A \sim \hbar\Omega$. The single back-action evading (BAE) transducer proposed by Thorne et al.[1] for which four designs have been published,[2-5] circumvents the SAL or SQL by reducing either ΔX_1 (or ΔX_2) below A, in exchange for increased uncertainty in the other (unwanted) coordinate. Phase sensitive coupling in this device makes it selectively sensitive to one coordinate, say X_1, while simultaneously channelling most of the amplifier back-action noise into the unwanted coordinate (X_2). Thus a BAE measurement "squeezes" the uncertainties in the coordinates, yielding

$$(\Delta X_1)^2_{min} = A^2/\Sigma \ , \qquad (3)$$

where $\Sigma \equiv \Delta X_2/\Delta X_1 > 1$ is the squeezing factor.

Our realization of a BAE transducer is a superconducting reentrant cavity[5-7] which only exhibits the required selective sensitivity when two conditions are fulfilled. The first is that the quantity

$$T \equiv 2Q\omega/\Omega \ , \tag{4}$$

where Q is the cavity electrical quality factor and Ω the resonant frequency, be much greater than unity. The second is that the cavity be excited by a pair of carriers of the same quadrature at $\Omega+\omega$ and $\Omega-\omega$. The magnitude of both the selective sensitivity to X_1 on the output and insensitivity to noise fed back into X_1 is enhanced by the cavity filtering factor, T. Selective sensitivity on the output does exist with only one carrier present (at $\Omega-\omega$ or $\Omega+\omega$) but this configuration exhibits no selective insensitivity to back-action noise. Further, operation with a single carrier at $\Omega+\omega$ is even potentially unstable because of parametric oscillation.[7] Modelling the cavity as a parallel LCR circuit, the excitation signal can be expressed as a constant current source:

$$I_{in} = I[\cos(\Omega+\omega)t + (1+2\delta)\cos(\Omega-\omega)t + \gamma \cos \Omega t] + i_n(t) \ . \tag{5}$$

Here δ and γ represent imperfections in the technique used to generate the pair of carriers and $i_n(t)$ represents the noise currents due to the linear amplifier and the pump, at Ω, $\Omega\pm\omega$ and $\Omega\pm2\omega$. Motion induces

modulation sidebands in the output voltage which are predominantly at the carrier frequency (Ω) when $T >> 1$. Ignoring noise terms we have

$$V_{out} \approx x_0^{-1} IR(\Omega/\omega) \{[X_1+X_2/T] \sin \Omega t + [\delta X_2 + x_0(\omega/\Omega)\gamma] \cos \Omega t\} , \quad (6)$$

where $x_0 \equiv (d \ell n\, C/dx)^{-1}$ is the dynamic capacitor plate spacing. The recovered output signal ($\sin \Omega t$) is essentially X_1, with a small fraction (T^{-1}) of X_2 contamination. Unless one wants to make a very wideband transducer, one can ignore the X_2 contamination on the output which appears at the sideband frequencies $\Omega \pm 2\omega$ since it is easily removed by postdetection filtering.

Since the back-action force, F_{ba}, on the mechanical oscillator arises from the rf time average of the square of the capacitor plate voltage one only has to consider pairs of currents (noise x carrier, or noise x noise) with a frequency separation ω. Under ideal conditions ($\delta = \gamma = 0$ and $T >> 1$) the only appreciable noise currents are those at Ω, i.e.

$$i_n(t) = i_c(t) \cos \Omega t + i_s(t) \sin \Omega t ,$$

in which case

$$F_{ba}(t) = \frac{i_c(t)\,ICR^2}{x_0(1+T^2)}\,(T \sin \omega t + \cos \omega t) \ . \qquad (7)$$

Since at resonance F_{ba} is in quadrature to x, Eq. (7) implies that the noise injected into the X_1 coordinate is T^{-1} times smaller than that injected into X_2. Thus our transducer has the required selective sensitivity to X_1 at the output and insensitivity to noise injected into X_1 at the input. One can show that even for frequencies outside the bandwidth of the mechanical oscillator the square root ratio of spectral densities, $(S_{\Delta X_2}/S_{\Delta X_1})^{1/2}$, is identically T for frequency offsets as large as $2\omega/T^2$.

A more rigorous analysis, assuming amplifier thermal noise dominates pump noise and considering all currents at Ω and $\Omega \pm \omega$, yields a squeezing factor

$$\Sigma = T\left[\frac{1 + (\eta^2 + \frac{1}{2}\gamma^2)(1 + 1/T^2) + (\delta/T)^2}{1 + T^2[(\eta^2 + \frac{1}{2}\gamma^2)(1 + 1/T^2) + \delta^2]}\right]^{1/2} , \qquad (8)$$

where η is approximately the ratio of the thermal noise current in the mechanical resonator bandwidth to the sideband currents (I). Normally η is entirely negligible,

being of order 10^{-7}, but not for the experiment described here. The imperfections δ and γ severely limit the squeezing obtainable at high $T(\Sigma \sim (\delta^2+\frac{1}{2}\gamma^2)^{-\frac{1}{2}})$ since they represent contamination of the excitation currents by currents appropriate for an A&P measurement scheme. Intuitively one expects the squeezing factor appropriate to Eq. (3) to be T [or its non-ideal value, Eq. (8)]. This is essentially the same result given by Braginsky et al.,[8] Blair[4] and Caves.[9] We defer a full discussion of this question and a complete noise analysis of the transducer for a future publication.

The experimental apparatus to study the properties of our BAE transducer is shown schematically in Fig. 1. The transducer is designed with two reentrant cavities capacitively coupled to a tensioned diaphragm which is the mechanical resonator. The diaphragm has a fundamental mode frequency $\omega/2\pi$ = 4.1 kHz, a mechanical quality factor of 800 and an effective mass $m \sim 2\times10^{-5}$ kg. Such a low mass provides strong coupling between the rf fields and the mechanical resonator. The monitor cavity (A) is driven at a low power level ($\sim10^{-9}$ W) and coupled through an amplifier to a double balanced mixer to produce a voltage proportional to the diaphragm displacement x. A two phase lock-in detector recovers the X_1 and X_2 components. Although the monitor cavity constitutes an A&P measurement of the diaphragm, the

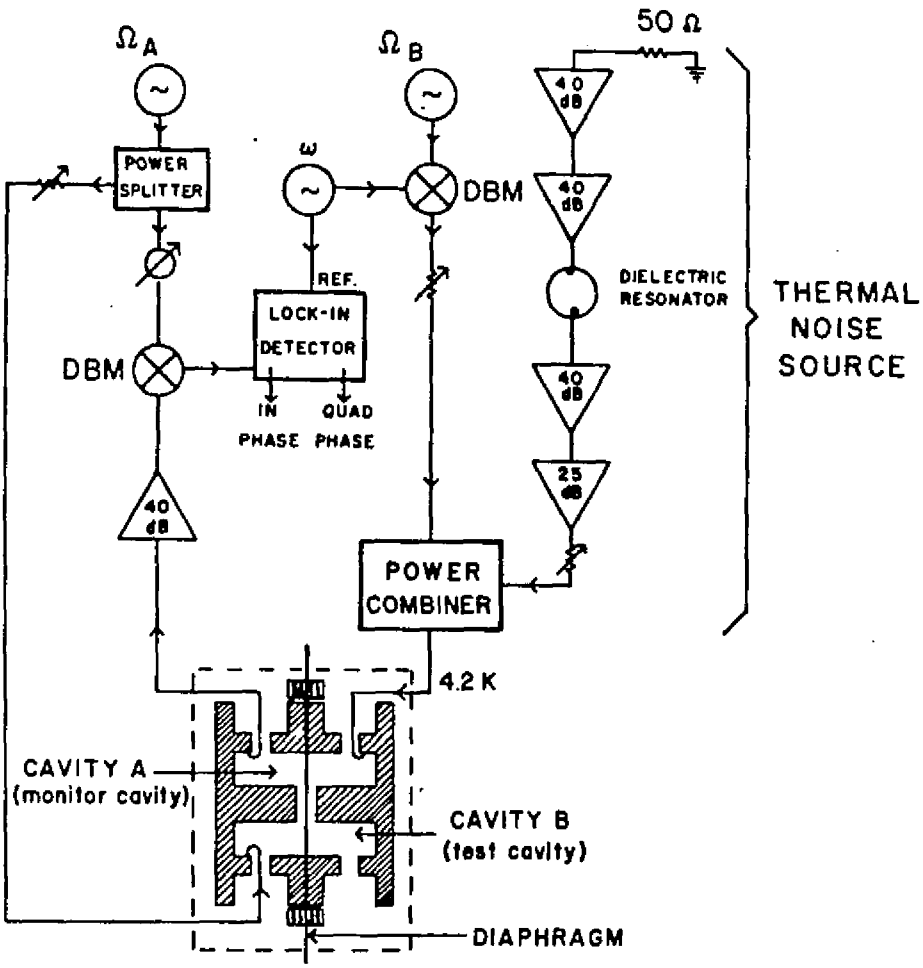

Fig. 1 Schematic diagram of the experimental BAE transducer.

back-action produced is too low to be seen above the diaphragm's brownian motion at 4.2 K ($\sim 10^{-14}$ m). Therefore the monitor cavity negligibly perturbs the mechanical oscillator. On the other hand, the test cavity (B) is driven at rf power levels of 10^{-7} to 10^{-5} W to produce easily observable back-action noise ($x_{rms} \sim 10^{-12}$ m). To achieve this the amplifier noise is elevated to an artificially high level ($\eta \sim 0.1$), 10^{-6} W Hz^{-1}, using an amplifier chain with a gain of 145 dB and a high Q ($\sim 10^4$) dielectric resonator[10] transmission filter to prevent saturation in the later stages. The two cavities are totally independent of one another electromagnetically; A being resonant at 602 MHz and B at 618 MHz, with Q's of $3x10^5$ and $6x10^5$ respectively.

By driving the mechanical oscillator with fixed X_1 and X_2 via a piezoelectric transducer attached to the cavity end wall we have verified the form of the output voltage, Eq. (6). The signal demodulation scheme for cavity B (suppressed in Fig. 1 for clarity) is essentially similar to cavity A, with the exception that the information is available at dc, hence no lock-in detector is required. The qualitative difference between A&P and BAE is illustrated in Fig. 2 where actual time-lapse photographs of the X_1, X_2 phase plane are displayed. In Fig. 2 on the left (A&P) the excitation current has the conventional form $I_{in} = I \cos \Omega t$ and

Fig. 2 Time-lapse display of the X_1, X_2 phase plane; left: No equeezing is evident, with X_1 and X_2 receiving equal noise; right: Squeezing is evident here, with the ellipse indicating squeezing of the injected noise. The two ellipses differ by a shift in the lock-in reference phase of 90°.

it is seen that there is equal uncertainty in X_1 and X_2; the noise is confined to a circular area no (no squeezing). In Fig. 2 on the right (BAE) the noise is squeezed into an elliptical area. The two ellipses obtained by shifting the lock-in reference phase by 90° diaplay a squeezing factor (major axis/minor axis) of about 4.

The pair of quadrature outputs of the lock-in detector, denoted by X_1' and X_2', are related to X_1 and X_2 by

$$X_1' = X_1 \cos\theta - X_2 \sin\theta, \quad X_2' = X_1 \sin\theta + X_2 \cos\theta, \tag{9}$$

where θ is the reference phase. Thus the observed squeezing factor, $\Delta X_2'/\Delta X_1'$, depends on the reference phase. To correctly measure Σ requires setting $\sin\theta = 0$. For other values of θ the observed squeezing factor is, in geneal, less than Σ. For $|\sin\theta| = 2^{-1/2}$ it is approximately unity; while for $|\sin\theta| = 1$ the quadratures interchange, hence $\Delta X_2'/\Delta X_1' = 1/\Sigma$. This behavior is clearly seen in Fig. 3 where spectra of $\Delta X_1'$ and $\Delta X_2'$ for the 4.1 kHz mode are displayed on the left and the corresponding phase plot on the right, for $\theta = 0°$, 45°, 90° and 135°. The roll-off outside the mechanical

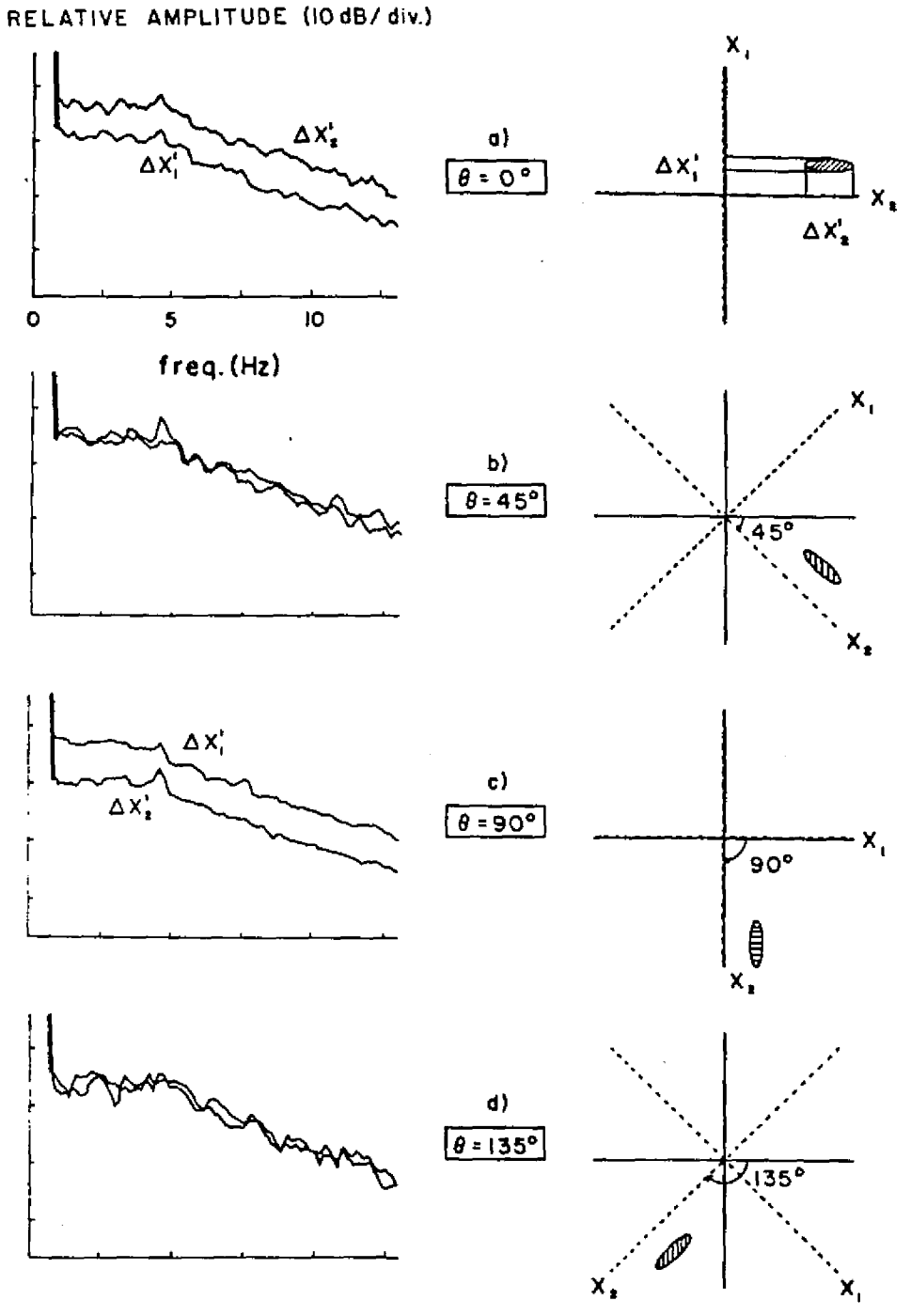

Fig. 3 On the left side are spectra of X_1' and X_2' for (a) $\theta = 0°$, (b) $\theta = 45°$, (c) $\theta = 90°$, and (d) $\theta = 135°$ and the corresponding phase plane representation on the right. Maximum squeezing occur in (a) and (c), and no squeezing is seen in (b) and (d).

resonator's bandwith is clearly visible above 4 Hz. The corresponding phase plane plot exhibits rotation of the noise ellipse by the reference angles in accordance with Eq. (9).

The maximum squeezing factor inferred from the spectra (corresponding to Fig. 2b) is 4.0±0.5 (12±1 dB). This is approximately half the ideal value, T = 8.2 and about 3 dB larger than that inferred from Fig. 3a or c. For two other diaphragm modes at 8.5 and 13.9 kHz, the maximum squeezing factors inferred from the spectra are 6.3±0.7 and 15±3, respectively, which are also lower than the ideal values, T = 16.9 and 27.8. To explain the less than ideal squeezing one has to invoke Eq. (8). This is plotted in Fig. 4 for the three values of T and typical parameters of the modulating mixer ($\delta = 0.3$, $\gamma = 0.06$) and noise source ($0.005 < \eta < 0.3$). Given the uncertainty in determining η there is reasonable agreement between Eq. (8) and our three experimental points. Clearly if one could reduce η to 0.01 one would only be limited by mixer imperfections: $\Sigma \sim T/[1 + T^2(\delta^2 + \frac{1}{2}\gamma^2)]^{\frac{1}{2}}$. Because of the relatively poor vibration isolation of our cryostat, especially at the lower modes, one has to keep $\eta \sim 0.1$ to override environmental noise which competes with F_{ba} and acts to reduce the squeezing. However if η were increased to near unity one observes a phase plane

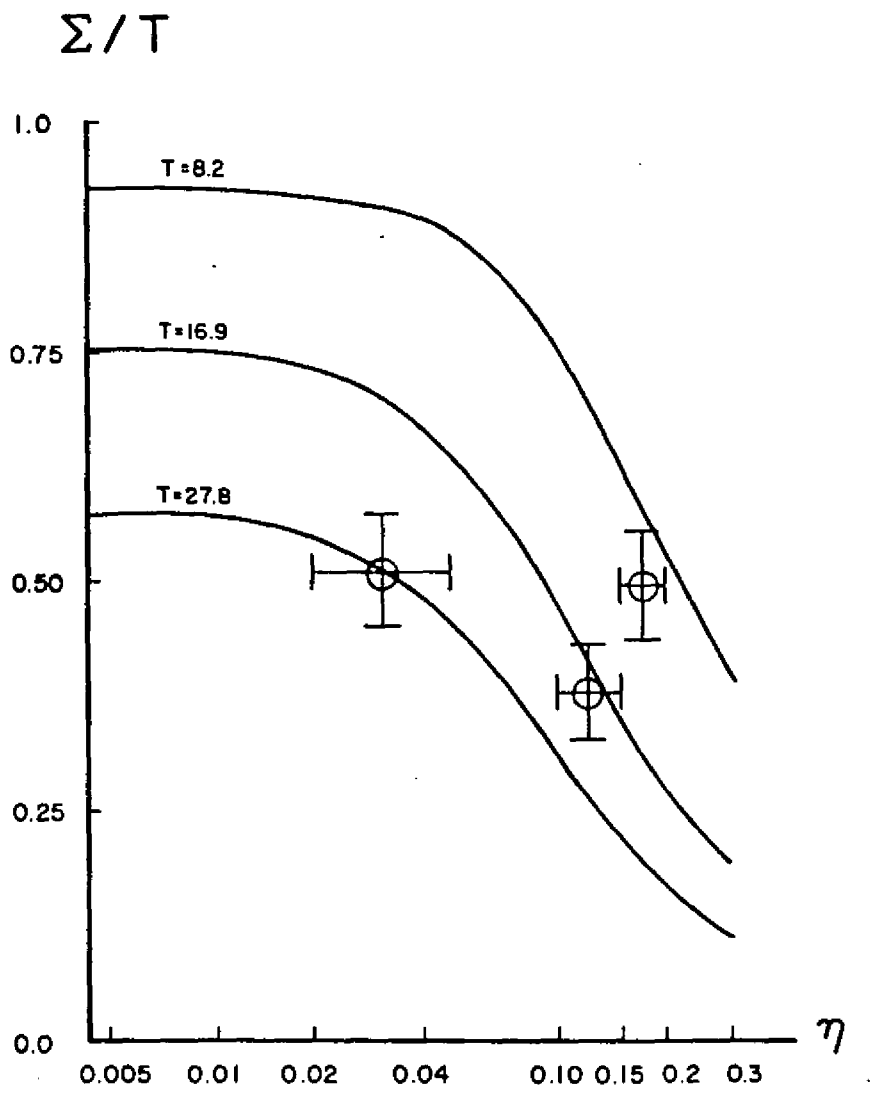

Fig. 4 Σ/T versus η for three values of T. The cross-bars indicate the experimental regime in which data was taken at each T value.

plot like on the left of Fig. 2 (no squeezing). Physically this means that the force noise is predominantly due to the cross-product of thermal noise currents at Ω and $\Omega \pm \omega$, which is obviously carrying the simulation too far.

In conclusion, a BAE transducer with a configuration described has demonstrated squeezing of the back-action noise of a simulated readout amplifier, in accordance with theory. Squeezing is limited primarily by cavity Q, and imperfections in the modulator providing the excitation signal.

This work was supported in part by a National Science Foundation grant PHY-81-07388 to LSU and an NBS Precision Measurements grant NB80-NADA-1049 to the University of Central Florida.

References

1. K. S. Thorne, C. M. Caves, V. D. Sandberg, M. Zimmerman and R. W. P. Drever, in: Sources of gravitational radiation, ed. L. L. Smarr, (Cambridge Univ. Press, London, 1979) p. 55.

2. V. I. Panov and J. Y. Khalili, 9th Intern. Conf. on General relativity and gravitation, Abstracts 2 (1980) 397.

3. M. F. Bocko, L. Narici, D. H. Douglass and W. W. Johnson, Phys. Lett. 97A (1983) 259.

4. D. Blair, Phys. Lett. 91A (1982) 197.

5. W. C. Oelfke, G. Spetz and W. O. Hamilton, Bull. Am. Phys. Soc. 26 (1981) 1215.

6. W. C. Oelfke, in: Quantum optics, experimental gravitation and measurement theory, eds. P. Meystre and M. O. Scully (Plenum, New York, 1983) p. 675.

7. W. C. Oelfke and W. O. Hamilton, Rev. Sci. Instrum. 54 (1983) 410.

8. V. B. Braginsky, Yu. I. Vorontsov and K. S. Thorne, Science 209 (1980) 547.

9. C. M. Caves, in: Quantum optics, experimental gravitation and measurement theory, eds. P. Meystre and M. O. Scully (Plenum, New York, 1983) p. 567.

10. A. G. Mann, Active stabilization of crystal oscillator FM noise at UHF using a dielectric resonator, submitted to IEEE Trans. MTT.

References

1. A. G. Mann, IEEE Trans. MIT-33, 51 (1985).

2. G. W. Spetz, A. G. Mann, W. O. Hamilton, and W. C. Oelfke, Physics Letters 104A, 335 (1984).

3. 1984 Radio Amateur's Handbook (American Radio Relay League, Newport, 1983).

CHAPTER 7

EXPERIMENTAL RESULTS FOR INDEPENDENTLY-GENERATED PS/BAE CAVITY INPUT

A. Introduction

In this chapter we provide more evidence for phase sensitive detection and back-action evasion using independently-generated dual-sideband input signals. We take advantage of the inherent flexibility offered by this coupling scheme by testing PS and BAE response to various input signal parameters. We also show the response of squeezing to amplifier back reaction and environmental noise levels. We conclude by determining the effect of oscillator phase noise and detuning of the two-stick pair on squeezing.

B. Experimental Evidence for Phase Sensitive Detection

We present evidence for PS coupling to the diaphragm by determining the DC voltage output, for the BAE LO phase, as a function of the PZT driving phase. Figure 7.1a is for a given PZT drive ($\approx 10^{-13}$ m), while Figure 7.1b is for a PZT drive amplitude 4 dB less than that in Figure 7.1b. (The theoretical curves are for T = 16). As stated in Chapter 6, it is this output component

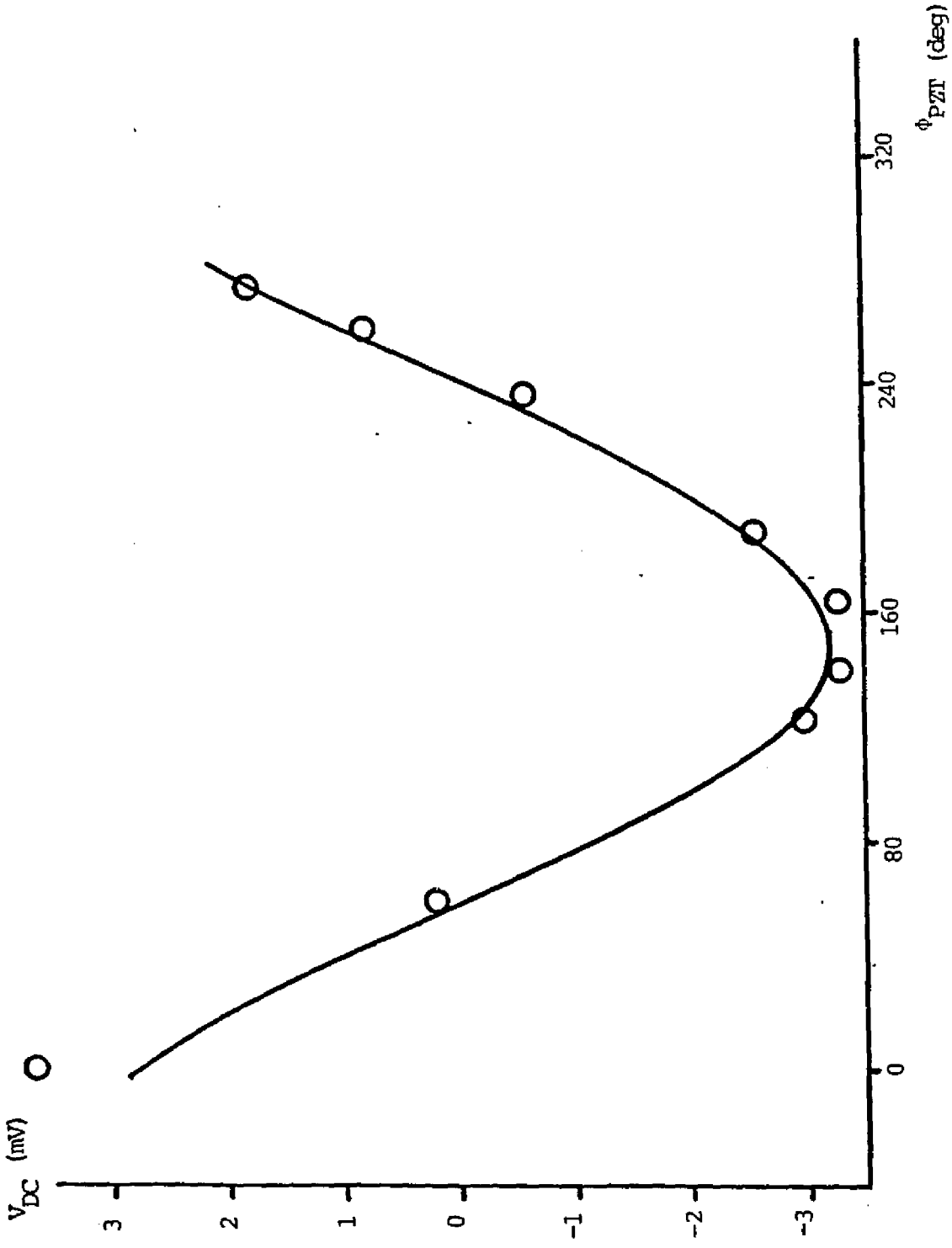

Figure 7.1 a) DBM DC-Component versus PZT Drive Phase for a Given Drive Amplitude

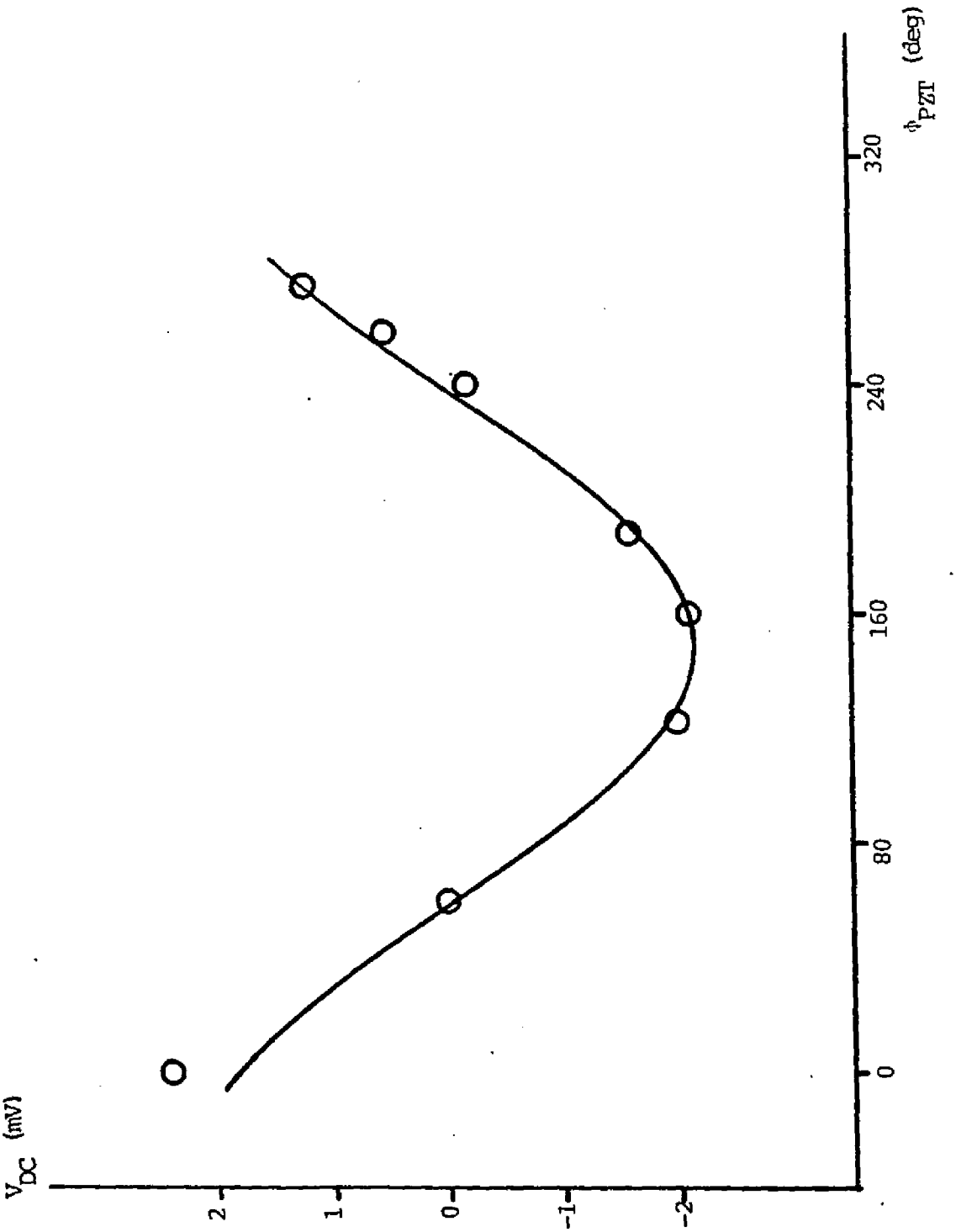

Figure 7.1 b) DBM DC-Component versus PZT Drive Phase for the Drive Amplitude in a) reduced by 4 dB

that would be monitored if the system was operated as a transducer.

Indirect support for the existence of PS coupling can be seen by examining the dependence of the output ω-component on the phases of the individual input sidebands, a test which can not be performed with a mixer-generated signal. One such set of data is presented in Figure 7.2 a-b, which show the lockin in-phase/quad-phase ratios, for the BAE LO phase, as a function of the phase of the upper and lower sideband, respectively (for T = 12.9). Each plot displays the response appropriate for phase sensitive coupling.

Figure 7.3a and 7.3b continue the indirect support by showing the in-phase/quad-phase (ω-component, BAE phase) response as a function of phase when only i_{-c} and i_{+c}, respectively, are present (with theoretical curves for T = 19.7). The responses shown in Figures 7.2 and 7.3 reinforce our identification of the individual sideband and mixer LO phases and confirm the establishment of PS detection.

As of this writing, only one other group[1] has published corraborating evidence indicating phase sensitive coupling to a harmonic oscillator. Our evidence, however, is much more comprehensive and provides a stepping stone to the goal of this research: does PS coupling allow amplifier back reaction force noise to be evaded

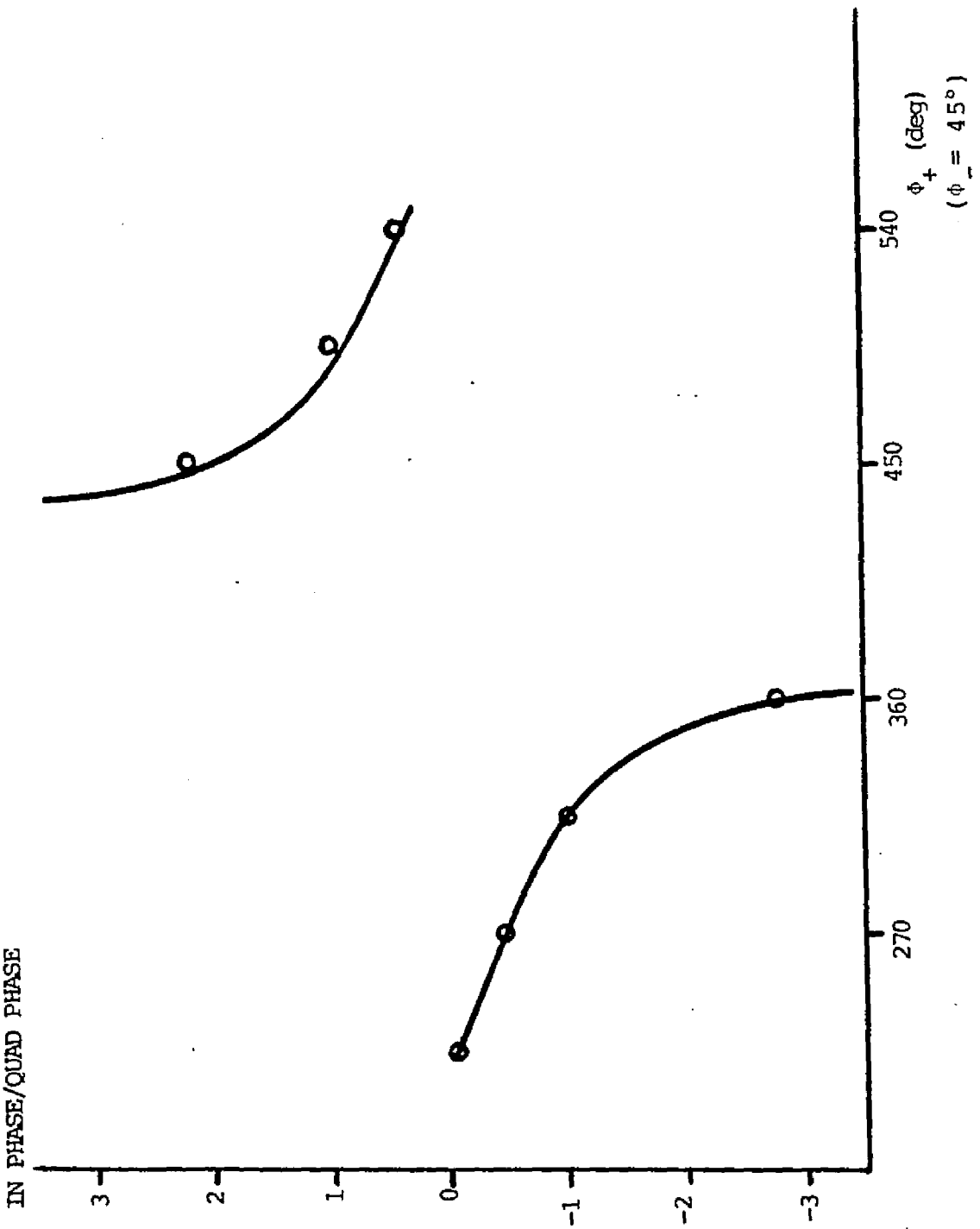

Figure 7.2 a) DBM ω-Component versus Upper Sideband Phase

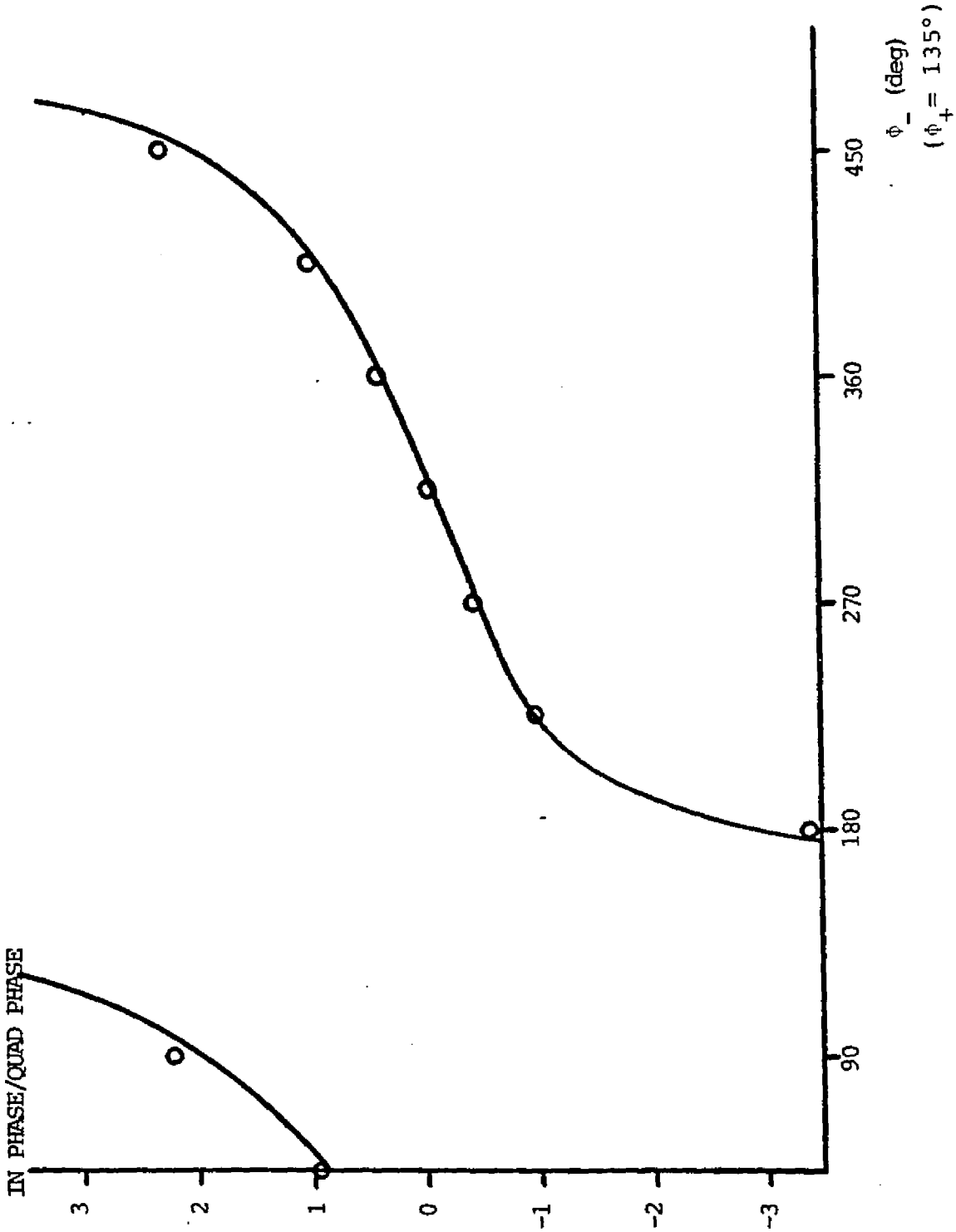

Figure 7.2 b) DBM ω-Component versus Lower Sideband Phase

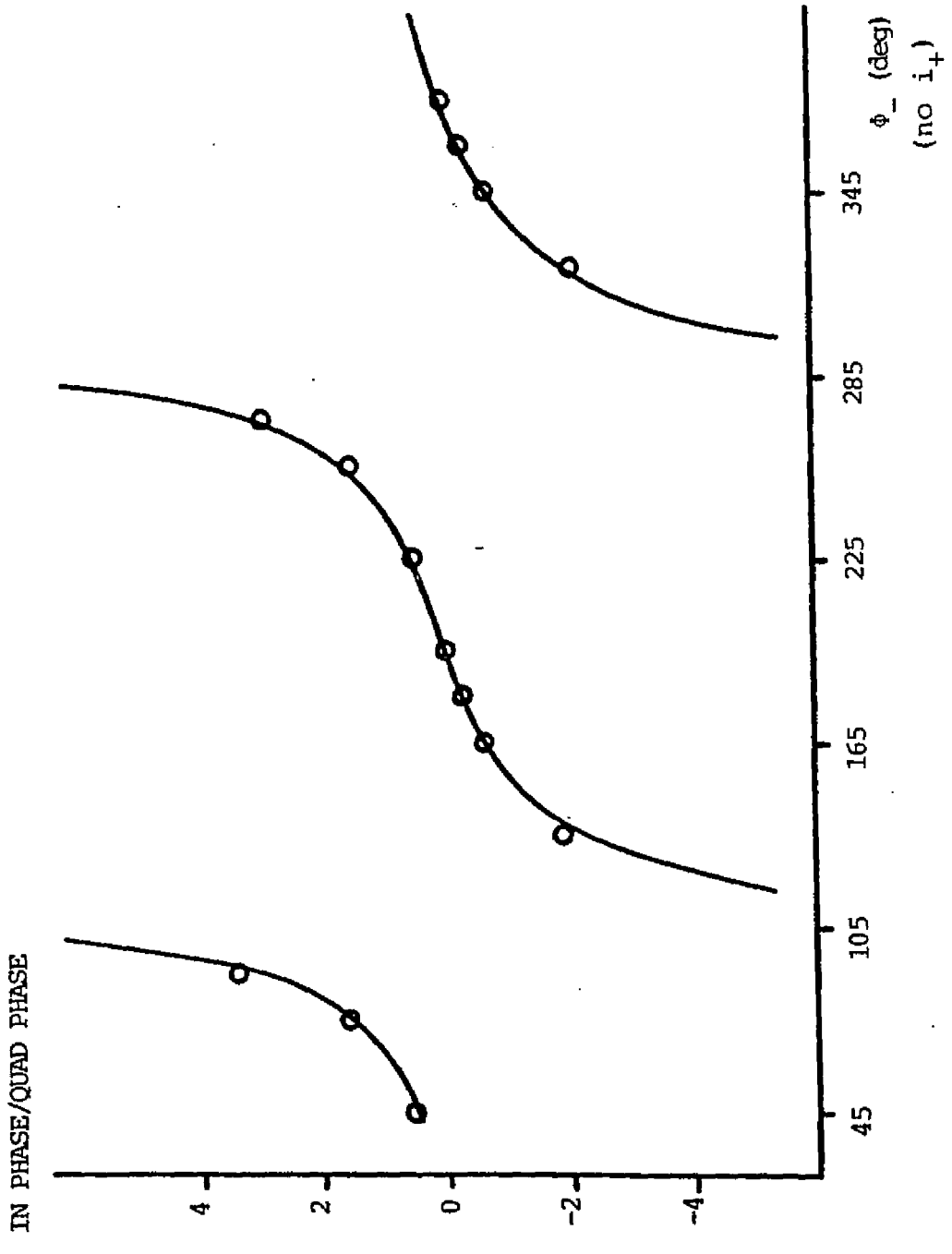

Figure 7.3 a) Ratio of In-Phase to Quad-Phase DBM ω-Component versus Lower Sideband Phase (Upper Sideband Turned Off)

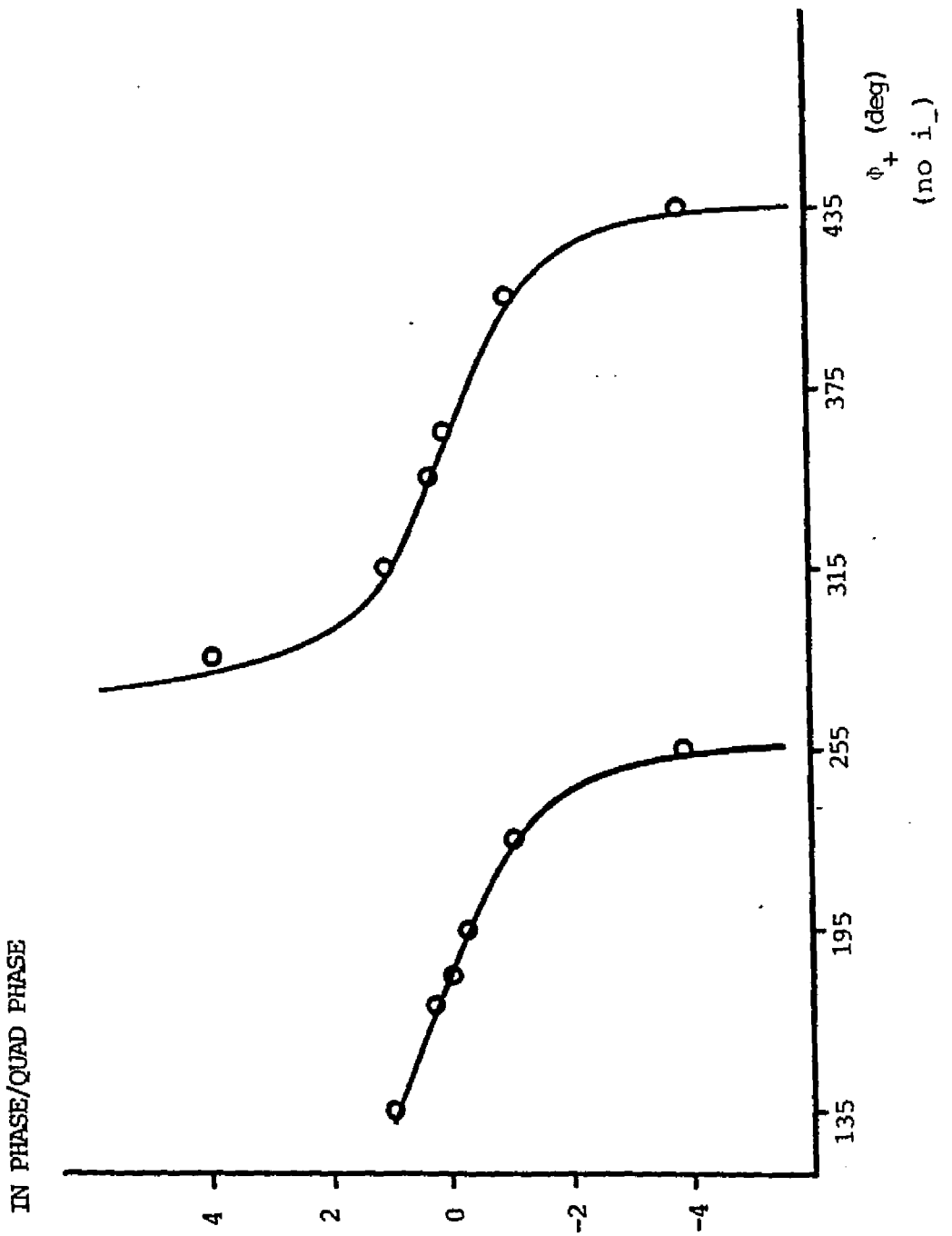

Figure 7.3 b) Ratio of In-Phase to Quad-Phase DBM ω-Component versus Upper Sideband Phase (Lower Sideband Turned Off)

and let the standard amplifier/quantum limits to be tested and surpassed? Although the Physics Letters article reprinted in the last chapter contained the first squeezing data published in the literature, we next present the results of more comprehensive tests.

C. Experimental Evidence for Back-Action Evasion

In the previous chapter, we presented conclusive evidence for the existence of the squeezing of amplifier force noise for (mixer-created) BAE input currents. We showed the dependence of squeezing on T and η (remember, η is the ratio of the rms noise current amplitude at frequency Ω_0 to the sideband amplitude). As we have stated earlier, however, the flexibility offered by independent sidebands provides a more comprehensive testing, and a better understanding, of the relevant principles of PS measurements and BAE.

In (3.9), we presented a general input current as a function of the phases of the individual sidebands in order to test phase sensitive coupling to the oscillator (diaphragm):

$$I_p = (i_+ \cos \phi_+)\cos \Omega_+ t - (i_+ \sin \phi_+)\sin \Omega_+ t$$

$$+ (i_- \cos \phi_-)\cos \Omega_- t - (i_- \sin \phi_-)\sin \Omega_- t \qquad (7.1)$$

The required input current for PS detection and BAE is recovered for $\phi_{+,-} = 0$.

If we let $i_+ = i_-$, then (7.1) implies a squeezing factor of

$$\Sigma = \left\{4(1+T^2)\eta^2 + \sin\phi_+ - \sin\phi_-)^2 + T^2(\cos\phi_+ + \cos\phi_-)^2 + T^2(\sin\phi_+ + \sin\phi_-)^2 + (\cos\phi_+ - \cos\phi_-)^2\right\}^{1/2} \Big/ \left\{4(1+T^2)\eta^2 + T^2(\sin\phi_+ - \sin\phi_-)^2 + (\cos\phi_+ + \cos\phi_-)^2 + (\sin\phi_+ + \sin\phi_-)^2 + T^2(\cos\phi_+ - \cos\phi_-)^2\right\}^{1/2} \tag{7.2}$$

Equations (7.1) and (7.2) provide a means of testing the correlation between PS detection and BAE by allowing the variation of the phase relationship between the two sidebands. In the previous section we saw the correct system response to phase differences in the two sticks and that PS measurements were convincingly verified. We now show the squeezing data obtained using independent two-stick input signals.

We first display the squeezing dependence on the phase difference between the two sticks for a given value of η, the relative strength of the injected amplifier noise.

Figures 7.4a and 7.4b show the experimentally determined squeezing as a function of phase of the upper and lower sidebands; a theoretical curve (loosely fitted to the data with η as a free parameter, due to the imprecision in measuring η) for $T = 13$ and $\eta = 0.08$ is shown for reference.

Figure 7.5 shows a sequence of data from another run, with a theoretical curve for $\eta = 0.186$ and $T = 13.4$. It is clear that BAE is a concomitant product of PS detection and depends upon the phase difference between the sidebands, thus laying a classical cornerstone for the foundation of quantum nondemolition.

These results are not trivial. Bocko[1] has presented evidence for phase sensitive coupling to an oscillator, and concludes that therefore back-action evasion has been achieved. This is putting the cart before the horse: the purpose of establishing phase sensitive detection schemes is to effect back-action evasion. PS detection offers nothing if it does not offer BAE.

The imprecision in determining the absolute value of the injected amplifier noise is most likely due to a combination of the high-Q of the resonator cavity (needed to prevent saturation of the final amplifier in the amplifier chain) and the (temperature-dependent) frequency drift of the amplifier output. This combination can account for the up to 10 dB corrections in η

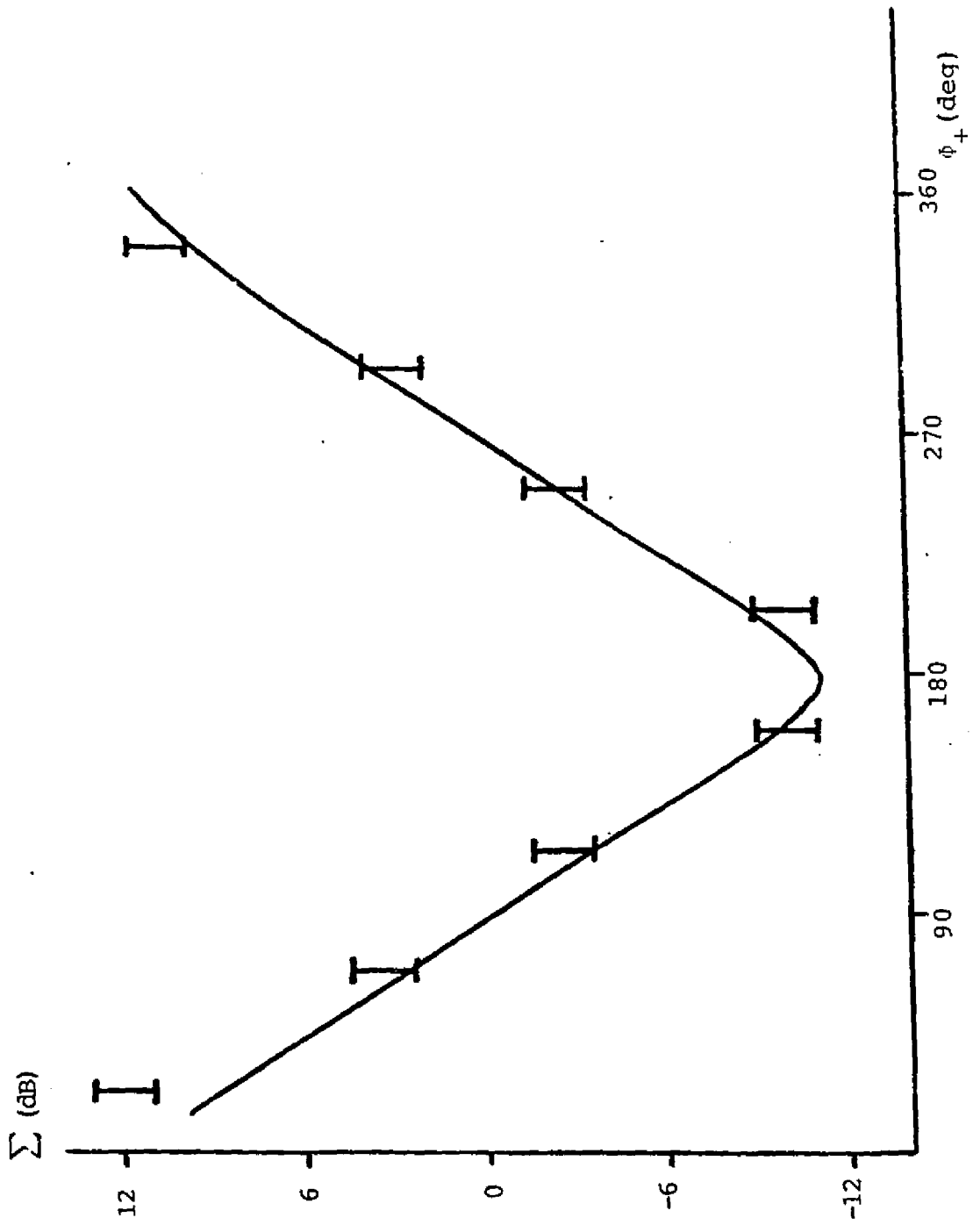

Figure 7.4 a) Squeezing as a Function of Upper Sideband Phase (Lower Sideband Phase = 0°)

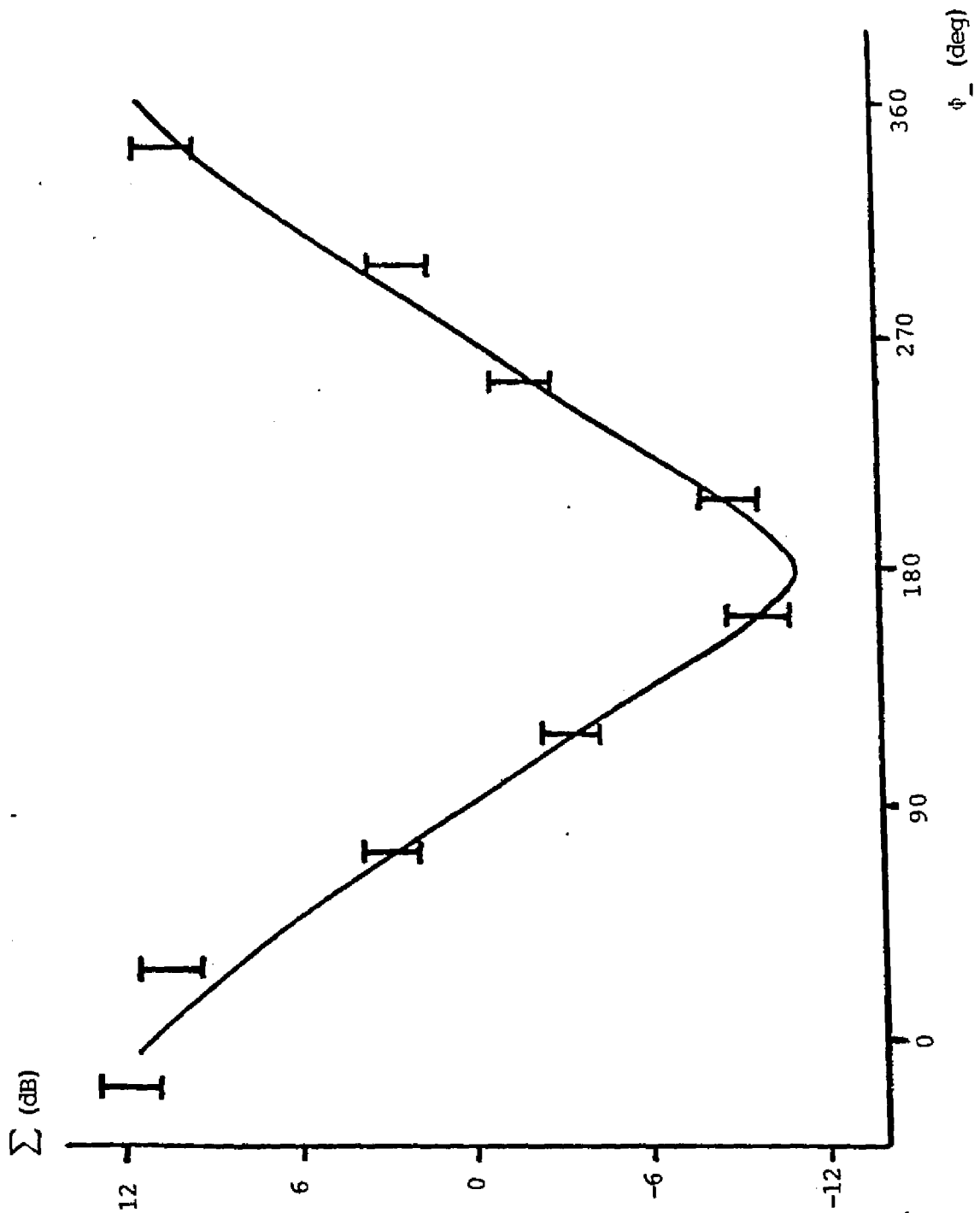

Figure 7.4 b) Squeezing as a Function of Lower Sideband Phase (Upper Sideband Phase = 0°)

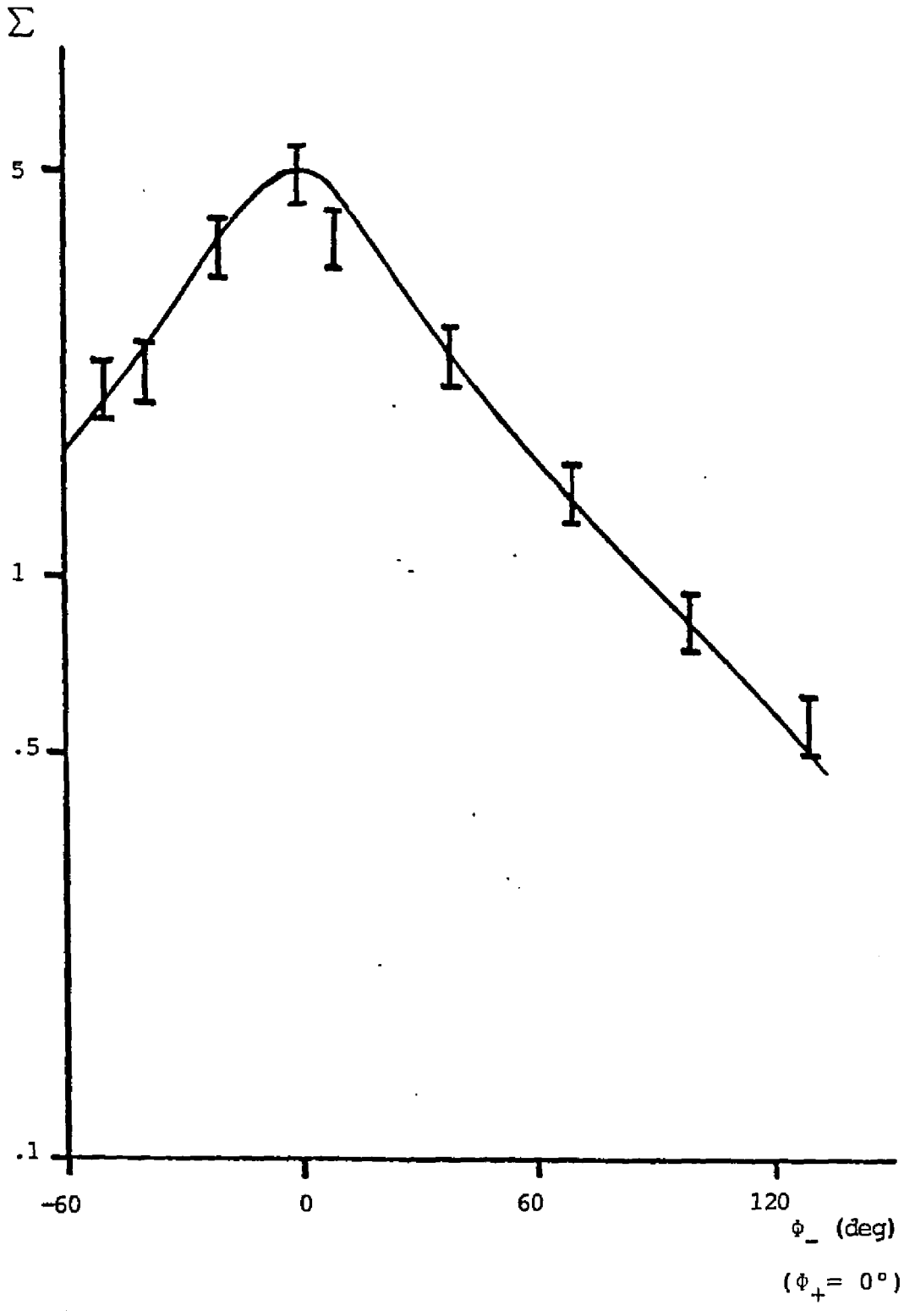

Figure 7.5 Squeezing as a Function of Lower Sideband Phase (Upper Sideband Phase = 0°)

that matching to the data can require.

D. Cavity Input Signal Preparation and Back-Action Evasion

Chapter 6 first mentions the imperfection of the input signal and amplifier noise level on squeezing: Figure 4 (Phys. Letts. paper) shows the expected squeezing response to amplifier noise levels, for one set of (mixer-created) two stick imperfections, as a function of T, and the actual squeezing data. We now take advantage of the independent sideband input to explore these imperfections and squeezing in more detail.

Input signal imperfections addressed are: 1) unequal amplitudes of i_+ and i_-; 2) coherent signal contributions at Ω_0 and $\Omega_{2\pm}$; 3) unequal amplitudes in the coherent contributions at $\Omega_{2\pm}$; and 4) frequency offset (detuning) of the two sticks from their nominal values at $\Omega_\pm$. This last item is not a very serious problem; spectral analysis (see Appendix 1) reveals that detuning does not play a role if the following condition is satisfied:

$$\frac{2Q_e\ \delta\Omega_0}{\Omega_0} = \frac{2\delta\Omega_0}{\Delta\Omega_0} << 1 \qquad (7.3)$$

where $\delta\Omega_0$ is the frequency offset. Since the microwave superconducting cavities used have bandwidths on the order of a kilohertz, (7.3) is a relatively easy criterion

to meet with frequency locking techniques employed to counter long term cavity drift.[2]

We can express the squeezing response to 1)-3), assuming that the amplifier back reaction is of uniform spectral density within several harmonics of ω about Ω_0, by

$$\Sigma = T\left\{\frac{(1+\delta_1)+(\eta^2+\frac{\gamma_1^2}{2})(1+\frac{1}{T^2})+\frac{\eta^2}{4T^2}+\frac{\gamma_2^2}{8T^2}(1+2\delta_2)+\frac{(1+2\delta_1)}{4T^2}}{(1+\delta_1)+T^2[(\eta^2+\frac{\gamma_1^2}{2})(1+\frac{1}{T^2})+\frac{\eta^2}{4T^2}+\frac{(1+2\delta_1)}{4T^2}+\delta_1^2+\frac{\gamma_2^2(1+2\delta_2)}{8T^2}]}\right\}^{\frac{1}{2}} \tag{7.4}$$

where γ_1, γ_2 are the relative coherent contributions (with respect to the coherent signal at Ω_+) at Ω_0 and Ω_{2+}, respectively, and γ_1, γ_2 are the relative amplitude imbalances in the $\Omega_\pm$ and $\Omega_{2\pm}$ signals (relative to the coherent signal amplitudes at Ω_+ and Ω_{2+}, respectively). Notice that the terms involving δ_2 and γ_2 are approximately T^2 times smaller than their δ_1 and γ_1 counterparts, and henceforth will be neglected.

The predicted effects of δ_1 on Σ can be seen for three values of T in Figure 7.6a (for $\gamma_1 = 0$). The figure shows that the higher the T of the system the more sensitive it will be to sideband imbalance. Figure 7.6b shows squeezing data for four different values

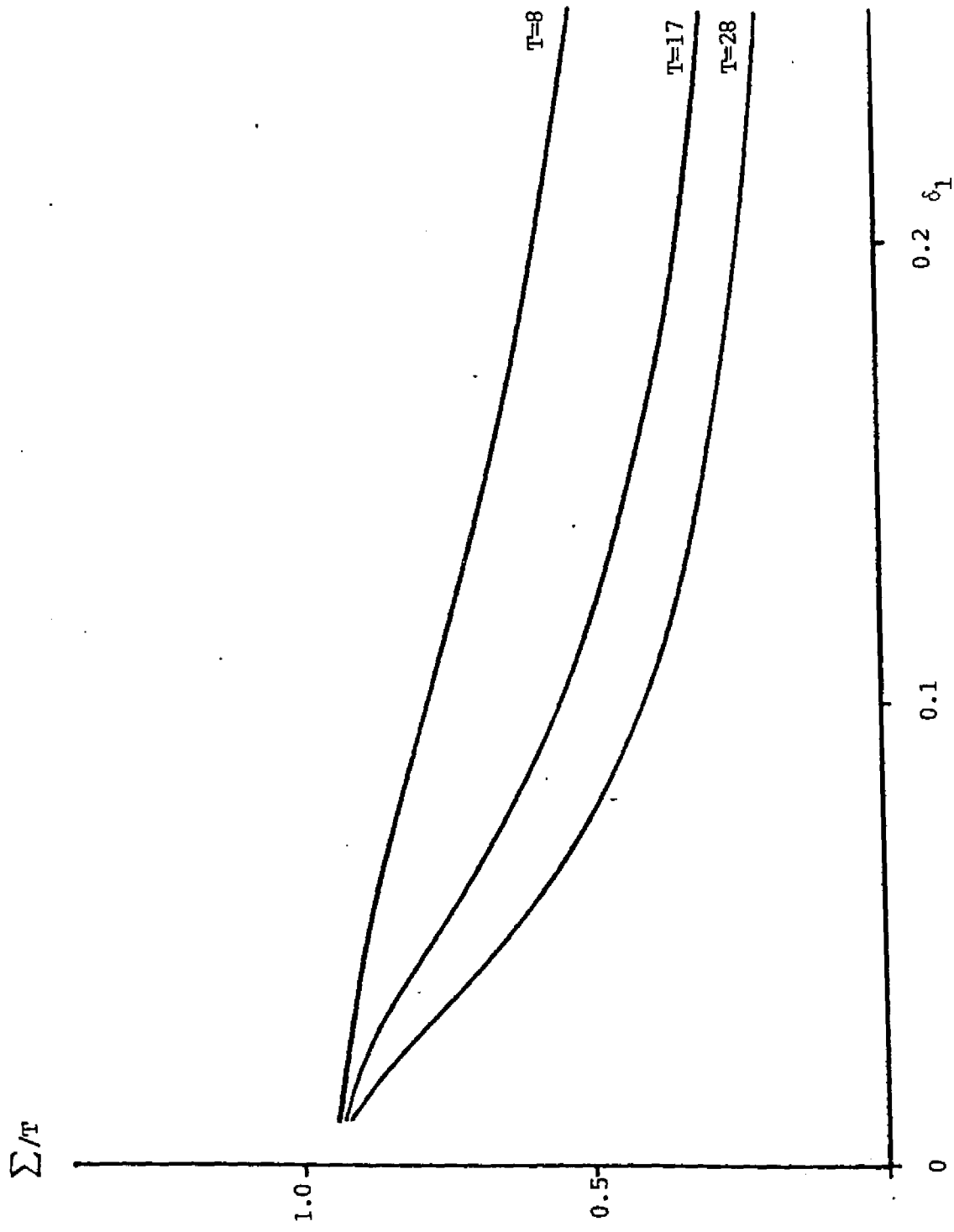

Figure 7.6 a) Predicted Squeezing versus Sideband Amplitude Imbalance

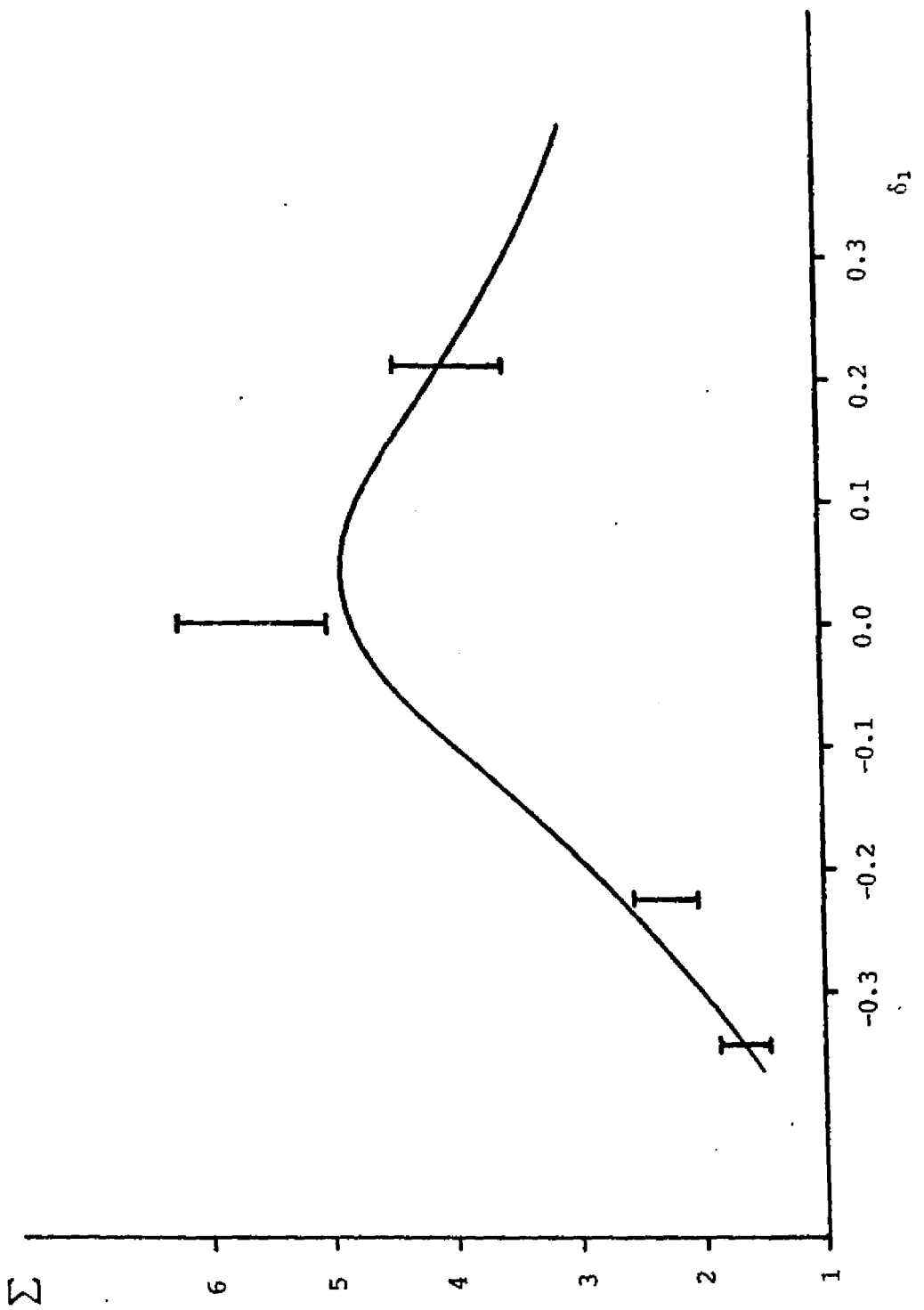

Figure 7.6 b) Squeezing versus Sideband Amplitude Imbalance

of δ_1, along with a theoretical curve for T = 19 and $\eta = 0.15$.

The amount of coherent carrier at Ω_0 is an important consideration in squeezing in that it mimicks an AP input; Figure 7.7 shows the predicted effect of γ_1 on Σ for three values of T (for $\delta_1 = 0$ and $\eta = 0$). As in Figure 7.6a, squeezing is much more sensitive to γ_1 at higher T values. One verification of the effect of carrier suppression (i.e., reducing γ_1) was performed: the effect of suppressing from a value of 0.25 to 0.05 improved the sensitivity by a factor of 1.68 ± 0.10, while the theoretically expected improvement factor for T = 12 and $\eta = 0.09$ is 1.63.

E. Effects of Amplifier Back Reaction and Environmental Noise on Back-Action Evasion

In our experiments, squeezing degradation due to signal imperfection is less of a problem than degradation due to sufficiently large amplifier noise and environmental noise levels. We stated in Chapter 5 that the amplifier back reaction was amplified by 145 dB in order for the diaphragm effects to be noticeable. At such high levels the product of noise at Ω_0 with the sideband coherent currents gives rise to AP simulations severe enough to compete with phase sensitive coupling. Furthermore, environmental noise also competes with the back-

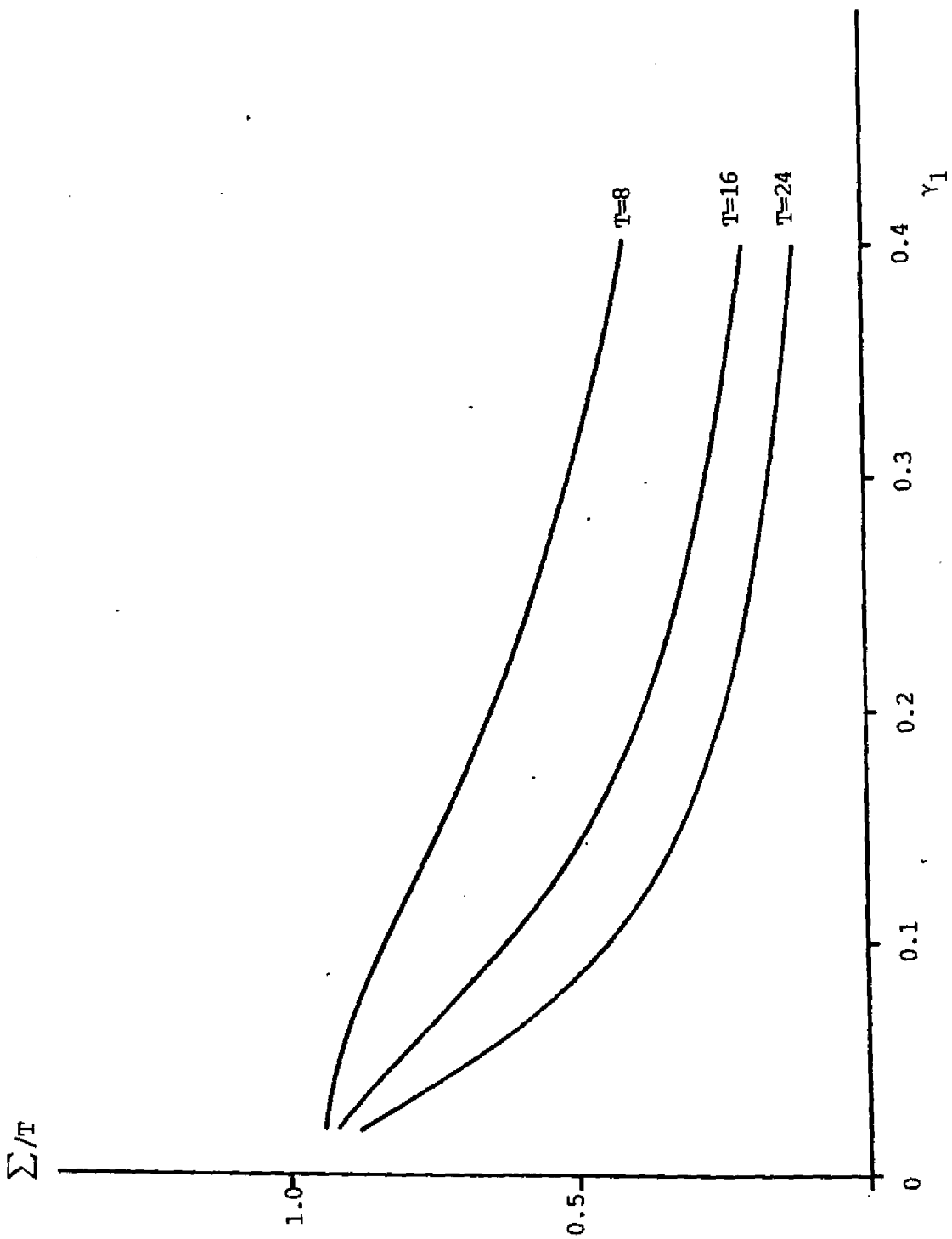

Figure 7.7 Predicted Squeezing versus Amplitude of Coherent Signal at Cavity Resonance Frequency

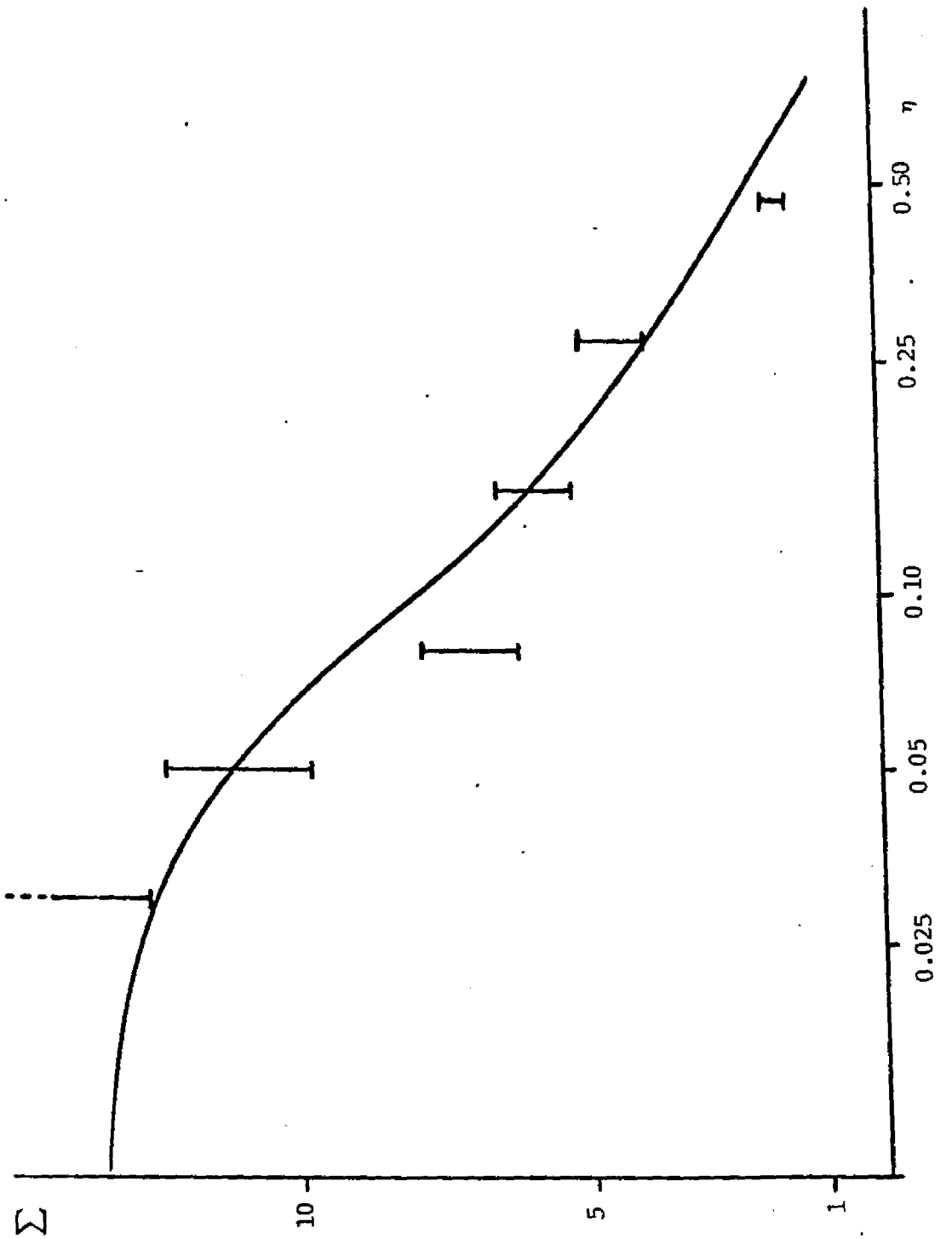

Figure 7.8 a) Squeezing as a Function of Amplifier Back Reaction Noise for Low Background Noise Level

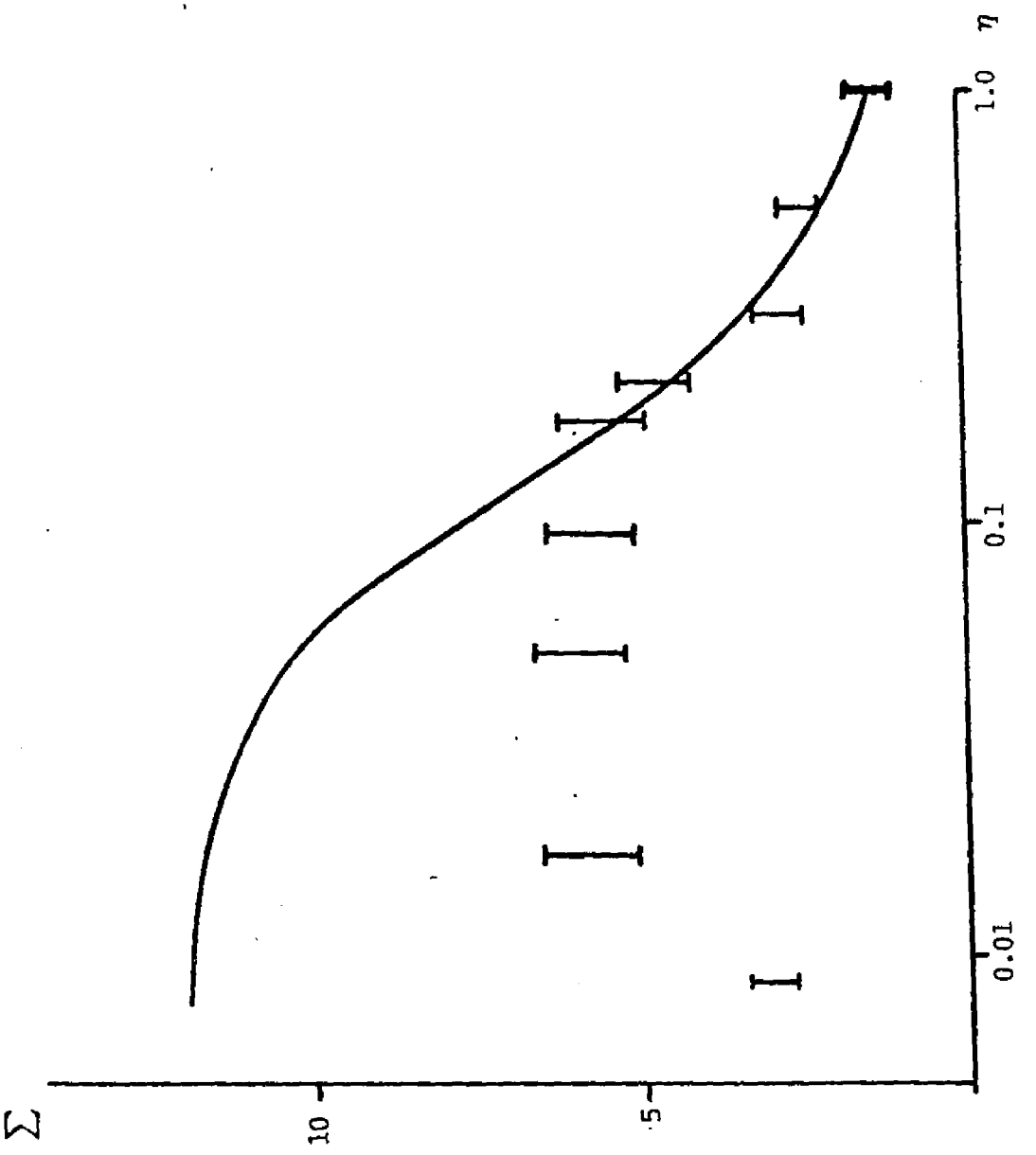

Figure 7.8 b) Squeezing as a Function of Amplifier Back Reaction Noise for a Relatively High Background Noise Level

action effects on the diaphragm, requiring that high η levels be present.

We can see both of these effects on squeezing in Figure 7.8. In Figure 7.8a, we present squeezing data as a function of η, along with a theoretical curve for $T = 15$ and γ_1, $\delta_1 = 0$ (the curve was matched to the data point at $\eta = 0.15$). In this figure, the data was taken late at night, and the lab was particularly quiet. This is to be contrasted with Figure 7.8b, where squeezing data is also presented as a function of but where squeezing is suppressed for $\eta < 0.17$. This is due to the ambient environmental noise effecting the diaphragm. Looking at the diaphragm behavior on the oscilloscope shows that in fact no squeezing occurs when the amplifier noise levels are reduced to that of the "background" noise. This conclusion is supported by Figure 7.9: the upper plot (data points represented by squares) shows Σ vs η for one value of the sideband amplitude, and the lower plot (data represented by triangles) is for an amplitude 4 dB lower but having the same η values. The stronger coherent sideband current data is less degraded because the relative environmental noise contribution is less than that for the lower coherent sideband data. Our test platform was not designed to have extraordinary vibration and acoustic isolation; typically these levels are at $\approx 10^{-15}$ m. The isolation of the

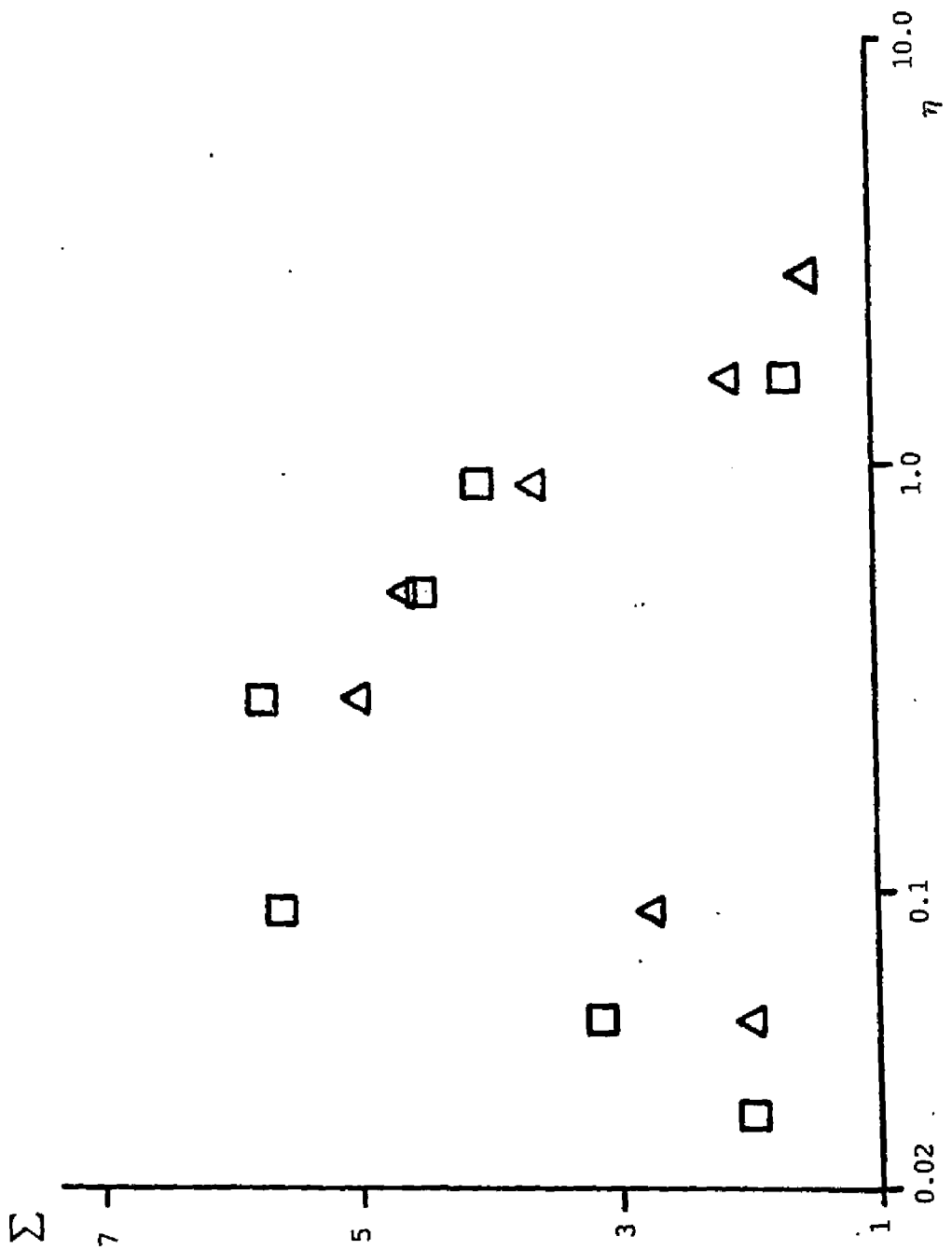

Figure 7.9 Squeezing versus Amplifier Back Reaction Noise for Two Different Sideband Amplitudes

gravity wave antenna is at least two orders of magnitude better.

F. Effects of Oscillator Phase Noise and Detuning on Back-Action Evasion

We turn now to two other potential sources of squeezing degradation. One is due to the noise introduced by the signal generators (at Ω_+ and Ω_-) and the other is due to the tuning of the input frequencies.

The former is of purely academic interest, as the level of pump noise needed to contaminate squeezing is much higher than that of off-the-shelf oscillators and synthesizers. This is shown in Figure 7.10, where predicted squeezing is plotted against Ψ, the dimensionless parameter used to approximate the pump phase noise strength, equal to the ratio of the rms pump phase noise current and the coherent sideband amplitude. According to the figure, degradation starts to occur at levels many orders of magnitude higher than those likely to be encountered. The effect of low level pump phase noise does have a very profound effect on the use of this transducer to detect gravitational radiation, as is discussed in Chapter 4.

A seemingly more serious problem is the ability to properly tune the dual sidebands, particularly in light of the fact that the cavity resonance frequency

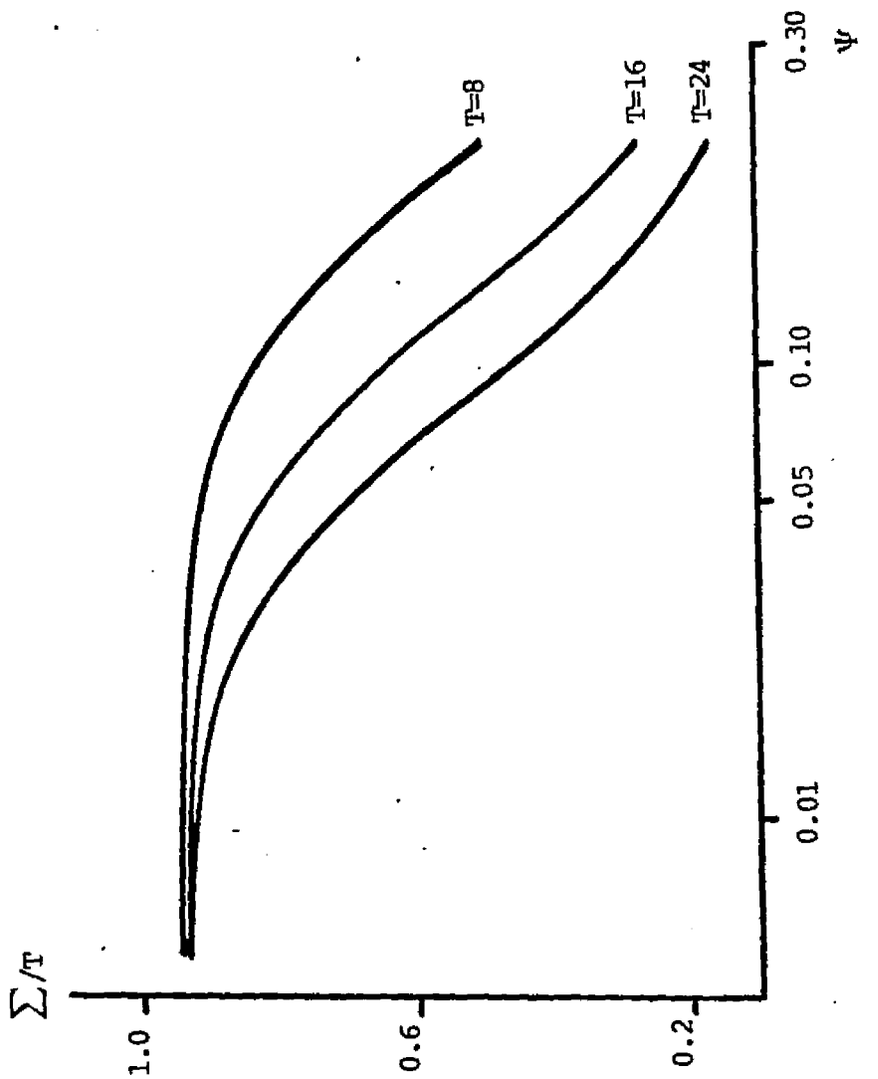

Figure 7.10 Predicted Squeezing as a Function of Oscillator Phase Noise

can drift. Appendix 3 presents an analysis of the squeezing spectrum for both an arbitrary back-action force and for the specific BAE back-action force. We present in Figure 7.11 a data sequence showing experimental results of detuning (by shifting the two stick frequencies simultaneously and in tandem) on squeezing. The analysis predicts relative insensitivity to detuning; the data presented here shows that cavity drifts on the order of tenths of kilohertz do not significantly affect BAE.

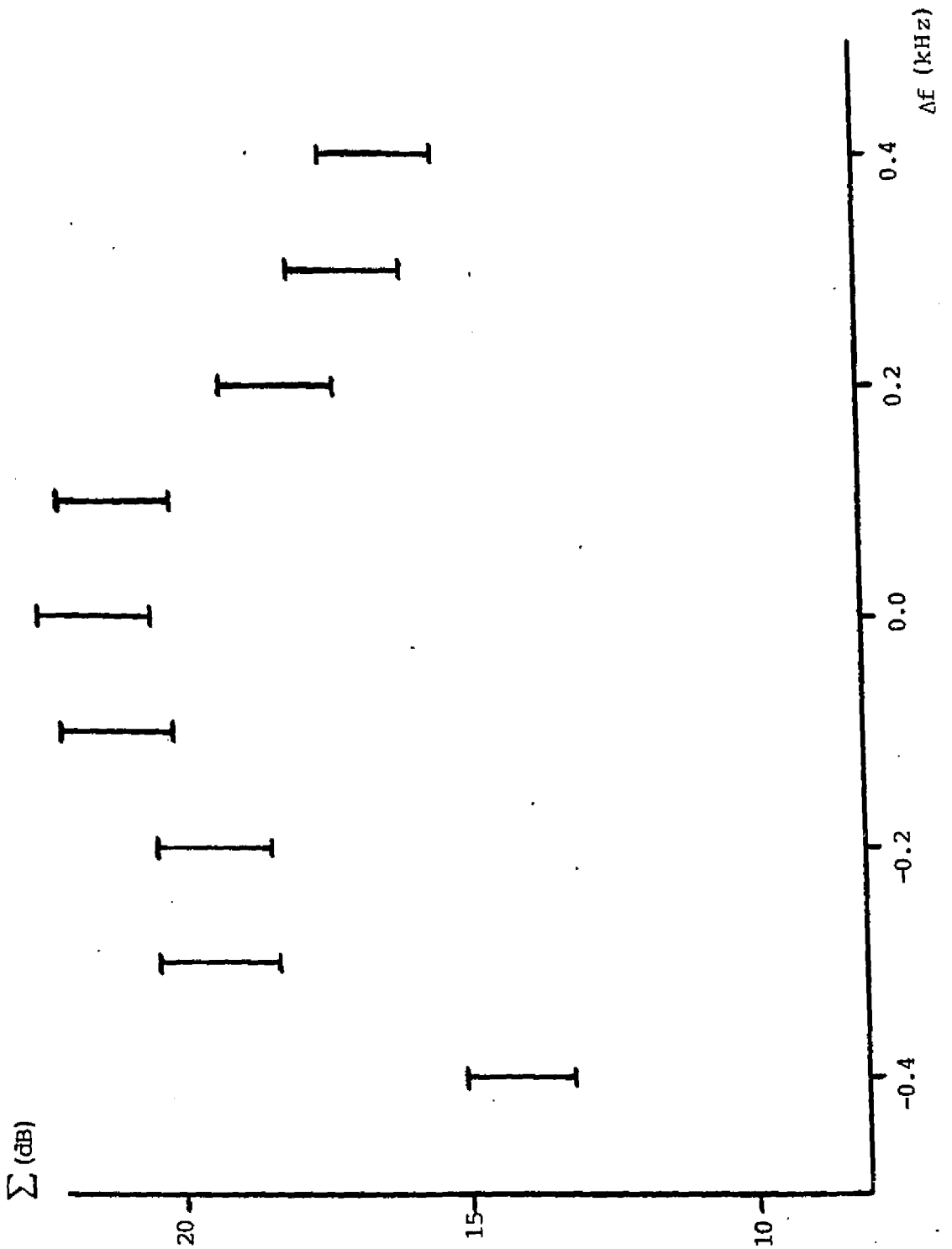

Figure 7.11 Squeezing Response to the Detuning of the BAE Input Signal

References

1. M. F. Bocko and W. W. Johnson, Phys. Rev. Letts. 48, 1371 (1982), Phys. Rev. A30, 2135 (1984).

2. See, e.g., A. G. Mann, Ph.D. Dissertation, Univ. of Western Australia, (1982).

CHAPTER 8

CONCLUSION

The last two chapters have presented conclusive evidence supporting the conclusion that our accelerometer test platform has, with the appropriate input signal, coupled predominantly to the imaginary component (X_2) of the diaphragm complex amplitude. The evidence also indicates that, for this phase-sensitive coupling, the amplifier back reaction noise is shunted to the real component (X_1) of the complex amplitude. Various parameter dependences and other indirect evidence also support these conclusions. The thoroughness of the tests of phase-sensitive detection of the oscillator motion and, in particular, the evidence for the back-action evasion of amplifier force noise, are the first to be achieved and reported in the literature.

Although the opening chapters introduce some of the semiclassical motivation behind the concepts of quantum nondemolition and back-action evasion, the experimental results presented herein are entirely classical. The squeezing of amplifier force noise does have a visible real world application, and that is in the detection of gravitational radiation. The analysis in Chapter 4 explores the response of detection

sensitivity as a function of squeezing. Although in the lab we were able to get squeezing factors as high as twenty for artificially high amplifier noise temperatures, the conclusions drawn from Chapter 4 indicate that, for realistic (and sometimes optimistic) experimental parameters, squeezing does not always guarantee improved antenna sensitivity. However, operation of the transducer in a resonant mode does help improve the system response to squeezing. Under very optimistic, yet achievable, conditions (dilution refrigerator temperatures, large antenna quality factor, and negligible transducer and pump oscillator noise), it is possible to reach and surpass the standard quantum limit with our system.

Although quantum limits were not approachable in these experiments, the back-action evasion demonstrated in the course of our research provides strong classical support for the circumvention of these limits, and for quantum measurement theory as well. These results should brace the efforts of researchers in experimental general relativity and quantum and nonlinear optics, just as the indirect evidence provided by the binary pulsar 1913+16 did for those earthbound searchers of gravitational radiation.

APPENDIX 1

CAPACITOR OUTPUT VOLTAGE COEFFICIENTS FOR EQUIVALENT CIRCUIT MODEL

We present the output voltage coefficients for the current input of (3.1) (see Chapter 3 for definitions of terms and other discussion), where the voltage is of the form

$$V(t) = V_p \Big[c_0 \cos \Omega_0 t + s_0 \sin \Omega_0 t + s_+ \sin \Omega_+ t + s_- \sin \Omega_- t + c_+ \cos \Omega_+ t + c_- \cos \Omega_- t + s_{2+} \sin \Omega_{2+} t + s_{2-} \sin \Omega_{2-} t + c_{2+} \cos \Omega_{2+} t + c_{2-} \cos \Omega_{2-} t \Big] \tag{A1.1}$$

The coefficients are:

$$c_0 = \frac{i_{0c}}{I} + \frac{\alpha Q_e}{2I(1+T^2)} \{-i_{+s} - T_{i+c} - i_{-s} + Ti_{-c}\} \cos \phi + \frac{\alpha Q_e}{2I(1+T^2)} \{Ti_{+s} - i_{+c} + Ti_{-s} + i_{-c}\} \sin \phi$$

$$s_0 = \frac{i_{0s}}{I} + \frac{\alpha Q_e}{2I(1+T^2)} \{-Ti_{+s} + i_{+c} + Ti_{-s} + i_{-c}\} \cos \phi$$

$$+ \frac{-\alpha Q_e}{2I(1+T^2)} \{-i_{+s} - Ti_{+c} + i_{+s} - Ti_{-c}\} \sin \phi$$

$$s_- = \frac{1}{I(1+T^2)} \{i_{-s} - Ti_{-c}\} + \frac{\alpha Q_e}{2I(1+T^2)} \{Ti_{0s} + i_{0c}\} \cos \phi$$

$$+ \frac{\alpha Q_e}{2I(1+T^2)} \{-i_{0s} + Ti_{-c}\} \sin \phi$$

$$c_- = \frac{1}{I(1+T^2)} \{Ti_{-s} + i_{-c}\} + \frac{\alpha Q_e}{2I(1+T^2)} \{-i_{0s} + Ti_{0c}\} \cos \phi$$

$$+ \frac{\alpha Q_e}{2I(1+T^2)} \{-Ti_{0s} - i_{0c}\} \sin \phi$$

$$s_+ = \frac{1}{I(1+T^2)} \{i_{+s} + Ti_{+c}\} + \frac{\alpha Q_e}{2I(1+T^2)} \{-Ti_{0s} + i_{oc}\} \cos \phi$$

$$+ \frac{\alpha Q_e}{2I(1+T^2)} \{i_{0s} + Ti_{0c}\} \sin \phi$$

$$c_+ = \frac{1}{I(1+T^2)} \{-Ti_{+s} + i_{+c}\} + \frac{\alpha Q_e}{2I(1+T^2)} \{-i_{0s} - Ti_{0c}\} \cos\phi$$

$$+ \frac{\alpha Q_e}{2I(1+T^2)} \{-Ti_{0s} + i_{0c}\} \sin \phi$$

$$s_{2+} = \frac{1}{I(1+4T^2)} \{i_{2+s} + 2Ti_{2+c}\} + \frac{\alpha Q_e}{2I(1+T^2)(1+4T^2)}$$

$$\{-3Ti_{+s} + (1-2T^2)i_{+c}\} \cos \phi$$

$$+ \frac{\alpha Q_e}{2I(1+T^2)(1+4T^2)} \{(1-2T^2)i_{+s} + 3Ti_{+c}\} \sin \phi$$

$$c_{2+} = \frac{1}{I(1+4T^2)} \{-2Ti_{2+s} + i_{2+c}\}$$

$$+ \frac{\alpha Q_e}{2I(1+T^2)(1+4T^2)} \{-(1-2T^2)i_{+s} - eTi_{+c}\} \cos \phi$$

$$+ \frac{\alpha Q_e}{2I(1+T^2)(1+4T^2)} \{-3Ti_{+s} + (1-2T^2)i_{+c}\} \sin \phi$$

$$s_{2-} = \frac{1}{I(1+4T^2)} \{i_{2-s} - 2Ti_{2-c}\} + \frac{\alpha Q_e}{2I(1+T^2)(1+4T^2)}$$

$$\{3Ti_{-s} + (1-2T^2)i_{-c}\} \cos \phi$$

$$+ \frac{\alpha Q_e}{2I(1+T^2)(1+4T^2)} \{-(1-2T^2)i_{-s} + 3Ti_{-c}\} \sin \phi$$

$$c_{2-} = \frac{1}{I(1+4T^2)} \{2Ti_{2-c} + i_{2-c}\}$$

$$+ \frac{\alpha Q_e}{2I(1+T^2)(1+4T^2)} \{-(1-2T^2)i_{-s} + 3Ti_{-c}\} \cos \phi$$

$$+ \frac{\alpha Q_e}{2I(1+T^2)(1+4T^2)} \{-3Ti_{-s} - (1-2T^2)i_{-c}\} \sin \phi$$

APPENDIX 2

TIME EVOLUTION OF X_1 UNDER OSCILLATOR INTERACTION WITH THERMAL RESERVOIR

The analysis in this appendix was motivated by a private communication from Carl Caves.[1] The statistics of a random force acting on a harmonic oscillator can be found in various texts, including the collection edited by Wax.[2]

Recall the definitions of X_1 and X_2, and assume that X_1 is the coupled component of the oscillator motion. The variance of X_1 is defined by:

$$(\Delta X_1(t))^2 = \langle X_1^2 \rangle - \langle X_1 \rangle^2 \qquad \text{(A2.1)}$$

Substituting the definitions of X_1 and X_2 into (A2.1) and rearranging and collecting terms gives

$$(\Delta X_1)^2 = \frac{1}{2} \langle X_1^2 \rangle + \frac{1}{2m\omega_0^2} \langle p^2 \rangle \qquad \text{(A2.2)}$$

We express the equation of motion for a harmonic oscillator as

$$\ddot{x} + \left(\frac{2}{\tau_*}\right)\dot{x} + \omega_0^2 x = \frac{F(t)}{m} \qquad \text{(A2.3)}$$

where $F(t)$ represents the thermal fluctuation forces of

the oscillator. The spectral density of F(t) is assumed to be equal to $4Dm^2$, and that $\langle F(t)\rangle = 0$ and $\langle F(t_1)F(t_2)\rangle = 2Dm^2\delta(t_1-t_2)$. The other assumption made is that F(t) is Gaussian, with a Gaussian coefficient $\sigma^2 = 4D/T$, where T is the physical temperature of the oscillator.

The substitution v = dx/dt can be made in this (Langevin) equation, giving

$$\frac{dv}{dt} + \left(\frac{2}{\tau_*} v + \omega_0^2 x\right) = \frac{F(t)}{m} \qquad \text{(A2.4)}$$

Wang and Uhlenbeck[3] solve this (Fokker-Planck) equation for a Gaussian force and obtain the average values and variances for the oscillator coordinate and velocity. Applying their solutions to (A2.2) gives, after some algebra and collection of terms,

$$(\Delta X_1)^2(t) = \frac{1}{2}\left[(\Delta x)^2 + \langle x\rangle^2\right] + \frac{1}{2\omega_0^2}\left[(\Delta v)^2 + \langle v\rangle^2\right]$$

$$= \frac{D}{\beta\omega_0^2}\left(1 - e^{-\beta t} - \frac{e^{-\beta t}}{2\omega_1^2}\beta^2 \sin^2 \omega_1 t\right)$$

$$+ v_o^2 e^{-\beta t}\left(\frac{\sin^2 \omega_1 t}{2\omega_1^2} + \frac{\cos^2 \omega_1 t}{2\omega_0^2}\right.$$

$$+ \frac{\beta^2 \sin^2 \omega_1 t}{8\omega_0^2 \omega_1^2} - \frac{\beta \sin \omega_1 t \cos \omega_1 t}{2\omega_0^2 \omega_1})$$

$$+ x_0^2 e^{-\beta t} (\frac{\cos^2 \omega_1 t}{2} + \frac{\beta^2 \sin^2 \omega_1 t}{8\omega_1^2}$$

$$+ \frac{\omega_0^2 \sin^2 \omega_1 t}{2\omega_1^2} + \frac{\beta}{2\omega_1} \sin \omega_1 t \cos \omega_1 t)$$

$$+ v_0 x_0 e^{-\beta +} (\frac{\beta}{\omega_1^2} \sin^2 \omega_1 t) \qquad \text{(A2.5)}$$

where

$$\beta \equiv \frac{2}{\tau_*} \; ; \; \omega_1^2 = \omega_0^2 - \frac{\beta^2}{y} \; ; \quad x_0 \equiv x(0) \; ; \quad v_0 = \frac{dx}{dt}|_{t=0}$$

This equation does not contain any approximations. If we now make the (reasonable) assumption that period of oscillation is much less than the decay time then $\omega_1 \approx \omega_0$ and $\beta/\omega_1 \approx \beta/\omega \approx 0$. Also, from the equation of motion we use the transfer function to relate the spectral density of x to the spectral density of F via

$$S_x(\omega) = \frac{S_F(\omega)}{m^2[(\omega-\omega_0)^2 + \frac{4}{\tau_*^2}\ ^2]} = \frac{4D}{m^2[(\omega-\omega_0)^2 + \frac{4}{\tau_*^2}\,\omega^2]} \qquad \text{(A2.6)}$$

Incorporating (A2.6) and the approximations just mentioned into (A2.5) gives the following expression for the variance in X_1

$$(\Delta X_1)^2(t) = (\frac{v_0^2}{2\omega_0^2} + \frac{x_0^2}{2})e^{-2t/\tau_*} + \frac{\tau_* S_F}{2m^2\omega_0^2}(1 - e^{-2t/\tau_*})$$

$$\equiv (\Delta X_1)^2_{t=0}\ e^{-2t/\tau_*} + (\Delta X_1)^2_{\text{fluct}} \qquad \text{(A2.7)}$$

where $(\Delta X_1)_{t=0}$ is the initial uncertainty in X_1; as t grows to infinity, the uncertainty in X_1 approaches $(\tau_* S_F/8m^2\omega_0^2)^{1/2}$. Of course, optimum measurement times are very much less than the decay time of the oscillator.

Since the random force is assumed to be produced by interaction with a heat bath at temperature T, we can determine S_F.[4] Results for the variance σ^2 are

$$\sigma^2 = \frac{2\beta kT}{m} \quad \text{and} \quad D = \frac{\beta kT}{m} \qquad \text{(A2.8)}$$

Thus

$$S_F = \frac{8mkT}{\tau_*} = \frac{8m\hbar\omega}{\tau_*}\left(\bar{n} + \frac{1}{2}\right) \qquad \text{(A2.9)}$$

where

$$\bar{n} = \frac{1}{e^{\hbar\omega/kT} - 1}$$

This last equation is the usual Nyquist theorem extended to low temperatures. Equations (A2.9) and (A2.7) are the standard results of classical fluctuation-dissipation theory.

References

1. Dated March 26, 1980.

2. Noise and Stochastic Processes, N. Wax, ed., (Dover, New York, 1954).

3. M. C. Wang and G. E. Uhlenbeck, in Noise and Stochastic Processes.

4. Ibid.

APPENDIX 3

SQUEEZING DETUNING AND FREQUENCY OFFSET DEPENDENCE

The classical squeezing results presented in the main body of this work were derived by making certain statistical assumptions for the input current amplitudes. In this appendix, we generalize the treatment by presenting squeezing as a function of the spectral densities of the back action force on the mechanical oscillator. We also show, for a white noise amplifier back reaction, that the squeezing is relatively insensitive to frequency offset.

The equation of motion of the mechanical oscillator (i.e. transducer diaphragm) acted upon by back action forces created by gap electric fields can be written as

$$\ddot{x} + (\frac{\omega_0}{Q_m})\dot{x} + {\omega_0}^2 x = \frac{F_{ba}(t)}{m} \qquad \text{(A3.1)}$$

where I have used ω_0 as the diaphragm resonant frequency (instead of ω as in the text). If I make the substitutions $x = X_1 \cos \omega_0 t + X_2 \sin \omega_0 t$ and $F_{ba}(t) = I \cos \omega_0 t + Q \sin \omega_0 t$, (A3.1) can be rewritten as

$$\ddot{X}_1 + (\frac{\omega_0}{Q_m})\dot{X}_1 + 2\omega_0\dot{X}_2 + \frac{{\omega_0}^2}{Q_m} X_2 = I/m \qquad \text{(A3.2a)}$$

$$\ddot{X}_2 + \left(\frac{\omega_0}{Q_m}\right)\dot{X}_2 - 2\omega_0\dot{X}_1 - \frac{\omega_0^2}{Q_m} X_1 = \dot{Q}/m \qquad \text{(A3.2b)}$$

Equations (3.2) are then Fourier-transformed (transforms are denoted by ~); solving for X_1 and X_2 gives

$$|\tilde{X}_1|^2 = \left|\frac{A}{m(A^2+B^2)}\right|^2 |\tilde{I}|^2 + \left|\frac{B}{m(A^2+B^2)}\right|^2 |\tilde{Q}|^2$$

$$- \frac{2\,\mathrm{Re}(AB^*)}{m^2\,A^2+B^2\,^2} \tilde{(IQ)} \qquad \text{(A3.3a)}$$

$$|\tilde{X}_2|^2 = \left|\frac{B}{m(A^2+B^2)}\right|^2 |\tilde{I}|^2 + \left|\frac{A}{m(A^2+B^2)}\right|^2 |\tilde{Q}|^2$$

$$+ \frac{2\,\mathrm{Re}(AB^*)}{m^2\,|A^2+B^2|^2} \tilde{(IQ)} \qquad \text{(A3.3b)}$$

where $A \equiv -\omega^2 - i\omega\omega_0/Q_m$ and $B \equiv -2\omega\omega_0 i + \omega_0^2/Q_m$. Applying the well-known relationship between the Fourier transform and its spectral density[1] gives

$$S_{X_1} = \left|\frac{A}{m(A^2+B^2)}\right|^2 S_I + \left|\frac{B}{m(A^2+B^2)}\right|^2 S_Q$$

$$- \frac{2\,\mathrm{Re}(AB^*)}{m^2\,|A^2+B^2|^2} S_{IQ} \qquad \text{(A3.4a)}$$

$$S_{X_2} = \left| \frac{B}{m(A^2+B^2)} \right|^2 S_I + \left| \frac{A}{m(A^2+B^2)} \right|^2 S_Q$$

$$+ \frac{2\,\mathrm{Re}(AB^*)}{m^2 |A^2+B^2|} S_{IQ} \qquad \text{(A3.4b)}$$

where S_f is the spectral density (power spectrum) of process f and S_{fg} is the cross spectral density (cross-power spectrum)[1] of processes f and g.

Dividing (A3.4a) by (A3.4b) and taking the square root gives the squeezing factor Σ as a function of frequency, but without having yet specified the form of the back action force (i.e., I and Q).

The discussion in the text introduced squeezing by examining the ratio of the in- and quad-phase components of the back action force and by assuming that the rms noise amplitudes for the input currents were all equal. Here, we consider the expressions for the force components without making assumptions on the current amplitudes. Instead, we determine the spectral densities of I and Q and their cross spectral density, making only the assumption that the spectral density of the amplifier noise back reaction is equal at each Fourier current component. These steps are tedious but essentially trivial; the results give for the squeezing factor the following expression:

$$\Sigma(\omega) = \left(\frac{S_{X_1}}{S_{X_2}} \right)^{1/2} = \left\{ \omega^2(\omega^2 + (\omega_0/Q_m)^2) + \alpha^2 \omega_0^2(4\omega^2 + (\omega_0/Q_m)^2) - 2\beta^2\omega^2(\omega_0/Q_m)^2 Q_m \right\}^{1/2} \Big/ \left\{ \omega_0^2(4\omega^2 + (\omega_0/Q_m)^2) + \alpha^2\omega^2(\omega^2 + (\omega_0/Q_m)^2) + 2\beta^2\omega^2(\omega_0/Q_m)^2 Q_m \right\}^{1/2} \tag{A3.5}$$

where

$$\alpha^2 \equiv \frac{2\eta^2 + \gamma_1^2 + 2\left(\frac{T^2}{1+T^2}\right)}{2\eta^2 + \gamma_1^2 + 2\delta_1^2\left(\frac{T^2}{1+T^2}\right) + \left(\frac{2}{1+T^2}\right)} \tag{A3.6a}$$

$$\beta^2 \equiv \frac{2(1+2\delta_1)\left(\frac{T}{1+T^2}\right)}{2\eta^2 + \gamma_1^2 + 2\delta_1^2\left(\frac{T^2}{1+T^2}\right) + \left(\frac{2}{1+T^2}\right)} \tag{A3.6b}$$

and where, as in the main text, δ_1 is the relative coherent two stick amplitude imbalance, γ_1 the coherent contribution at Ω_0, and η the rms amplitude (relative to the upper sideband) of the amplifier back reaction.

We present in Table A.1 squeezing vs. frequency offset for three different values of η (with $T = 10$, a diaphragm frequency of 4000 kHz, and δ_1 and $\gamma_1 = 0$). We see that for offsets as high as 200 Hz the squeezing is affected less than a few percent. Since the diaphragm bandwidth is less than 1 Hz, these results indicate that very high-Q diaphragms won't require frequency tunings and stabilities that could be difficult to implement and maintain.

Table A.1

Frequency Offset (Hz)	Squeezing Factor (η=.01)	(η=.05)	(η=0.1)
0	9.95	8.95	7.09
50	9.93	8.93	7.08
100	9.87	8.89	7.06
200	9.65	8.73	6.98
500	8.45	7.81	6.48
1000	6.23	5.96	5.31
2000	3.71	3.65	3.49

References

1. A. Papoulis, Probability, Random Variables, and Stochastic Processes, (McGraw-Hill, New York, 1965).

VITA

Gary Wayne Spetz was born on July 19, 1952 in Chicago, Illinois to Robert and Ann Spetz. Graduating class valedictorian from D. D. Eisenhower High School in 1970, he attended the University of Illinois and received a Bachelor of Science degree in engineering physics in 1974. He entered the University of Illinois physics graduate program in 1975, and received his Master of Science degree in physics in 1977.

In the summer of 1977 he was hired by the University of Southern Mississippi as an Instructor of Physics, where he remained for one year. In the fall of 1978 he entered the graduate physics program at Louisiana State University, and one year later joined the gravitational radiation detection group of Prof. William O. Hamilton. He began his research into measurement strategies and the fundamental sensitivity limits associated with these strategies in the summer of 1980, and is presently a candidate for the degree of Doctor of Philosophy.

On November 6, 1982 he was married to Martha Ruston, and daughter Lauren was born to them on March 13, 1985.

DOCTORAL EXAMINATION AND DISSERTATION REPORT

Candidate: Gary Spetz

Major Field: Physics and Astronomy

Title of Dissertation: Phase-Sensitive Detection and the Back-Action Evasion of Amplifier Force Noise.

Approved:

Major Professor and Chairman

Dean of the Graduate School

EXAMINING COMMITTEE:

R. F. O'Connell

Date of Examination:

April 11, 1985